University of Alberta
Department of Civil &
Environmental Engineering

Structural Engineering Report No. 227

Fatigue of Bearing-Type Shear Splice

by

Georg Josi

Gilbert Y. Grondin

and

Geoffrey L. Kulak

June, 1999

FATIGUE OF BEARING-TYPE SHEAR SPLICES

by

Georg Josi

Gilbert Y. Grondin

and

Geoffrey L. Kulak

STRUCTURAL ENGINEERING REPORT 227

Department of Civil and Environmental Engineering
University of Alberta
Edmonton, Alberta, Canada

June, 1999

ABSTRACT

An investigation of the fatigue resistance of bearing-type shear splices was carried out to assess the effect of bolt hole pattern on fatigue resistance. A finite element stress analysis of shear splices consisting of flat plates was conducted to investigate the influence of bolt hole stagger, gage dimension, and edge distance on the stress concentration around the bolt holes. A test program, consisting of 31 fatigue test specimens, was designed on the basis of the analysis. The test specimens consisted of symmetrical bearing-type shear splices with varying stagger and gage dimension and they were tested at different stress ranges. Staggers varying from zero to 75 mm were investigated on four sets of three specimens and two different gage dimensions were investigated at two stress range levels. A statistical analysis of the test results indicated that neither the stagger nor the gage dimension significantly influenced the fatigue life of the test specimens.

An analysis of the test results also indicated that none of the commonly used cross-sectional area definitions is adequate for stress range calculations. An approach that accounts for stress concentration in the calculation of the effective stress range was therefore proposed. This approach consists of multiplying the gross cross-section stress range by a correction factor that was determined using a finite element analysis. A fatigue curve with a slope of 7.0 and stress correction factors for most common flat plate geometries are presented for design use.

ACKNOWLEDGEMENTS

This project was conducted with the research funding from the Natural Sciences and Engineering Research Council of Canada. The first author wishes also to acknowledge personal financial support in the form of scholarships from the Swiss National Fund (Fonds National), the Faculty of Graduate Studies and Research and the C.W. Carry Chair of the University of Alberta.

TABLE OF CONTENTS

LIST OF TABLES

LIST OF FIGURES

LIST OF ABBREVIATIONS AND SYMBOLS

Abbreviations

AASHTO	American Association of State Highway and Transportation Officials
AREA	American Railway Engineering Association
ASTM	American Society for Testing and Materials
CAFL	Constant Amplitude Fatigue Limit
CSA	Canadian Standards Association
DOF	Degrees of Freedom
ECCS	European Convention for Constructional Steelwork

Symbols

a	intercept of regression line
A_g	gross cross-sectional area
A_n	net cross-sectional area
$A_{n,1}$	net cross-sectional area deducting one hole
$A_{n,2}$	net cross-sectional area deducting two holes
$A_{n,C}$	net cross-sectional area using Cochrane's rule
b	slope of regression analysis curve
C	clamping force; fatigue life constant
D	hole diameter
d_s	nominal fastener diameter
e	edge distance
F	statistical test
F_{sc}	stress range correction factor
F'_{sc}	simplified stress range correction factor
F_y	yield strength
g	gage dimension

k_s	slip coefficient
l	distance from the grip ends to the first bolt holes
m	slope of $\Delta s - N$ curve
N	number of stress cycles (to failure)
N_c	reference number of stress cycles (= 2 000 000)
N_d	numbers of stress cycles corresponding to the detection of a crack
N_e	number of stress cycles at which the crack reached the edge of a plate
N_f	number of stress cycles corresponding to the end of a test
n	number of holes in static failure path; number of tests
n_l	number of lines of bolts (parallel to applied load)
n_r	number of rows of bolts (perpendicular to applied load)
P	pretension load in fastener
$P_{\max}$	maximum applied load
p_i	projected load at node i
p_n	percentage of fatigue life
Q	total load applied at one bolt hole (i.e., the load in the bolt).
q_i	projected load at node i of a bolt hole
R	stress ratio
RD_{kf}	relative difference in stresses
r	correlation coefficient
r_i	ratio between the largest and smallest values of SCF_i
SCF	stress concentration factor
SCF_{S0}	stress concentration factor for the reference plate S0
SCF_i	stress concentration factor using effective cross-sectional area i
SCF_k	stress concentration factor for any plate geometry k
s	stagger
s_b	standard deviation of the slope b in a regression analysis

s_e	standard error of estimate
s_y	variance
T	tensile force
t	plate thickness; value of the *t*-distribution
t_m	main plate thickness
t_s	splice plate thickness
V	load transmitted by fastener(s)
w	plate width
w_g	gross section width
x	coordinate; independent variable in statistical analysis ($\log(\Delta s)$)
$\bar{x}$	mean value of x
y	coordinate; dependent variable in statistical analysis ($\log(N)$)
$\bar{y}$	mean value of y
y_i	coordinate at node i
z	coordinate
ΔP	applied load range
Δs	stress range
Δs_c	reference fatigue strength at two million cycles
Δs_D	constant amplitude fatigue limit stress range
Δs_g	gross section stress range
Δs_n	net section stress range
Δs_{sc}	corrected stress range (accounting for stress concentration)
Σ	summation
s	stress
s_b	bearing stress
s_f	stress obtained with the fine mesh model

s_g	gross section stress
$\sigma_{g,S0}$	gross section stress for reference plate (plate S0)
$\sigma_{g,k}$	gross section stress for any plate geometry k
σ_i	stress obtained using effective cross-sectional area i
s_k	stress obtained with the intermediate or coarse mesh model
$s_{\max}$	maximum applied stress
$s_{\min}$	minimum applied stress
s_n	net section stress
σ_{peak}	peak stress in a plate with holes
$\sigma_{peak,S0}$	peak stress in reference plate (plate S0)
$\sigma_{peak,k}$	peak stress in any plate k
s_x	normal stress on a plane perpendicular to applied load

1. INTRODUCTION

1.1 Connections

Connections play a vital role in structural designs by linking the individual members to form a continuous configuration. In new steel structures, this is commonly performed by welding or bolting. Although no longer used in contemporary civil engineering structures, rivets are common fasteners in older structures. This report will only deal with bolted and riveted connections.

Because of the complexity of connections, our understanding of connection behavior is sometimes less than our understanding of the behaviour of the members that are being connected. It is highly desirable that the connections not fail before the main members: such behavior would be catastrophic [1.1]. To minimize the risk of a failure within a connection, additional safety margins are prescribed in codes. This approach is justified for the design of new structures where the result is a more secure connection at the expense of a relatively small increase of the overall cost of the structure. However, for existing structures this approach may be too conservative and may lead to unnecessary rehabilitation or replacement of a structure or structural components.

Mechanically fastened joints are conveniently classified according to the type of forces to which the connectors are subjected [1.2]. The different types of actions are (1) shear, (2) tension, and (3) combined tension and shear. Shear cases can further be divided into slip-resistant and bearing-type joints, depending on the specifics of the load transfer mechanism. This report will mainly deal with bearing-type shear connections. A further complication often arises: if the width of the connected material is restricted, a staggered bolt or rivet configuration is adopted to accommodate the required number of fasteners for the load transfer while minimizing the length of the connection.

1.2 Fatigue of Fabricated Steel Components

Fatigue is, with corrosion, one of the principal causes of deterioration of steel structures. Fabricated steel components normally contain microcracks. When subjected to cyclic stresses these microcracks may grow to macroscopic proportions, eventually leading to failure of the member by brittle or ductile fracture, net section plastification, leakage (pressure vessels), or a combination of these failure modes. Steel structures subjected to the repeated action of loads (bridges, overhead cranes, transmission towers, offshore platforms, and the like) are susceptible to fatigue cracking. Many examples of catastrophic failures caused by fatigue cracking have been documented [1.3], illustrating the importance of a better understanding of fatigue.

The research into the behavior of fatigue of fabricated steel structures has shown that the combined effect of stress concentrations (at locations of so-called stress raisers) and high residual tensile stresses can be the source of fatigue cracks. This phenomenon even occurs if the maximum applied stress is well below the elastic limit of the material. A mechanically fastened connection is therefore particularly susceptible to fatigue cracking since stress raisers created by abrupt changes in geometry and high residual stress fields due to punching or drilling of holes cannot be avoided.

1.3 Statement of the Problem

The type of load transfer mechanism present in bolted or riveted shear splices directly influences the behavior of the connection under repeated loading. The applied load can either be transferred by friction at the interface of the connected plates, by bearing and shear of the bolts, or by a combination of both mechanisms. The load transfer mechanism is influenced by factors such as:

- the magnitude of the clamping force
- the slip coefficient of the faying surfaces
- the magnitude and direction of the applied load.

Quite different crack patterns can be observed for the two extreme cases of the load transfer mechanism. Slip-resistant joints, where the load is entirely transferred by friction, imply a high concentration of shear stresses at the discontinuities of the lap and main plates and of the bolts or rivets and the lap plates (see Figure 1.1). This results from large differences in strain between the two respective parts in contact. In order to relieve some of those strains, microslips take place at these locations, and this can damage the surface of the plates. This is termed fretting fatigue. Under the combined effects of stress concentration and plate damage, crack growth can occur under cyclic loading. In this case, the crack usually propagates through the gross section of the plate(s) and does not intersect a bolt or rivet hole.

In bearing-type joints the load is entirely transferred by shear and bearing of the bolts. This type of load transfer implies a stress concentration at the edge of the bolt or rivet holes, which is also the location where the cross-sectional area is the smallest. Cracks initiate at these points of high stresses and propagate through the net section of the plate(s), as illustrated in Figure 1.2.

It is generally accepted that the stress range associated with the fatigue strength of bolted and riveted shear splices should be calculated on the net cross-section for bearing-type connections and on the gross cross-section for slip-resistant connections [1.4, 1.5]. This is consistent with observed behavior. However, there are no research data to define the boundary between a bearing-type and a slip-resistant joint. The question about the critical cross-section for fatigue calculations becomes even more confusing in the presence of bearing-type connections with staggered holes. Such configurations are often encountered in older structures, where savings on the material were important, thus restricting plate widths of the members being connected. Observations of crack patterns, which always seem to be perpendicular to the applied loads, have indicated that the relevant net cross-section approaches used for the design of the plates under static loading might not be applicable for net cross-section calculations under cyclic loading.

1.4 Scope, Objectives, and Structure of the Report

The scope and objectives of this study are to:

1. Review the existing literature on fatigue of bolted shear splices with particular attention to bearing-type shear splices that have staggered holes.
2. To investigate the stress distribution near the holes of the lap plates for different staggers using the finite element method.
3. To conduct fatigue tests on bolted bearing-type shear splices where the hole-stagger (from zero to a value at which the effective net section for static loads no longer depends on the stagger) and the gage distance is varied.
4. To derive a simple procedure to calculate the fatigue strength of joints with staggered holes under repeated loading, using the results of the analysis and the test results.

Other important issues of bolted shear splices, such as the minimum clamping force and slip coefficient to guarantee a slip-resistant joint or the influence of mean stress on fatigue life, as well as other types of mechanically fastened connections, are not investigated in this report.

The *Literature Review* (Chapter 2) summarizes the current knowledge about: (1) the behavior of bearing-type shear splices under static loading; (2) the mechanisms of fatigue damage and failure; (3) the behavior of shear splices under repeated loading; and (4) the estimation of the effective fatigue net cross-section in the presence of staggered holes. In Chapter 3, *Analytical Investigations*, finite element models are developed that illustrate the magnitude of the stress concentrations around bolt holes for different joint geometries. Based on the analytical investigations, a series of fatigue tests on bearing-type shear splices with and without staggered holes was planned and then carried out. *Experimental Program*, including the test results, is presented in Chapter 4. *Discussion of Results* (Chapter 5) demonstrates the correlation between the tests and the analytical model, providing the basis for *Recommendations*, which—together with a *Summary* and *Conclusions*—are proposed in the last chapter (Chapter 6) of this report.

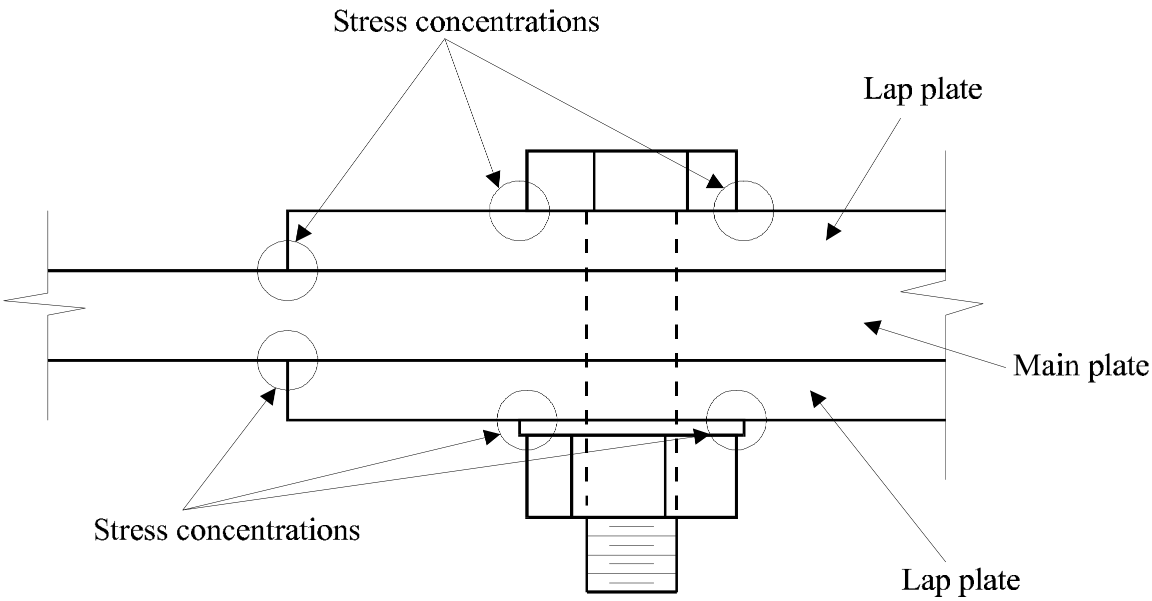

Figure 1.1 – Stress concentrations at discontinuities of slip-resistant shear splices.

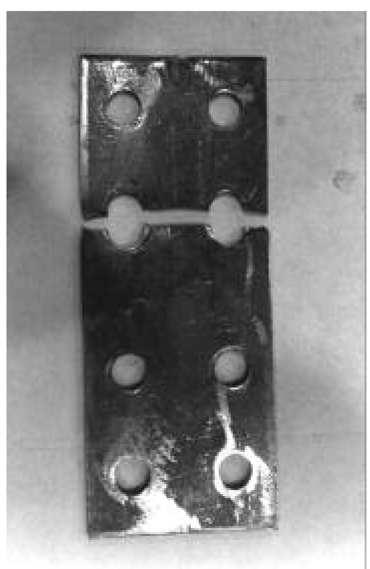

Figure 1.2 – Failure at net section of bearing-type joint.

2. Background Information and Literature Review

2.1 Introduction

Although the behavior of bolted bearing-type shear splices under static loads is generally well understood, some of the important issues will be presented in the first part of this chapter. The general concepts of fatigue are explained in Section 2.3. The current state of knowledge concerning the fatigue strength and the influence of the most important parameters on fatigue life of symmetric shear splices are summarized in Section 2.4. Finally, the issue of bolt or rivet stagger and its consequences on the fatigue behavior of shear splices is addressed in Section 2.5.

2.2 Static Behavior of Symmetric Shear Splices

2.2.1 General

Mechanically fastened shear splices can be designed either as slip-critical or as bearing-type connections [2.1]. A slip-critical shear splice is one that has a low probability of slip at any time during the service life of the structure. In a bearing-type connection, the bolts either are initially in bearing upon completion of the joint or have been brought into bearing as the connection slips under service loading. In limit states design, it has to be assumed that the bolts will be in bearing under the action of the factored loads, whether the connection was designed as slip-critical or bearing-type. This report will mainly deal with symmetric bearing-type shear splices, as shown in Figure 2.1.

Fatigue loading usually is included in the definition of service load. Thus, the expectation is that joints subjected to fatigue loading should be designed as slip-critical. However, there are situations in which an understanding of fatigue behavior of a bearing-type joint is important. If rivets have been used to make the joint, there is no guarantee that the joint will not slip at service load levels and place the rivets into bearing: rivet pretension is both unknown and unreliable [2.2]. If pretensioned high-strength bolts have been used to make the connection, it is not known *a priori* whether the fatigue life of a bolted joint will be governed by conditions at the service load level in a slip-critical state or by conditions when the bolts are in bearing because the preload was lost at some higher load level. In any event, the bearing case is the limiting condition.

2.2.2 Slip Resistance of Shear Splices

The cooling shrinkage of hot driven rivets or the tightening of high-strength bolts introduces clamping forces in the connection—even if the bolts are only snug-tight, as is the case for bearing-type joints. As a result, a frictional resistance is mobilized between the connected plates. As long as the axial load applied on the shear splice does not exceed the frictional resistance, no slip occurs in the connection and the bolts are not subjected to shear and bearing. The frictional resistance depends on the following factors:

- the number of slip planes;
- the number of bolts;
- the slip coefficient of the connected material; and
- the tension force in each bolt or rivet.

The first two are geometrical properties and are known exactly for a given connection. However, the slip coefficient, k_s, which can only be determined experimentally [2.3, 2.4], and the clamping force, C, are both subject to variability about their mean values. Information about the parameters affecting k_s and C can be found elsewhere [2.5–2.13].

2.2.3 Shear Splices in Bearing

In bearing-type connections, the bolts or rivets are often in bearing from the beginning of loading. However, at low load levels some of the load can still be transferred by friction. As the frictional resistance of a joint is exceeded, the load is mainly transferred by shear and bearing of the fasteners. At this stage the critical parameters for the behavior of the joint are no longer the slip coefficient and the clamping force, but the joint geometry as it affects the stresses in the connected material and the local bearing pressures in the connected material.

The load partition among the bolts in a shear splice depends primarily upon the type of bolt and grade of material being connected and geometrical features like joint length. More information about these parameters can be found elsewhere [2.14–2.19]. In order to assess the fatigue behavior of bearing-type shear splices with staggered holes it is necessary to discuss the following two issues in more detail:

- bearing stresses on the holes

- effect of hole stagger on the ultimate strength of the connection.

Bearing Stresses

After the slip resistance of a connection is exceeded, one or more fasteners are in bearing against the side of the hole. Bearing stresses, s_b, are developed at the point of contact between the fastener and the plate. Although the bearing area is a function of the applied load and varies through the thickness of the plate, it is usual to assume that the resulting stresses are uniformly distributed and can be expressed as follows:

$$\sigma_b = \frac{V}{d_s t} \tag{2.1}$$

where

V	:	load transmitted by the fastener
d_s	:	nominal fastener diameter
t	:	plate thickness

Figure 2.2 shows a shear splice subjected to a tensile force T. If it is assumed that the load P is the same for all the fasteners, then the highest stresses in the splice plates are around the fastener holes of section A-A, where the entire load T has been introduced. Thus, these holes are critical for fatigue. In practice, some of the fasteners may come into bearing before others and the load P can vary from fastener hole to fastener hole. This can result in higher stresses around other holes than the ones in section A-A, and it is possible that a fatigue crack might initiate at a fastener hole in section B-B or C-C.

Staggered Holes

In many situations a staggered hole pattern (see Figure 2.3) is required to place all the bolts within the length of a shear splice. Figure 2.4 shows possible failure paths for a plate with staggered holes. In such a case, the governing cross-section required to calculate the stresses at ultimate limit state is a function of the stagger, s, and the gage, g. This cross-section is termed the "effective net section." The following formula for the calculation of the net section was developed by Cochrane in 1922 [2.20] and is widely used in North America for the design of tension connections:

$$A_n = t\left(w_g - nD + \sum \frac{s^2}{4g} \right) \tag{2.2}$$

where

t	:	plate thickness
w_g	:	gross section width of the member
n	:	number of holes in failure path
D	:	hole diameter (usually taken 2 mm greater than the bolt diameter for drilled and 4 mm greater for punched holes)
Σ	:	summation considering all inclined segments in the failure path

The least cross-sectional area of those depicted in Figure 2.4 is taken as governing.

Other approaches used for the net section calculation in the presence of staggered holes can be found elsewhere [2.21–2.23]. It has to be noted that all approaches—including

Cochrane's rule—are founded on the assumption that plastic deformation conditions are present over the entire width of the plate. Other than the limitations of some of the approaches themselves [2.24], their use for failure modes like fatigue, which take place at stress levels considerably less than the yield strength of the material, is questionable.

2.3 Fatigue

2.3.1 General

Repeated application of stress can initiate and cause the propagation of micro-cracks in metal. These cracks can grow to macroscopic proportions with continued application of stress. This is the process known as fatigue. Unless otherwise noted, in this report the term "fatigue" is intended to apply to mechanical and high-cycle fatigue. Mechanical fatigue is a result of the fluctuation of externally applied stresses, specifically without being influenced by environmental or time-dependent effects. High-cycle fatigue refers to crack initiation (seldom significant in fabricated steel structures) and propagation of (existing) microcracks under global maximum stresses that are less than the yield stress of the base material. These relatively moderate stresses result in fatigue lives that generally exceed 100,000 load cycles.

The aim of this section is to give a brief introduction of the theory of fatigue. *Parameters Influencing the Fatigue Life* are discussed in Section 2.3.2 and an overview of current *Fatigue Design Methods* is presented in Section 2.3.3.

2.3.2 Parameters Influencing Fatigue Life

The fatigue life of a member or structural detail is simply the number of stress cycles that can be sustained before failure. Some of the parameters that potentially can influence the fatigue life of a structural detail are [2.25]:

- the load spectrum;
- the geometry and fabrication of the detail;
- the material characteristics; and
- environmental effects.

Only the first three are discussed in this report, and attention is directed most closely at the first two.

Load Spectrum

Through a stress analysis, the load spectrum can be defined by the stress range, the mean stress, and the stress sequence to which a detail is subjected. Since this study considers only fatigue behavior under constant amplitude stresses, the effect of stress sequence on the fatigue strength of a detail is not discussed herein. Fatigue tests on many different welded details have shown that stress range, Δs , is the most important stress-related parameter that describes the fatigue life of a structure [2.26]. The stress range is defined as:

$$\Delta s = s_{\max} - s_{\min} \tag{2.3}$$

where $s_{\max}$ and $s_{\min}$ are the maximum and minimum applied stresses, respectively.

For welded details, it has been found that other stress parameters such as mean stress or the stress ratio, $R = s_{\min} / s_{\max}$, have a negligible effect on fatigue resistance. The dependence of fatigue life solely on stress range is largely a reflection of the presence of high tensile residual stresses, coupled with high stress concentration, at some locations of the detail. Since the residual stresses can be expected to be more moderate in bolted and riveted connections than in welded details, the conclusion that the stress ratio does not influence the fatigue life of such a detail has to be examined. This problem is discussed in Section 2.4.

Geometry and Fabrication of the Detail

At locations where both stress concentrations and tensile residual stresses are high, the detail will be particularly susceptible to fatigue cracks. The magnitude of stress concentration and tensile residual stresses is dictated by the geometry and fabrication of the detail. The highest stress concentrations in a bearing-type connection are usually around a hole. Furthermore, the fabrication of the holes, which is done by drilling or by punching, introduces residual stresses and micro-cracks, which can subsequently affect the fatigue strength of the detail.

Material Characteristics

Some researchers have observed in tests of non-welded specimens that material characteristics—or more precisely the microstructure of metals—can have an influence on the fatigue life of a member [2.27]. Whether this observation is also true for bolted connections is discussed in Section 2.4.

2.3.3 Fatigue Design Methods

Two basic approaches for the fatigue design of members and elements have been proposed. These are based on both extensive physical testing and on analytical studies. The two philosophies are [2.28]:

- Use of experimentally determined relationships between stress range and fatigue life ($\Delta s - N$ curves).

- application of fracture mechanics principles.

Because of its ease of application in design, use of the $\Delta s - N$ curves are preferred to the fracture mechanics approach, which is used primarily to explain fatigue failures. It is not discussed further here.

As was discussed in Section 2.3.2, the fatigue life of a given detail depends primarily on the applied stress range and the detail. Therefore, it is possible to represent the stress range Δs as a function of the fatigue life N for a given detail. It has been shown that when the log of Δs is plotted against the log of N, the test results fall more or less on a straight line [2.29]. This can be represented by the following equation:

$$\log(N) = \log(C) - m\log(\Delta s) \tag{2.4}$$

where C is the fatigue life constant and m is the slope of the straight line.

This way of representing the relationship between Δs and N is termed a $\Delta s - N$ curve. Such $\Delta s - N$ curves have been established for a large number of structural details. For design purposes, it is customary for design standards, specifications and codes to group these results into several categories.

Although based on the same test results and concepts, two somewhat different sets of curves and classifications are used in design: the $\Delta s - N$ curves given by the American Association of State Highway and Transportation Officials (AASHTO) Specification [1.4] and the $\Delta s - N$ curves given by the European Convention for Constructional Steelwork (ECCS) Recommendations [1.5]. The AASHTO curves, which are also used in the Canadian steel structures design standard CAN/CSA S16.1 [2.30], are illustrated in Figure 2.5. The same kind of information in the ECCS Recommendations, not shown here, are designated by a detail category number, which represents the reference fatigue strength at two million cycles, Δs_c.

Both constant amplitude and variable amplitude fatigue tests have shown that the fatigue life of steel structures is infinite if all the applied stress ranges are less than a threshold value, Δs_D. This is called the constant amplitude fatigue limit (CAFL) and it is the horizontal portion of the $\Delta s - N$ curves in Figure 2.5. As long as all stress ranges applied to a detail are smaller than the CAFL for that detail, no crack growth takes place and the detail is not susceptible to fatigue failure. However, this approach can lead to unsafe designs if just a few stress cycles exceed the CAFL, resulting in a deterioration of the structure and a reduction of Δs_D [2.31].

2.4 Fatigue of Symmetric Bolted Shear Splices

2.4.1 Introduction

Fatigue research has been conducted for over 150 years and has involved many different scientific disciplines. Early fatigue investigations on mechanically fastened connections were done by Wilson and Thomas in 1938 [2.32]. The introduction of high-strength bolts gave rise to several research programs to investigate the fatigue behavior of bolted shear splices. Research on single lap shear splices that were free to deform out-of-plane showed that the fatigue strength can be reduced significantly due to secondary stresses induced by the eccentricity of the connection and the resulting out-of-plane bending [2.33, 2.34]. However, the following review will focus on joints with symmetrical shear splices only.

A helpful starting point for the literature review already exists. This is the work of Albrecht *et al.* [2.35], who conducted a review of the literature on fatigue of bolted shear splices up to 1987. Section 2.4.2 outlines and evaluates this and the other literature presented since that time on the fatigue behavior of symmetrical shear splices. The different design specifications that have been established in North America and Europe on the basis of these test programs are summarized in Section 2.4.3, followed by a discussion and conclusions.

2.4.2 Basic Results from Research Projects

The following presents a review of sixteen major studies of the fatigue behavior of bolted shear splices conducted between 1938 and 1984. Over 500 test results have been reported. However, only about 80% of these results can be considered to have provided useful information: unexpected behavior, such as excessive slip or failure in the grips, invalidates some of the studies. Tests that were stopped at 5,000,000 cycles, before the formation of cracks, are not presented since they cannot really be considered run-outs and would therefore bias the data. Where $\Delta s - N$ diagrams were used to represent the test results, the curves for fatigue categories B, C, and D of the AASHTO Specification [1.4] are also shown for comparison.

Effective Cross-Section

Depending on the type of connection, fatigue crack initiation can either take place in the net section (bearing-type connections), or in the gross section (slip-critical connections) [2.35, 2.36]. The distinction between these two types of connections is often quite difficult to establish for fatigue loading and depends on such factors as the clamping force (bolt pretension), the slip coefficient provided by the contact surfaces , and the level of fatigue load that was applied. A number of test programs have indicated that failure can initiate either in the gross cross-section or in the net cross-section even with identical test specimens [2.37–2.42]. It has been shown that if no pretension, or only small pretension (up to about 10% of the bolt tensile strength), is applied, bolted connections behave similar to riveted connections [2.32, 2.43]. Early studies [2.43, 2.44] already indicated that an increase in preload leads to an increase in fatigue life of a connection. Tension splice specimens tested by Steinhardt and Möhler [2.38] failed through the gross cross-section when high friction between the connected plates was assured. (Sand-blasted plates and fully pretensioned bolts were used.) However, neither one of these studies indicates the level of bolt pretension needed to move the failure from the net cross-section to the gross cross-section and thus guaranteeing an increased fatigue strength.

The effect of surface preparation was investigated by Birkemoe *et al.* [2.40], Frank and Yura [2.36], and by Cullimore [2.45]. Birkemoe *et al.* tested pretensioned connections with mill scale and grit blasted surfaces. The results of their tests are presented in Figure 2.6. Birkemoe *et al.* concluded that sandblasting increased the fatigue strength of a joint, which was attributed to a higher slip coefficient. These conclusions, however, are based on a limited number of test data that show considerable scatter and no statistical analysis of the results was performed. Cullimore [2.45] did not observe a marked difference between the fatigue behavior of shot-blasted, epoxy-coated and non-treated plates in slip-critical shear splices. Frank and Yura [2.36] concluded that the fatigue strength of pretensioned shear splices made up of plates with different coatings is at least as high as the fatigue strength of similar specimens with untreated or blasted plates. In both the Cullimore and the Frank and Yura tests the bolt pretension was high, preventing the plates from slipping under fatigue loads. These test results suggest that, as long as a certain minimum bolt pretension is provided, the fatigue strength of shear splices is not affected by the surface preparation. However, no study has been conducted to determine the combination of minimum bolt pretension, surface preparation, and fatigue load level that ensures gross cross-section failure—and thus increased fatigue strength—under repeated loading.

Joint Geometry

The effect of joint geometry on the fatigue behavior of bolted shear splices has been investigated in several research projects. Variations in bolt grip length, joint length, and joint width have been considered.

Bolt Grip length—Munse *et al.* [2.46] and Baron and Larson [2.37] varied the grip length of the bolt from 44 to 95 mm and from 76 to 152 mm, respectively. In both studies it was found that the bolt grip length, *per se*, did not have a significant influence on the fatigue strength of pretensioned shear splices.

Joint length—Yin *et al.* [2.47] investigated the effect of joint length on the fatigue behavior of slip-critical shear splices. They varied the number of bolts in a line from two to eleven. These researchers observed that increasing the number of bolts in a line reduced the fatigue strength considerably, approaching the fatigue strength of a plate with an empty hole as the length of the joint increased. However, their test results are somewhat obscured by the fact that other geometric parameters, such as plate width and thickness, were varied along with the joint length. Other independent studies [2.38, 2.48], where the number of bolts in a line was varied from one to four, indicated that the number of bolts in a line does not affect the fatigue resistance of shear splices.

Joint width—The width of a joint has a direct influence on the net to gross cross-sectional area ratio, A_n / A_g. For a constant width specimen, the A_n / A_g ratio decreases with an increase in the number of bolts per row. Similarly, the A_n / A_g ratio increases with the plate width for a constant number of bolts per row. In the first part of their investigation, Steinhardt and Möhler [2.38] varied the A_n / A_g ratio from 0.83 for one bolt per row to 0.49 for three bolts per row. The results of these tests on slip-critical shear splices are presented in Figure 2.7. Although the test results show considerable scatter, it was concluded that the fatigue life decreased with the A_n / A_g ratio. This trend was, according to Steinhardt and Möhler, further confirmed by the second part of their investigation, where the A_n / A_g ratio was varied from 0.66 to 0.76.

Birkemoe and Srinivasan [2.49] investigated the effect of the joint width by comparing two test series that were identical except for the number of bolts in a row. All bolts were tightened to the snug plus one-half turn condition. The test results for A_n / A_g ratios of 0.69 and 0.85 are presented in Figure 2.8. Contrary to the findings of Steinhardt and Möhler, Birkemoe and Srinivasan concluded that the fatigue life decreased with an increase in A_n / A_g ratio. An earlier study by Birkemoe *et al.* [2.40] also arrived at this same conclusion. It should be noted that most of the cracks in the test specimens from Birkemoe *et al.* started in the net cross-section, whereas the cracks in the test specimens from Steinhardt and Möhler were generally located in the gross cross-section. These two different fracture paths—corresponding to the behavior of bearing-type and slip-critical shear splices—could provide the explanation for their differing conclusions.

The effect of A_n / A_g ratio on bearing-type shear splices will be further investigated in the study presented in the following chapters. Based on the results shown in Figure 2.7, the conclusion reached by Steinhardt and Möhler cannot be corroborated, and the effect of A_n / A_g ratio is most likely negligible for slip-critical shear splices. This is supported by test results from Cullimore [2.45], who examined the influence of two different edge distances on the fatigue behavior of slip-critical shear splices. He concluded that increasing the edge distance from 30 millimeters to 40 millimeters—and thus increasing the A_n / A_g ratio—did not change the performance of the shear splices significantly.

Other Parameters

Although the effects of material yield strength and stress ratio on the fatigue life of bolted connections have been investigated experimentally, their effect has often been considered of lesser importance. The investigations conducted to study the effect of these two parameters are summarized as follows.

Yield strength—Hansen [2.48], Steinhardt and Möhler [2.38], Birkemoe *et al.* [2.40, 2.49], Lieurade [2.41], and Cullimore [2.45] investigated the influence of yield strength of the connected plates on the fatigue behavior of pretensioned shear splices. They all noted an increase in fatigue life with the yield strength of the steel, as illustrated in Figure 2.9 using the test results from Lieurade [2.41]. Figure 2.9 shows that there is a lot of scatter in the data, suggesting that this increase is rather a trend and might be statistically insignificant. It is therefore possible that, if yield strength has an effect on the fatigue life, its effect is small and may be negligible for the design of connections. However, if the significance of the effect of yield strength is accepted, it seems to be reasonable to carry out fatigue tests with steel grades of a low yield strength, since they might, conservatively, yield lower fatigue lives.

Stress ratio—The effect of stress ratio on the fatigue life of pretensioned shear splices was investigated by Mas and Janss [2.50] and by Birkemoe *et al.* [2.40]. Figure 2.10 shows the stress range corresponding to failure at 2 million cycles (using equation (2.4) with a slope of $m = 3$) as a function of the stress ratio, R, according to the above cited references. Figure 2.10 indicates a trend that increasing the stress ratio decreases the fatigue strength. Again, the scatter in the data is large and, without further investigations of this parameter, no definitive conclusions can be drawn. However, similar to the observation made concerning the yield strength of the connected plates, it may be conservative to carry out fatigue tests with reasonably high stress ratios.

2.4.3 Current Design Specifications

Different stress range vs. number of cycles relationships have been proposed for the verification of the fatigue strength of symmetric bolted shear splices. It has to be noted that most of the guidelines are based on a comparison of test results with existing fatigue design curves (established for welded, hot rolled, and flame cut details, cf. Section 2.3.3). This section presents the approaches proposed in the following four publications:

- AASHTO Specification [1.4]

- CAN/CSA S16.1 [2.30]
- ECCS Recommendation [1.5]
- Eurocode 3 [2.51]

AASHTO Specification [1.4] and CAN/CSA S16.1 [2.30]

In the AASHTO Specification and in the Canadian steel design code CAN/CSA S16.1, all symmetric bolted shear splices are assigned to fatigue category B. The calculation of the stresses is to be carried out using the gross cross-section for slip-critical joints and the net cross-section for bearing-type connections.

ECCS Recommendation [1.5]

The ECCS Recommendation classifies all symmetric bolted shear splices as fatigue category 140. As for the AASHTO Specification, the calculation of the stresses is to be done based on the gross cross-section for slip-critical joints and on the net cross-section for bearing-type connections.

Eurocode 3 [2.51]

The following fatigue categories are defined in Eurocode 3 for the calculation of the fatigue strength of bolted shear splices:

- Fatigue category 112 for double covered symmetrical joints with preloaded high-strength bolts. Stresses are to be calculated on the gross cross-section.

- Fatigue category 112 for double covered symmetrical joints with injection bolts. Stresses are to be calculated on the net cross-section.

- Fatigue category 90 for double covered symmetrical joints with fitted bolts. Stresses are to be calculated on the net cross-section.

No guidelines are given specifically for the fatigue strength of symmetrical bearing-type shear splices. This is most likely due to the fact that of the 500 cited tests only a handful were carried out on truly bearing-type connections and that the goal of these tests was not to investigate the fatigue behavior of this type of connection, but to check the effect of increasing the bolt pretension [2.43].

Conclusions Concerning the Current Design Specifications

Figure 2.11 shows the different fatigue design curves for bolted shear splices according to the AASHTO Specification [1.4], the ECCS Recommendation [1.5], and Eurocode 3

[2.51]. It is evident from Figure 2.11 that the three different approaches result in significant discrepancies for the calculation of the fatigue strength of symmetric shear splices, leading to important disagreements in the prediction of the fatigue life of such connections.

2.4.4 Discussion and Conclusions

Over 500 tests from 16 research programs have been used to assess the fatigue behavior of symmetric bolted shear splices. Despite the large number of test data, many uncertainties concerning the fatigue strength of such connections remain, and there are significant differences between different standards. In order to obtain a more precise prediction of the fatigue strength of bolted shear splices the following questions should be further investigated:

- Is the approach with existing fatigue curves, which were established on the basis of tests on welded details, valid for bolted details? Regression analyses of most bolted joint test results give much shallower slopes, m, than 3, approaching 10 in some cases [2.45].

- What effective cross-sectional area should be used to calculate the stress range in bearing-type shear splices? Should it be the net cross-section as defined in most design codes, the gross cross-section as proposed in reference [2.35], or is there a need to find an alternative approach?

- Does the joint geometry (joint length and A_n/A_g ratio) affect the fatigue strength of shear splices?

- What is the effect of mean stress or yield strength of the connected plates on the fatigue strength of shear splices?

- What is the effect of bolt preload and slip coefficient on the fatigue strength of slip-critical shear splices?

Only with a thorough analysis of existing test results and possibly new tests—especially in stress ranges close to the constant amplitude fatigue limit—some of these questions can be answered and the uncertainties reduced.

2.5 Fatigue of Shear Splices with Staggered Holes

2.5.1 Introduction

The fastener pattern found in older structures, especially in built-up riveted members, is often staggered. However, most fatigue tests on riveted members have been carried out using members loaded in bending and the influence of hole stagger has generally not been investigated. Research on riveted shear splices subjected to fatigue loading is very limited. Although all of the tests had staggered holes, the effective net section for the specimens tested by Reemsnyder [2.52] was not affected by the bolt stagger. Therefore, the test results from Reemsnyder are not included in the following review. In the work of DiBattista and Kulak [2.53, 2.54] and Josi *et al.* [2.55] riveted tension members under fatigue loading were investigated. In these two research projects, the net effective area, calculated using Cochrane's method, consisted of a mixture of inclined and transverse segments. For this case, the net effective section is not well defined. The fatigue behavior of slip-critical shear splices with staggered holes was investigated by the Japanese National Railways [2.56], and their findings are also presented in this section.

2.5.2 DiBattista and Kulak [2.53]

Fatigue tests of full-scale gusset plate end connections from four riveted tension members were carried out. The test specimens consisted of diagonal members taken from a Canadian National Railway bridge built in 1911 and dismantled in 1991. Field measurement of strains in the bridge before dismantling and historical records of train traffic indicated that stresses on the critical details in the diagonal members likely never exceeded the fatigue Category D constant amplitude fatigue limit given in the AASHTO Specification [1.4].

Each diagonal member consisted of two end connections (bottom and top chord attachments) that were tested under constant amplitude fatigue loading. The critical cross-section of the bottom chord attachment was on a line orthogonal to the member and rivet stagger did not affect the effective net section stresses. In the case of the top chord connections, the rivets in the critical section were not on the same plane, as shown in Figure 2.12. Three different options were considered for the calculation of the effective net section:

1. Use of a straight line that passes only through the gusset-to-angle holes (upper bound for the effective net section designated as A_{n1} in Figure 2.12b).

2. The net section obtained by deducting both the gusset-to-angle holes and the web-to-angle holes from the gross section (lower bound for the effective net section designated as A_{n2} in Figure 2.12c).

3. Use of a staggered section that passes through both the gusset-to-angle and the web-to-angle holes. The area (A_{n3} in Figure 2.12d) was calculated using the $s^2/4g$ rule proposed by Cochrane [2.20].

Figure 2.13 shows a typical fracture path at the top connection of tension member tested by DiBattista and Kulak. Fracture started at the gusset-to-angle rivet hole and propagated on a plane perpendicular to the axis of the member. However, it was recognized that the close proximity of the holes in the flange to gusset plate connection may increase the stress calculated on the failure plane. Because of this uncertainty the test results were presented in terms of net section stress according to option 1 (deduction of one bolt hole from the gross section area) and option 2 (deduction of two bolt holes). These results are reproduced in Figure 2.14. It was noted that the actual stress range must lie between these two options. It is apparent that the effective net section used to calculate the stress range in the riveted connection affects the selection of a fatigue design curve. DiBattista and Kulak recommended further research to determine the effect of staggered rivet patterns on the fatigue strength of a riveted detail, so as to determine an appropriate definition of the critical net cross-sectional area.

2.5.3 Josi, Kunz, and Liechti [2.55]

End connections from four riveted tension diagonals were tested under fatigue loading. The diagonal members from a bridge built in 1935 were obtained when they had to be replaced in 1995. Fatigue tests were conducted on the diagonal members in order to determine their remaining fatigue life. At the time of their replacement, it was estimated that the members had reached the end of their predicted fatigue life [2.57]. Testing of the diagonal members was conducted in uniaxial constant amplitude cyclic tension. Six tests were conducted on four diagonals; namely, two tests on the full length of two diagonals, and four tests on the end connections of the remaining two diagonals.

The diagonals consisted of two angles back-to-back, connected to a gusset plate by rivets. The rivet holes in the legs of the angles were staggered, as shown in Figure 2.15. In the original end details, angle segments were added at the connections in order to minimize eccentricity at the connections. Since the rivets had to be removed when the diagonals were removed from the bridge, the tests had to be carried out with the rivets replaced by bolts. The bolt pretension was kept low (about 100 MPa) in four of the six test specimens. In order to assess the effect of fastener preload, one test each was carried out with a preload of 300 MPa and 700 MPa (full preload), respectively. In the remaining fatigue life calculations [2.57], the effective net section area of one angle from the double angle member was taken as the gross cross-section minus one hole, i.e., the net section was calculated on a section at right angle to the axis of the member. Although Josi *et al.* recognized that the hole in the other leg might influence the stresses at the critical hole, the net section defined above was used to calculate the stress range in the test specimens.

Fatigue crack growth leading to fracture was observed in all the test specimens except the one with fully preloaded bolts. In a manner similar to that observed in the DiBattista and

Kulak tests, the fracture surface of each specimen was perpendicular to the axis of the member and never went through two fastener holes. Since the amount of fatigue damage in the members before testing was not exactly known, only conclusions concerning the remaining fatigue life were drawn and the test results can not be compared to other tests or to existing fatigue curves.

2.5.4 Abe, Ichijo, and Takagi [2.56]

Fifty-five fatigue tests were conducted on slip-critical shear splices with staggered holes. The pitch and the gage distances were varied in order to investigate their influence on the fatigue resistance. The bolt stagger was chosen so that under static loads some of the specimens would fail along a straight line whereas others would have a failure path through the staggered holes. The following observations were presented by these researchers:

- The fracture path is always at right angles to the axis of the member and is not affected by hole stagger.

- The effective stress range for slip-critical joints, with or without staggered holes, should be calculated based on the gross cross-section.

- The same detail category is applicable for both staggered and non-staggered hole configurations.

2.6 Conclusions

The static behavior of mechanically fastened shear splices has been investigated in a large number of research projects. Two types of shear splices can be distinguished—slip-critical and bearing-type shear splices. The main parameters that influence the behavior of the connected plates before the slip resistance of the joint is exceeded are the joint geometry, the slip coefficient, and the fastener clamping force. In bearing-type connections the slip resistance is normally exceeded under service loads. Therefore, it is assumed that the bolts transfer the load in shear and in bearing for the entire life span of the structure. At this stage, the geometry of the connection and the load distribution among the fasteners become the critical parameters.

In spite of an important number of test results, the fatigue behavior of mechanically fastened symmetric shear splices is not well understood, and this has resulted in large discrepancies between different design codes. Additional analysis of existing test results and possibly the addition of new test data to the existing database of test results is required to clarify some of the uncertainties and to formulate better guidelines for the fatigue life prediction of shear splices.

Test results indicate clearly that the fatigue strength of slip-critical shear splices with staggered bolts can be based on stresses in the gross cross-section, no matter what the stagger pattern of the fasteners.

The definition of the effective cross-section in bearing-type shear splices with staggered holes under fatigue loading is not clear. Various sources agree on the need to base the calculations on some kind of net cross-section, however. As an upper bound for the net section, resulting in the smallest stresses, a net cross-section perpendicular to the axis of the member can be used. Alternatively, as a lower bound on the net section, resulting in the highest stresses, the gross cross-section minus all the holes that are in a possible static failure path can be used. The effective net cross-section has to be somewhere between these two bounds. If the lower bound approach for the net section is used for the evaluation of existing structures, the predicted remaining fatigue life may be too conservative, leading to a premature replacement of the structure. There is, therefore, a need for further investigation of the effect of hole stagger on the fatigue resistance of bearing-type shear splices.

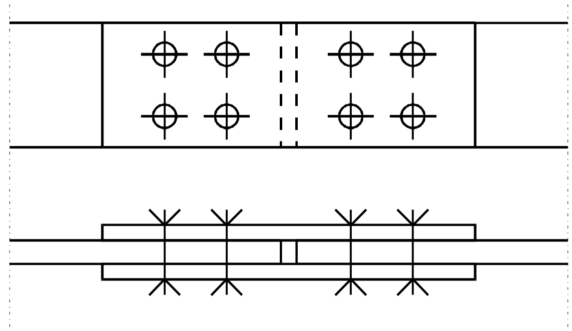

a) Symmetric butt splice

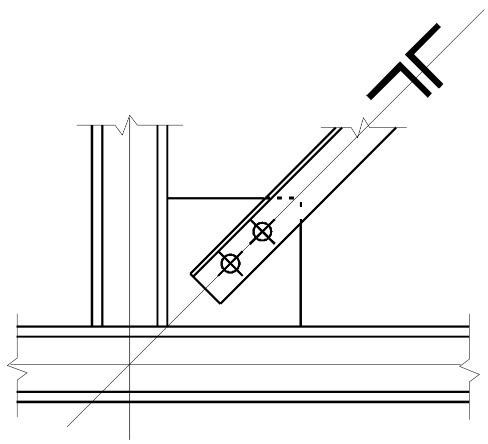

b) Bracing member connection

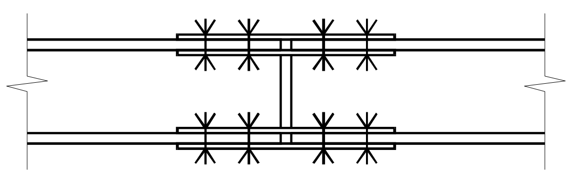

c) Girder flange splice

Figure 2.1 – Typical symmetric shear splices.

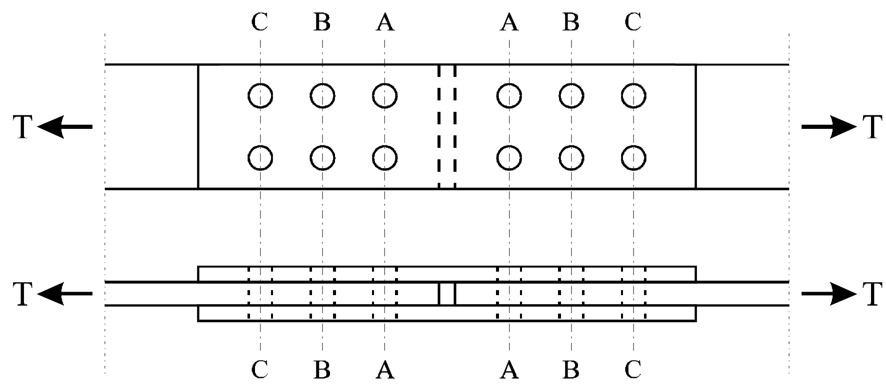

Figure 2.2 – Shear splice subjected to a tensile force T.

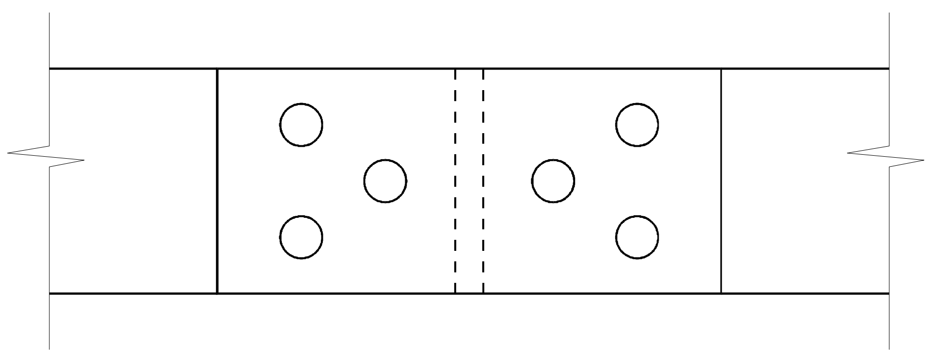

Figure 2.3 – Shear splice with staggered holes.

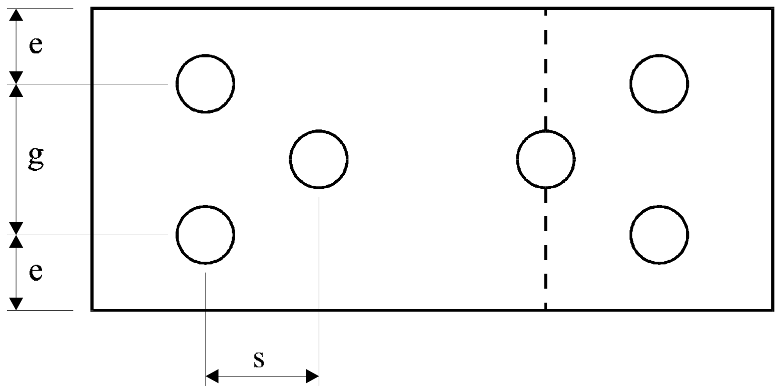

a) through first bolt hole

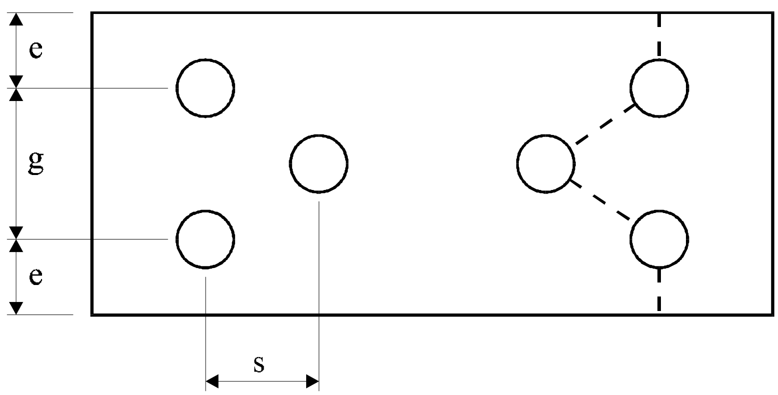

b) zigzag

Figure 2.4 – Possible failure paths for a plate with staggered holes.

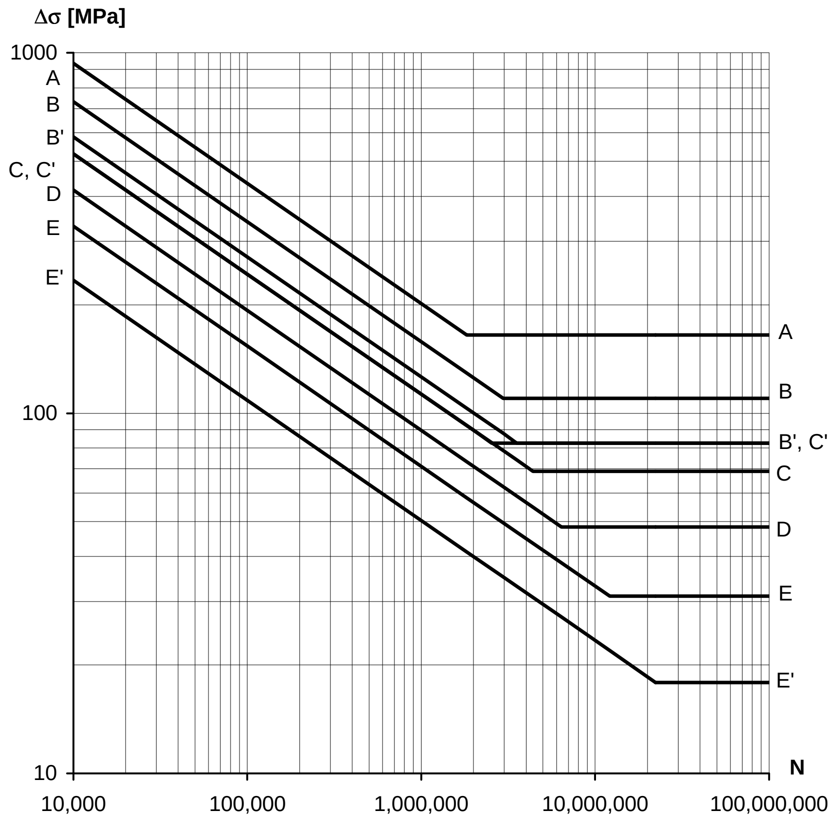

Figure 2.5 – $\Delta s - N$ curves according to AASHTO.

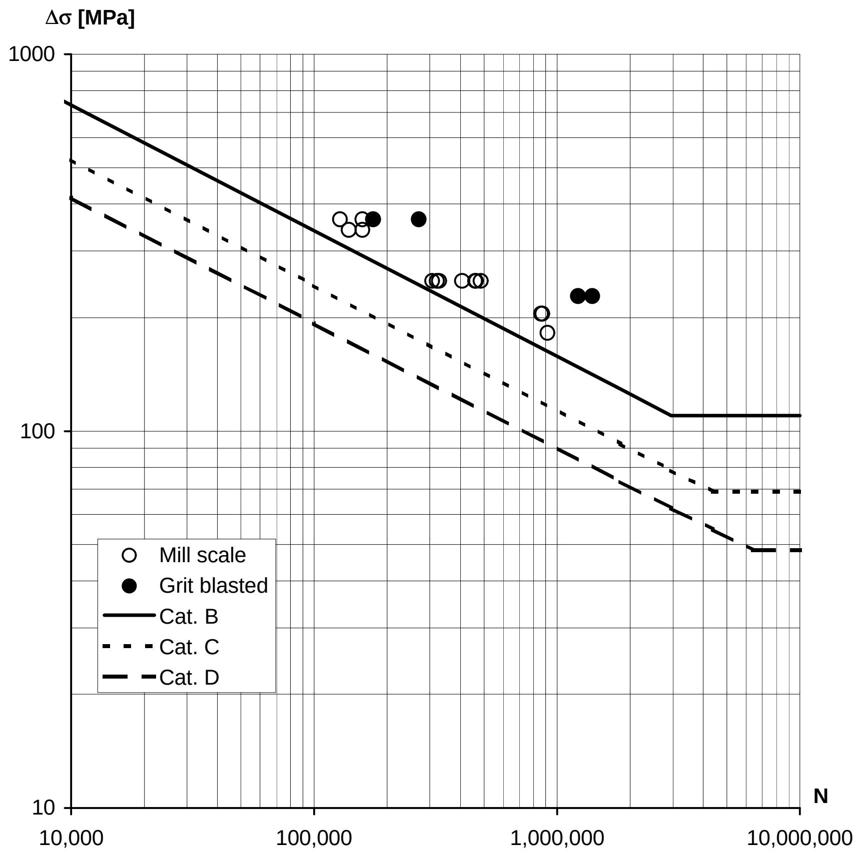

Figure 2.6 – Effect of surface treatment on the fatigue life of bolted shear splices using data from Birkemoe et al. [2.40].

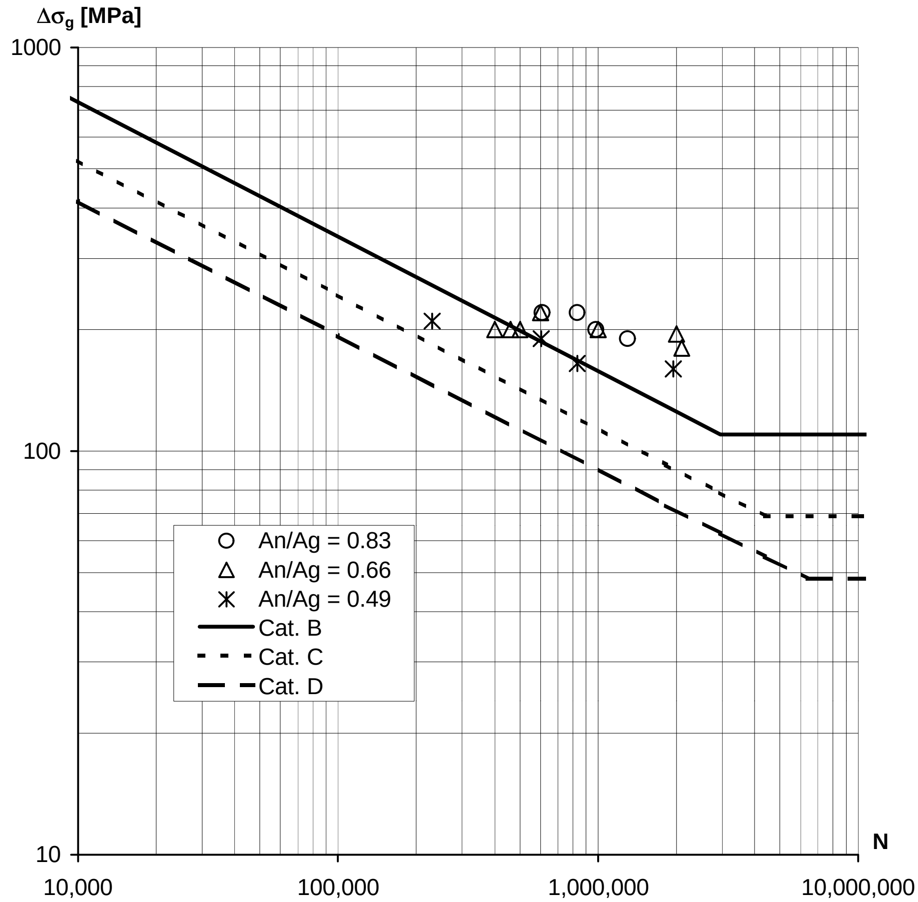

Figure 2.7 – Effect of A_n / A_g ratio on the fatigue life of bolted shear splices using data from Steinhardt and Möhler [2.38].

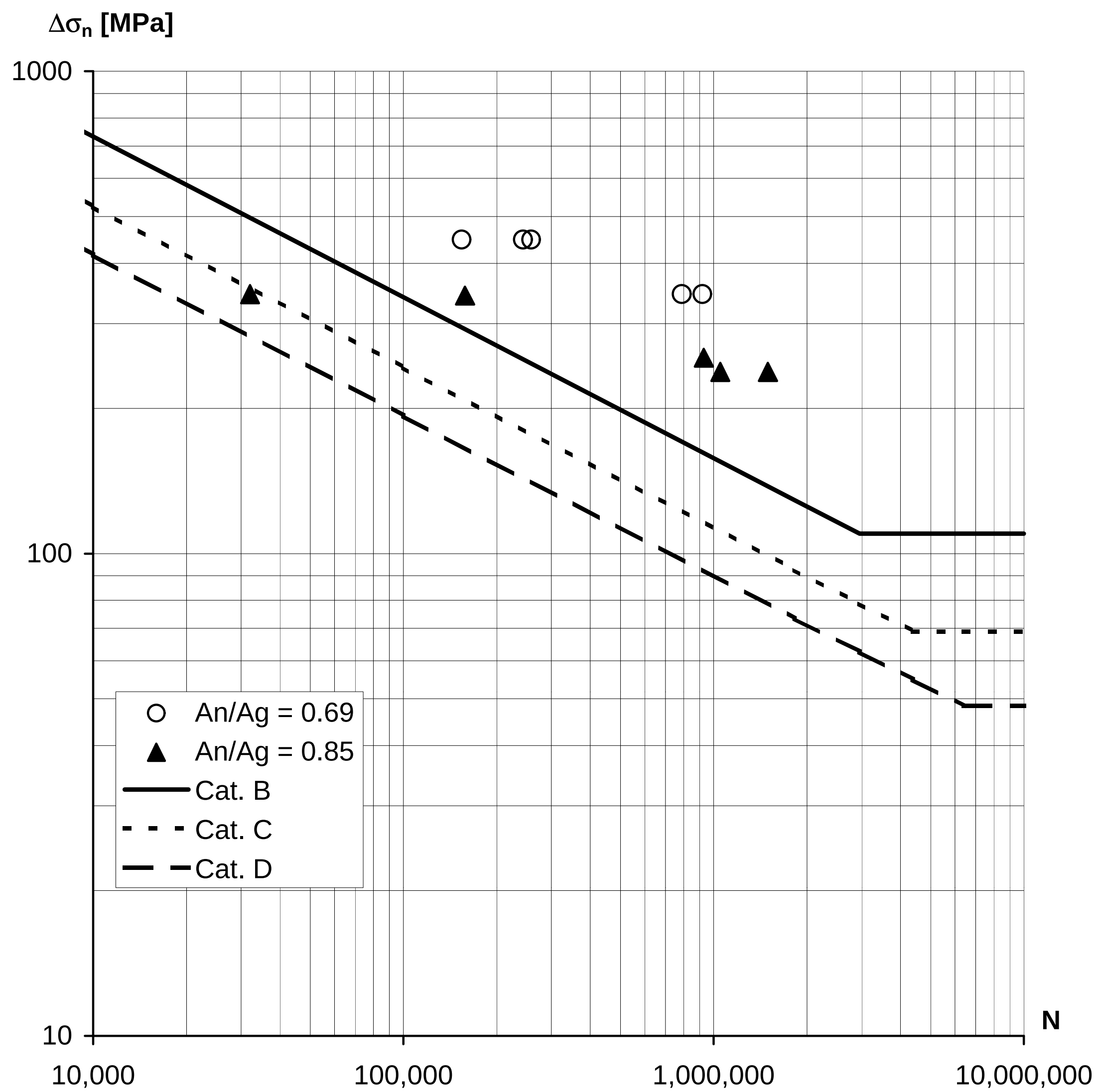

Figure 2.8 – Effect of A_n / A_g ratio on the fatigue life of bolted shear splices using data from Birkemoe and Srinivasan [2.49].

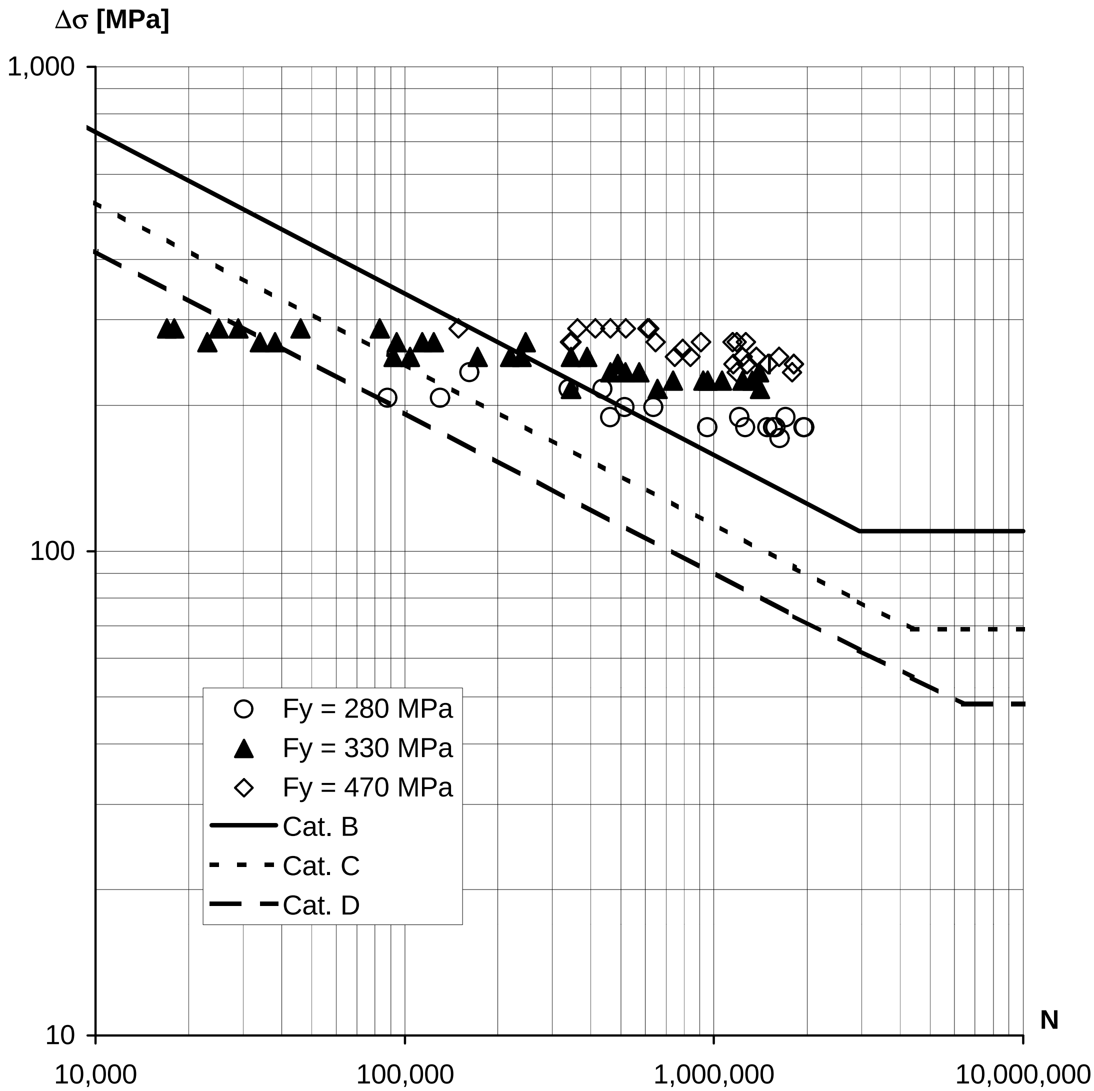

Figure 2.9 – Effect of yield strength of the base plates on the fatigue life of bolted shear splices using data from Lieurade [2.41].

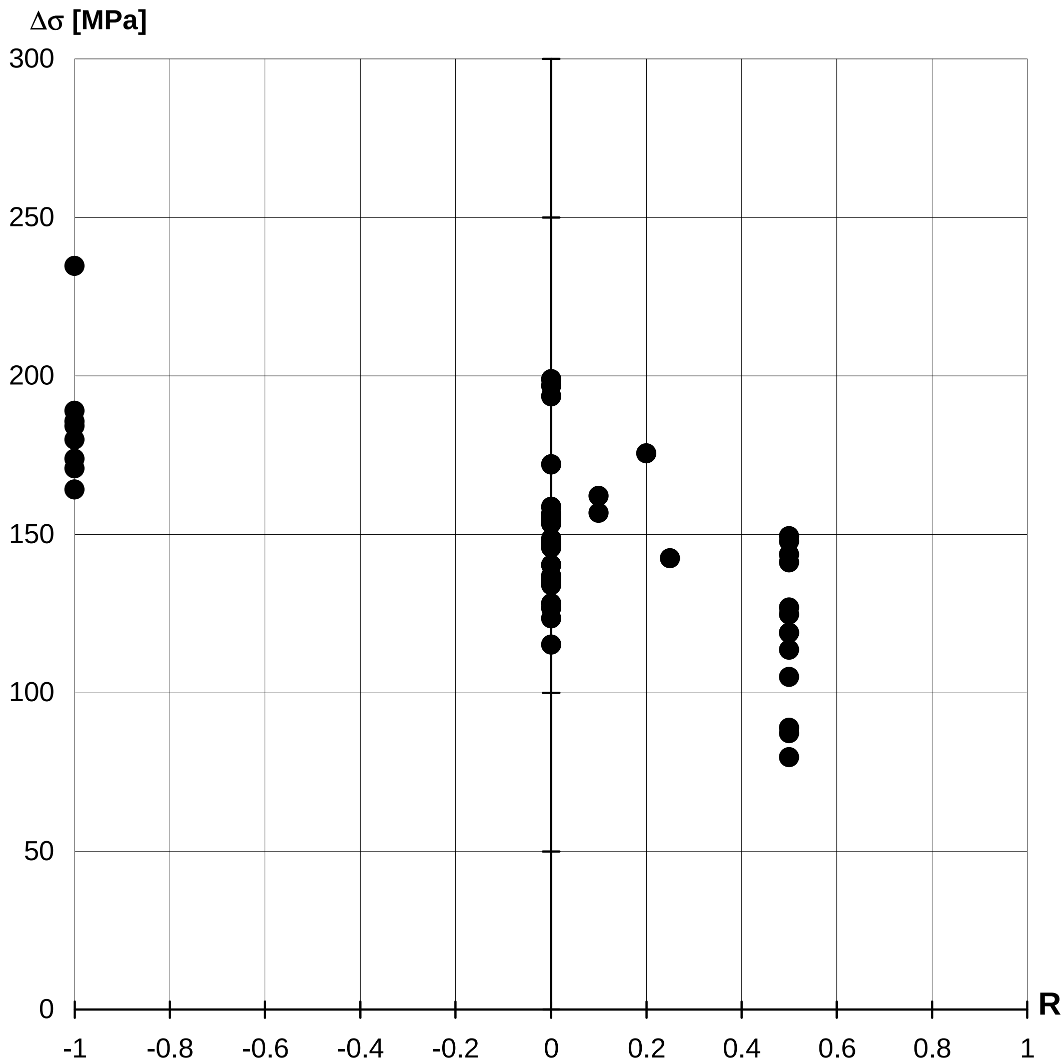

Figure 2.10 – Effect of the stress ratio, R, on the fatigue life of bolted shear splices using data from Birkemoe et al. [2.40] and from Mas and Janss [2.50].

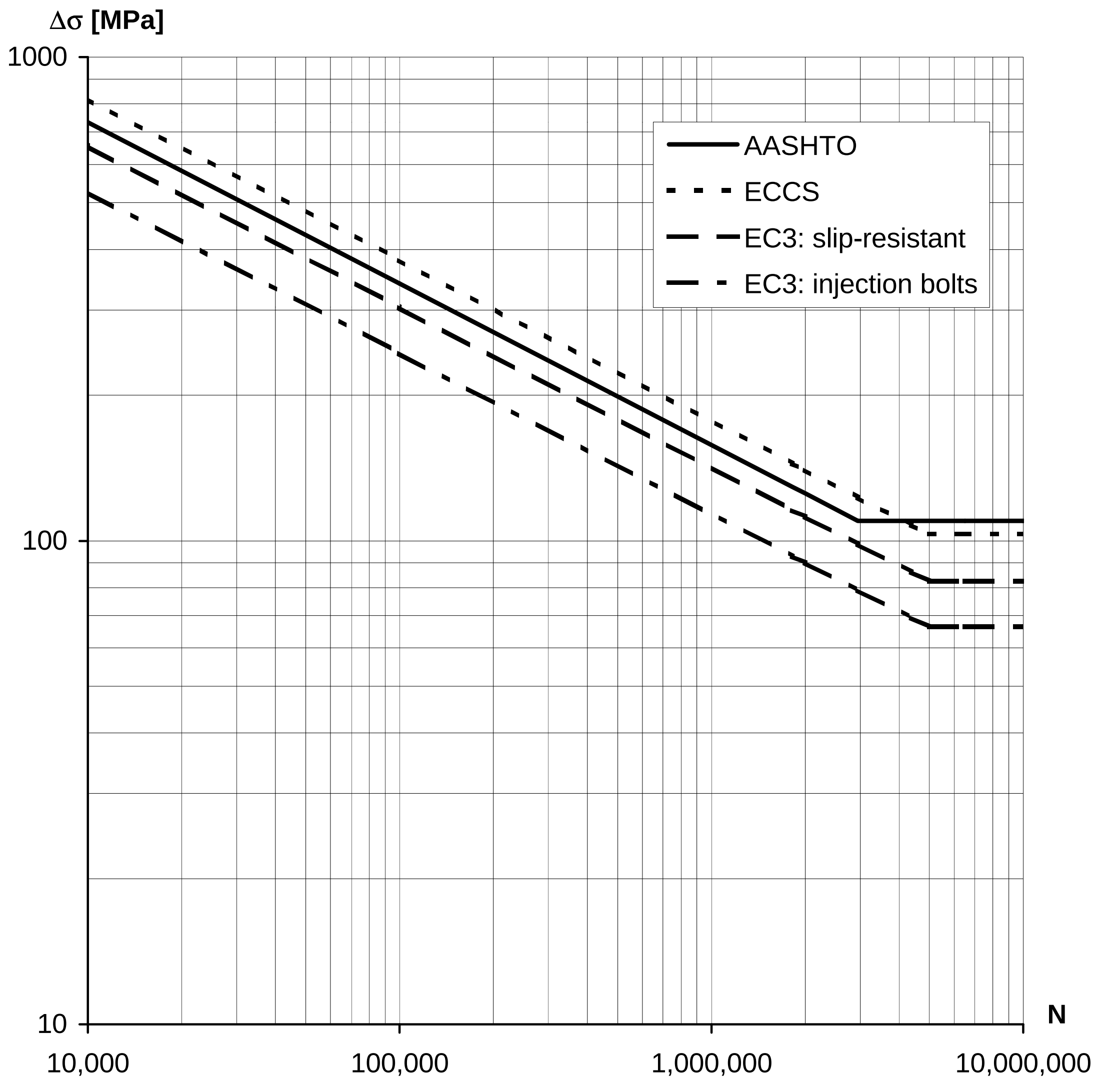

Figure 2.11 – Comparison of the fatigue strength of symmetric bolted shear splices according to different design specifications.

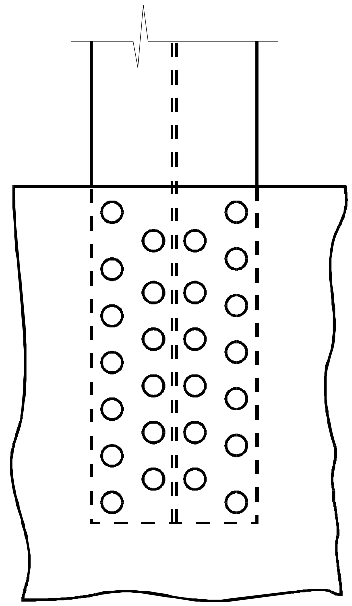

a) Gusset-to-angle connection

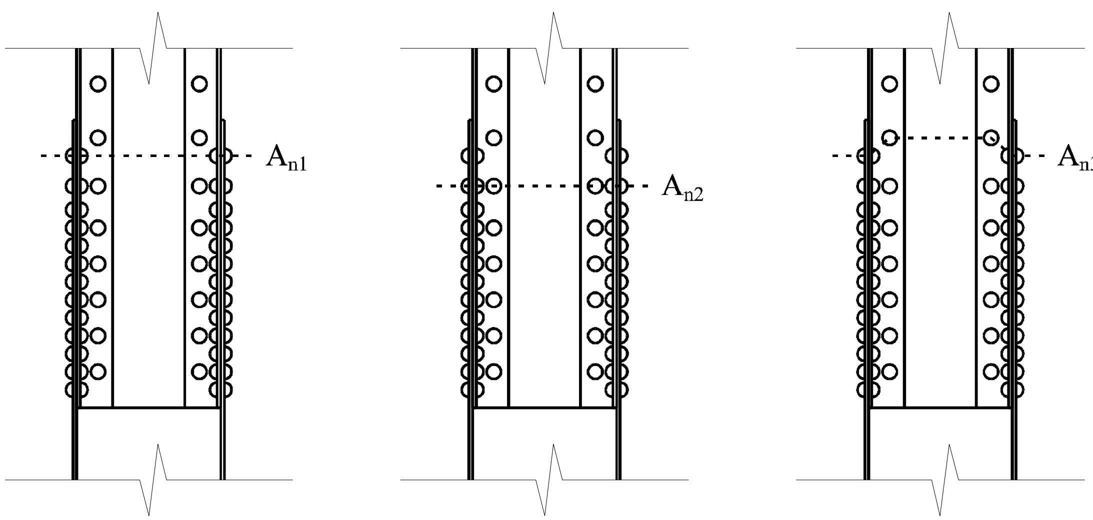

b) Option 1 c) Option 2 d) Option 3

Figure 2.12 – Rivet pattern and options for the net section calculation of the top chord connections tested by DiBattista and Kulak [2.53].

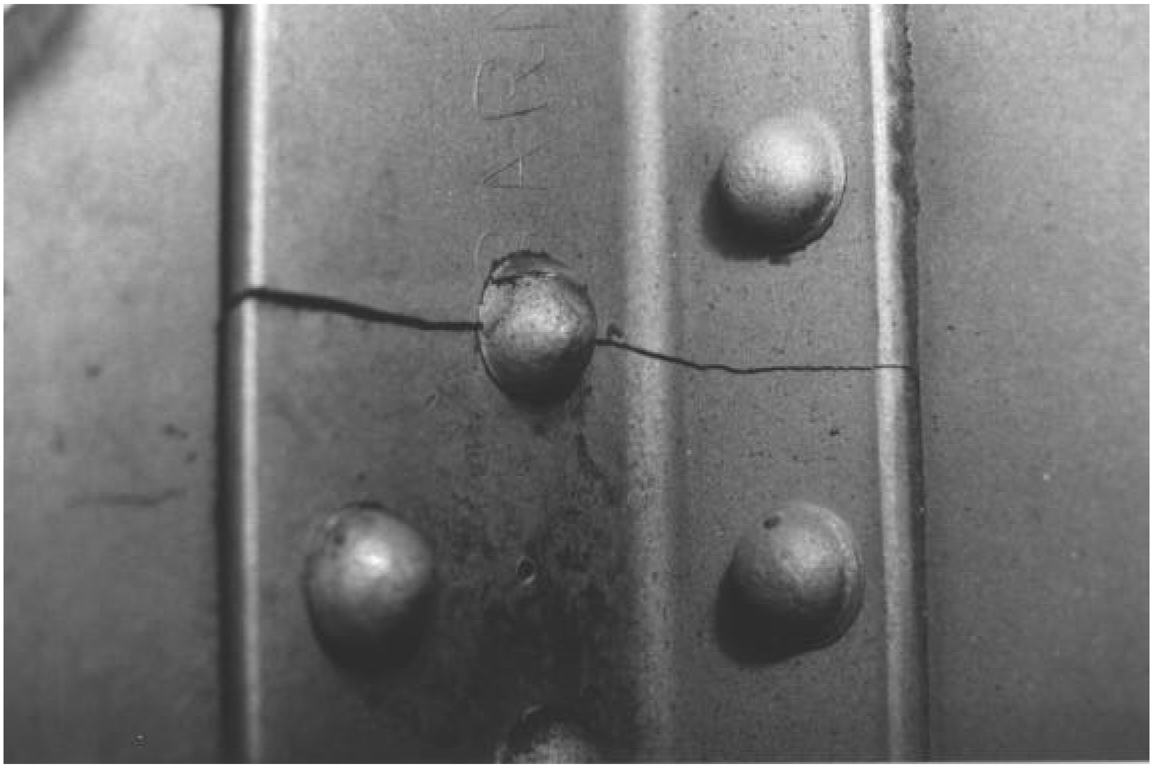

Figure 2.13 – Typical fracture path in top chord connections tested by DiBattista and Kulak [2.53] (Courtesy of University of Alberta).

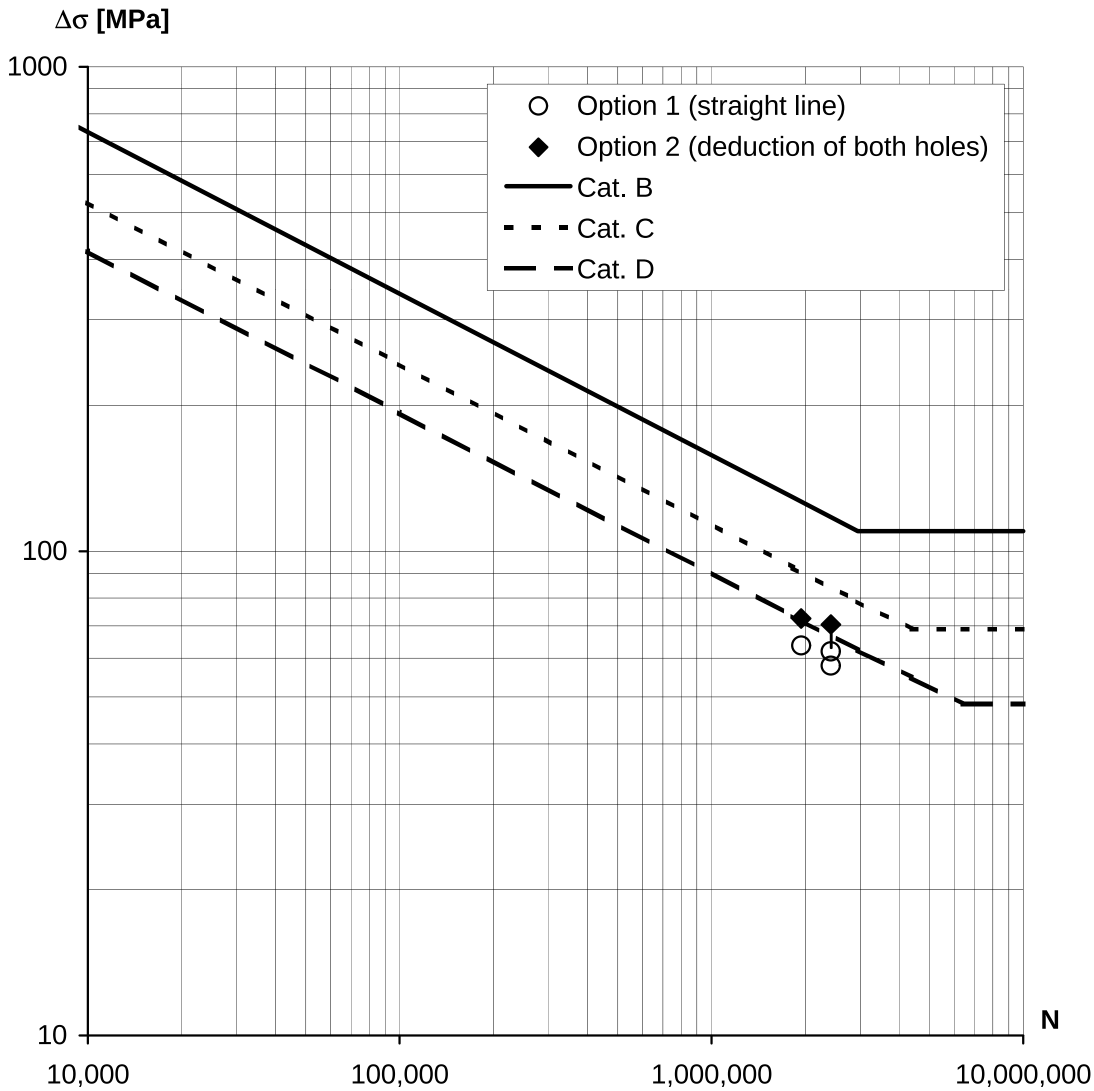

Figure 2.14 – Fatigue test results of top chord connections tested by DiBattista and Kulak [2.53].

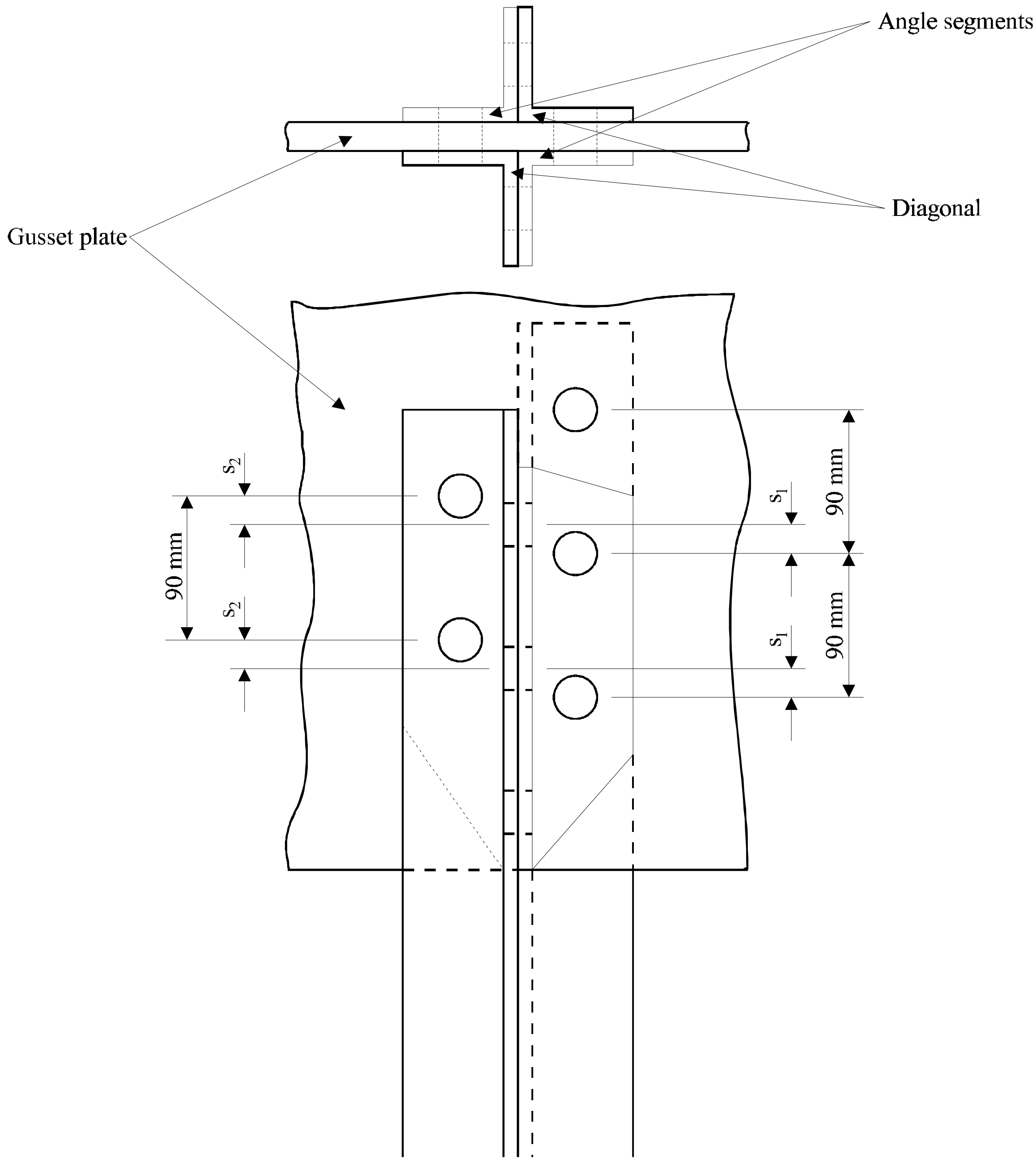

Figure 2.15 – End connection geometry of the diagonals tested by Josi et al. [2.55].

3. ANALYTICAL INVESTIGATIONS

3.1 Introduction

The literature review indicates that no guidelines for the design and evaluation of mechanically fastened shear splices with staggered holes exist. Therefore, the butt splice shown in Figure 3.1 was investigated in order to assess the effect of various parameters (bolt stagger, gage distance, and edge distance) on the fatigue behavior of this kind of connection. Although other shapes are used in structural engineering, the butt splice with flat plates investigated here covers a large number of applications. Using the finite element method, a preliminary numerical investigation was performed to assist in the design of an experimental program. This chapter describes the finite element model used to carry out this investigation and presents the numerical results.

3.2 Finite Element Model

3.2.1 *General*

The load transfer mechanism from the main plate into the splice plates of a bearing-type shear splice depends on several factors. These might include the relative alignment of the bolt holes, the frictional resistance developed on the faying surfaces, and the size of the main and splice plates. A finite element model taking all these factors into account could be quite complex, and simplifications are therefore desirable. In order to simplify the analytical model, it was assumed that the splice plates share the load equally and that negligible friction develops on the faying surfaces. It was therefore necessary to model only one splice plate.

3.2.2 Elements

The finite element program ABAQUS, Version 5.7 [3.1], was used to model one splice plate from the butt splice shown in Figure 3.1. Since only a small deformation analysis was used and because the splice plates are not subjected to bending or out-of-plane instability, membrane elements, with three translational degrees of freedom per node, were used for the model. The nine node quadrilateral element M3D9 from the ABAQUS finite element library was found to be suitable for accurate modeling of the curved shape of the bolt holes. The element has nine integration points and a constant thickness was used for the splice plate models. The node ordering and the numbering of the integration points for the M3D9 element are shown in Figure 3.2.

3.2.3 Mesh

The choice of the finite element mesh significantly affects the accuracy of the numerical results. The error in the strain energy—and thus in strains, stresses, reaction forces, etc.—decreases with decreasing element size [3.2]. However, as the element size decreases, the computational effort increases. It is therefore desirable to use the coarsest mesh that will lead to an accurate solution. Three different meshes—a coarse, an intermediate, and a fine mesh—were studied. In order to further simplify the model for the purpose of the mesh refinement study, a doubly symmetric splice plate with eight bolt holes, subjected to a uniform stress, s, was used (Figure 3.3a). Because of the symmetry of the model, only the lower left quarter of the plate had to be modeled (Figure 3.3b). In order to model the planes of symmetry, the nodes along the top edge were fully restrained in the y-direction and free in the x-direction (Figure 3.3b), while the nodes along the right hand boundary were fully restrained in x-direction and free to move in the y-direction. All the nodes in the models were restrained in the direction perpendicular to the plane of the plate (z-direction). Figure 3.4 illustrates the three different mesh refinements: the coarse mesh consists of 151 elements and 683 nodes, the intermediate mesh has 493 elements and 2127 nodes, and the fine mesh has 1972 elements and 8199 nodes.

A uniformly distributed tension load was applied to the left boundary of the model. A comparison of the relative difference in stresses along section A-A shown in Figure 3.4 is presented in Figure 3.5. The relative difference in stress, RD_{kf}, was calculated using:

$$RD_{kf} = \frac{s_k - s_f}{s_k} \cdot 100 \qquad (3.1)$$

where,

RD_{kf}	:	relative difference in stresses
s_k	:	stress obtained with the intermediate or coarse mesh model
s_f	:	stress obtained with the fine mesh model

Figure 3.5 shows that the difference between the stresses predicted using the fine and intermediate meshes is negligible (within 0.3%). On the other hand, the coarse mesh underestimates the peak stresses around the hole by as much as 8.0%. It is therefore believed that the intermediate mesh has converged to the exact solution. The convergence of the intermediate mesh was also confirmed for the load model and boundary conditions described in the next section.

3.2.4 Loads and Boundary Conditions

In order to simplify the analytical model, the following assumptions were made:

- The load transfer between the bolts and the plates are simulated with nodal loads applied at the edge of the holes.
- The entire load is transferred by bearing of the bolts on the bolt holes. Any load transfer by friction is neglected.
- The load is distributed equally to each bolt hole.
- The bolts and main plates are infinitely stiff, thereby preventing the bolt holes of the splice plate from deforming laterally (perpendicular to the applied load).

As illustrated in Figure 3.6, three different load models were considered: a) a single nodal load at each bolt hole, b) fifteen equal nodal loads at each hole, and c) fifteen projected nodal loads at each hole. Projected nodal loads are directly proportional to the area tributary to a node projected onto a plane perpendicular to the line of action of the load. The following equation was used to calculate the projected load at a node:

$$p_i = \frac{y_{i+1} - y_{i-1}}{2 \cdot (y_{15} - y_1)} \cdot V \tag{3.2}$$

where,

p_i	:	projected load at node *i*
y_{i+1}	:	y coordinate of node *i*+1
y_{i-1}	:	y coordinate of node *i*-1
y_1	:	y coordinate of first loaded node (node 1)
y_{15}	:	y coordinate of last loaded node (node 15)
V	:	total load applied at one bolt hole (i.e., the load in the bolt).

The three different load models were applied to a 9.5 mm plate discretized using the intermediate mesh. The boundary conditions were the same as defined in section 3.2.3. An elastic analysis with a load of 250 N per bolt hole and $E = 200\,000$ MPa was performed for all three load models.

The results of the analysis showed that the maximum normal stress, s_x, was equal to 3.72 MPa for all three different load models. This analysis was repeated using the fine mesh presented earlier to check solution convergence. The maximum normal stress, s_x, was again found to be 3.72 MPa. It was therefore concluded that any one of the three load models could be used in conjunction with the intermediate mesh.

Since the splice plates with staggered holes do not possess any axes of symmetry, the entire plates had to be modeled. The tension in the splice plates with staggered holes was introduced by loading the plate as shown in Figure 3.7 for a plate with a single nodal load at each hole. Figure 3.7 also shows the boundary conditions imposed on the plate. The center node is a point of symmetry and thus its translation was restrained in all three orthogonal directions (x, y, and z). In order to prevent the plate from rotating as a rigid body, additional restraints were necessary. These additional restraints were provided by preventing transverse (y) and out-of-plane (z) displacements at the points of loading.

3.2.5 Analysis

When loading a plate with a hole, high stress concentration fields around the hole can produce a localized plastic zone [3.3]. However, because of the difficulty in quantifying the effect of the plastic zone, most fatigue and fracture mechanics approaches only consider elastic stress fields. In fact, it can be expected that compressive residual stresses are introduced after the first load cycle because of plastic deformation of the material around the hole and that further cycling will result in elastic response of the stresses. To verify this, an inelastic cyclic analysis of the plate investigated in Section 3.2.4 was carried out. The analysis was performed using the measured stress versus strain relationship of the plate material (see Chapter 4), a maximum load, $P_{\max}$, of 280 kN, and a load range, ΔP, of 200 kN. These loads are similar to the loads applied in the physical tests (see Chapter 4).

The inelastic analysis of a splice plate through several loading cycles indicated that the normal stresses, s_x, around a bolt hole remain elastic after the first load cycle. Figure 3.8 shows the maximum value of the normal stress, s_x, as a function of the applied load. The maximum normal stress, s_x, reaches yield (460 MPa) at a load of about 200 kN and remains constant up to the full load of 280 kN. Upon unloading from the peak load of 280 kN, s_x decreases linearly and remains elastic during the subsequent load cycles. Figure 3.8 also indicates that residual compressive stresses of 170 MPa are created in the plate at the bolt hole as a result of the differential plastic deformations imposed in the first loading cycle. Since the stress range around a hole is elastic after the first load cycle, the following study only considers linear elastic analytical models.

3.3 Investigation of Test Specimens

3.3.1 Plate Geometry

A series of cover plates with varying hole patterns were analyzed. Three different hole staggers were investigated, namely, a minimum stagger of 25.4 mm (S1 Series) with the minimum hole spacing of three bolt diameters as recommended in CAN/CSA S16.1 [2.30]; a maximum stagger of 76.2 mm (S3 Series), for which, according to the Cochrane rule [2.20], the non-staggered net section becomes governing; and an intermediate stagger of 50.8 mm (S2 Series). A plate with non-staggered holes (S0 Series) was also analyzed as a basis of comparison. All plates were 95.25 mm wide and 9.5 mm thick, resulting in a gross section, A_g, of 905 mm^2. The hole diameter, D, was 21 mm in all cases. The geometry of the four plates is shown in Figure 3.9. A load of 250 N was applied at each hole, resulting in a total tensile force on the splice plate of 1 kN and a gross cross-section stress, s_g, of 1.102 MPa. On the basis of the observations made in the previous section, M3D9 elements with 15 equal loads per hole (Figure 3.6b) were used throughout. The same boundary conditions defined in Section 3.2.4 were employed. All plates were modeled using the intermediate mesh size shown in Figure 3.10 for the plate with a hole stagger of 25.4 mm. Only linear elastic analyses were carried out.

3.3.2 Results

Figure 3.11 shows the stress contours for the normal stress, s_x, in the plate with a hole stagger of 25.4 mm. Analysis of the plates with the other three hole patterns resulted in similar stress contours. The stress distribution within the edge distance at the critical holes (cf. Figure 3.9) is presented for the four hole patterns in Figure 3.12. The figure indicates that:

1. The three different hole staggers result in approximately identical stress concentrations. In fact, the stress concentrations calculated for the S2 and S3 Series are exactly the same and that for the S1 Series is only 1.6% smaller.
2. The stress concentration observed for the three cases of bolt stagger is about 6% higher than that for a plate with non-staggered holes.

Figure 3.13 shows a plot of the normal stress, s_x, within the central portion of the plate, i.e., from the edge of the critical bolt holes to the center of the plate, for the same hole patterns considered in Figure 3.12. It can be observed that the amount of stagger significantly influences the stress concentration in the central section of the plate. Because of the close proximity of the bolt holes in the S1 Series, the stress concentration is higher for the 25.4 mm stagger than for the other two cases. However, the stress concentration in the central portion of the plate for all three staggers is at least 5% smaller than within the edge distance.

3.3.3 Discussion of Analysis Results

The stress concentration within the edge distance was found to be higher than within the central portion of the plate for all bolt staggers investigated. It is concluded therefore that the presence of nearby holes as the bolt stagger decreases has a negligible influence on the governing stresses for fatigue design. However, a comparison between the staggered and non-staggered cases indicates higher stresses within the edge distance in a plate with staggered holes.

The difference in stress concentration between the staggered and non-staggered cases can be explained with the help of the plate with a center hole shown in Figure 3.14a. The plate of width w with a hole of diameter D is subjected to a uniform stress, s, at the gross cross-section. The stress concentration factor, SCF, obtained from photo-elastic studies [3.4], is plotted in Figure 3.14b as a function of the ratio of the hole diameter to the plate width, D/w. The stress concentration factor (SCF) presented in Figure 3.14b is based on the net section stress, σ_n, and is defined as:

$$SCF = \frac{\sigma_{peak}}{\sigma_n} \tag{3.3}$$

where,

σ_{peak} : peak stress in the plate (at hole)

σ_n : nominal net section stress in the plate $= \sigma \frac{A_g}{A_n}$

It can be seen that the SCF decreases as the ratio of the hole diameter to plate width increases. Since the ratio of the net section to the gross section area (A_n/A_g) is equal to $1-D/w$ for a plate with non-staggered holes, it follows that the SCF increases with an increase of A_n/A_g. According to the Cochrane rule [2.20], the net cross-sectional area of plates with staggered holes is larger than the net section of plates with non-staggered holes, resulting in a higher A_n/A_g ratio. From the observations on a plate with a single hole, it can be hypothesized that the stress concentration factor for plates with staggered holes is larger because of their larger A_n/A_g ratio. If this hypothesis is correct, the stress concentration factor should increase if the gage width or the edge distance of the splice plates with staggered holes is increased without making any other changes to their geometry. This is investigated in the following sections.

3.4 Effect of Gage Width

Two series of plates with gage widths of 52.5 mm and 60.4 mm were analyzed and compared to the plates investigated in the previous section, where the gage used was 44.5 mm. Both series included three different staggers, namely, 25.4 mm, 50.8 mm, and 76.2 mm. The 60.4 mm gage width corresponds to the minimum gage width allowed by CAN/CSA S16.1 [2.30] for non-staggered 20 mm bolts. Therefore, it would be unlikely for a designer to stagger the holes when the gage width is larger than 60.4 mm. The magnitude of the applied load was selected to create the same net section stress in specimens with varying gage distances. The net cross-sectional area of every plate with staggered holes was obtained by deducting one hole from its gross cross-sectional area. The maximum stress within the edge distance near the critical holes divided by the nominal net section stress is presented in Table 3.1. In all the cases investigated, the peak stress within the edge distance was greater than the peak stress within the middle portion of the plate. The data presented in Table 3.1 substantiate the observation made earlier, i.e., an increase in gage width results in an increase in stress concentration at the critical hole. The stresses in the plates with a 60.4 mm gage width exceed the stresses in the plate with a 44.5 mm gage width by up to 6%. Analysis of a plate with 60.4 mm gage width but non-staggered holes showed that the maximum stresses in this case are about 3% smaller than for a plate with a hole stagger of 25.4 mm. This is an important reduction of the stress difference compared to the 6% observed with a gage width of 44.5 mm.

3.5 Effect of Edge Distance

The effect of edge distance was investigated using plates with edge distances of 24.5 mm, 38.1 mm and 50.8 mm. For each case three bolt staggers were investigated, namely, 25.4 mm, 50.8 mm, and 76.2 mm. The 25.4 mm edge distance corresponds to the minimum edge distance allowed by CAN/CSA S16.1 [2.30] for 20 mm bolts. Once again, the magnitude of the applied load was selected to create the same net section stress in specimens with varying edge distance. The maximum stress divided by the net section stress on the inside and outside edges of the critical holes is presented in Table 3.2. These data indicate that:

- As expected, the stress concentration factor at the critical holes increases with the edge distance.
- The increase in stress concentration on the inside edge of the hole (towards the center of the plate) is more significant than the stress concentration on the outside edge. There is up to a 25% increase in stress concentration on the inside compared to 12% for the outside.
- The maximum stress on the inside edge of the hole increases with a decrease in bolt stagger. This makes the stress concentration on the inside edge of the hole more critical than that on the outside edge in the case of the 25.4 mm stagger. For the two other bolt hole staggers the stress concentration on the outside edge remains critical.

3.6 Conclusions

Linear elastic analyses were carried out on splice plates using the finite element analysis software ABAQUS. The effect of bolt stagger, gage distance, and edge distance were investigated. Bolt hole stagger was found to introduce higher stresses around the critical bolt hole, although the magnitude of the stagger did not seem to significantly affect the stress concentration. It was demonstrated that this increase in stress concentration is most likely due to an increase in the A_n/A_g ratio. The results also showed that both an increase in gage width and an increase in edge distance—and therefore an increase in

A_n/A_g ratio—result in higher stress concentrations around the critical holes. The stresses are more sensitive to an increase in edge distance than to an increase in gage distance. Since higher stress concentrations imply lower fatigue lives, the following conclusions, which will be verified with a testing program discussed in the next chapter, can be drawn from the analytical investigation:

- Bearing-type shear splices with staggered holes can be expected to have a reduced fatigue resistance as compared to shear splices with non-staggered holes. However, an increase in gage width of the specimens should lead to more moderate reduction of fatigue life.
- The amount of stagger should not significantly influence the fatigue life of bearing-type shear splices.
- An increase in A_n/A_g ratio should reduce the fatigue life of bearing-type shear splices.

Table 3.1 – Stress concentration factor for different gage dimensions and hole staggers.

Gage Width [mm]	Stagger [mm]		
	25.4	**50.8**	**76.2**
44.5	3.21	3.26	3.26
52.5	3.26	3.35	3.35
60.4	3.32	3.42	3.45

Table 3.2 – Stress concentration factor for different edge distances and hole staggers.

Edge Distance [mm]	Stagger [mm]					
	25.4		**50.8**		**76.2**	
	inside	**outside**	**inside**	**outside**	**inside**	**outside**
25.4	3.04	3.21	2.95	3.26	2.91	3.26
38.1	3.33	3.26	3.19	3.31	3.13	3.30
50.8	3.78	3.57	3.48	3.53	3.40	3.53

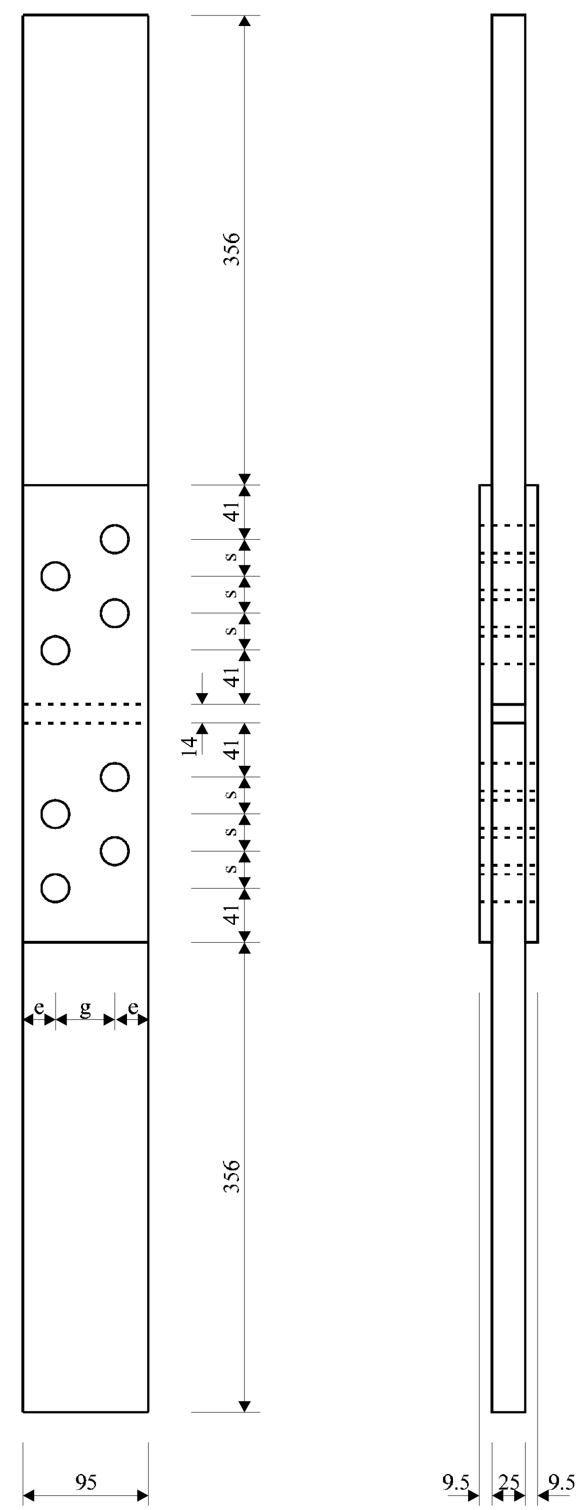

Figure 3.1 – Butt splice investigated in this project.

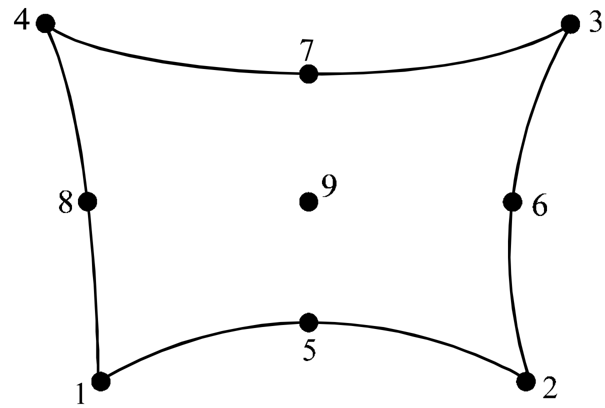

a) Node ordering

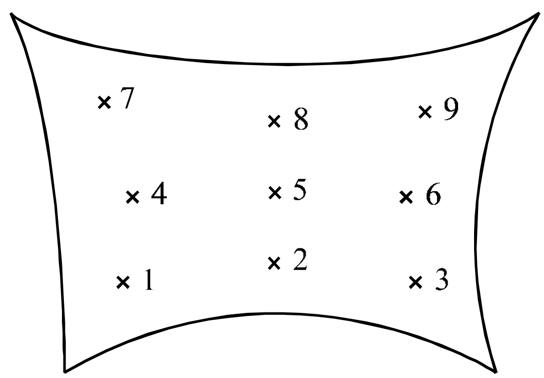

b) Numbering of integration points

Figure 3.2 – Typical M3D9 element.

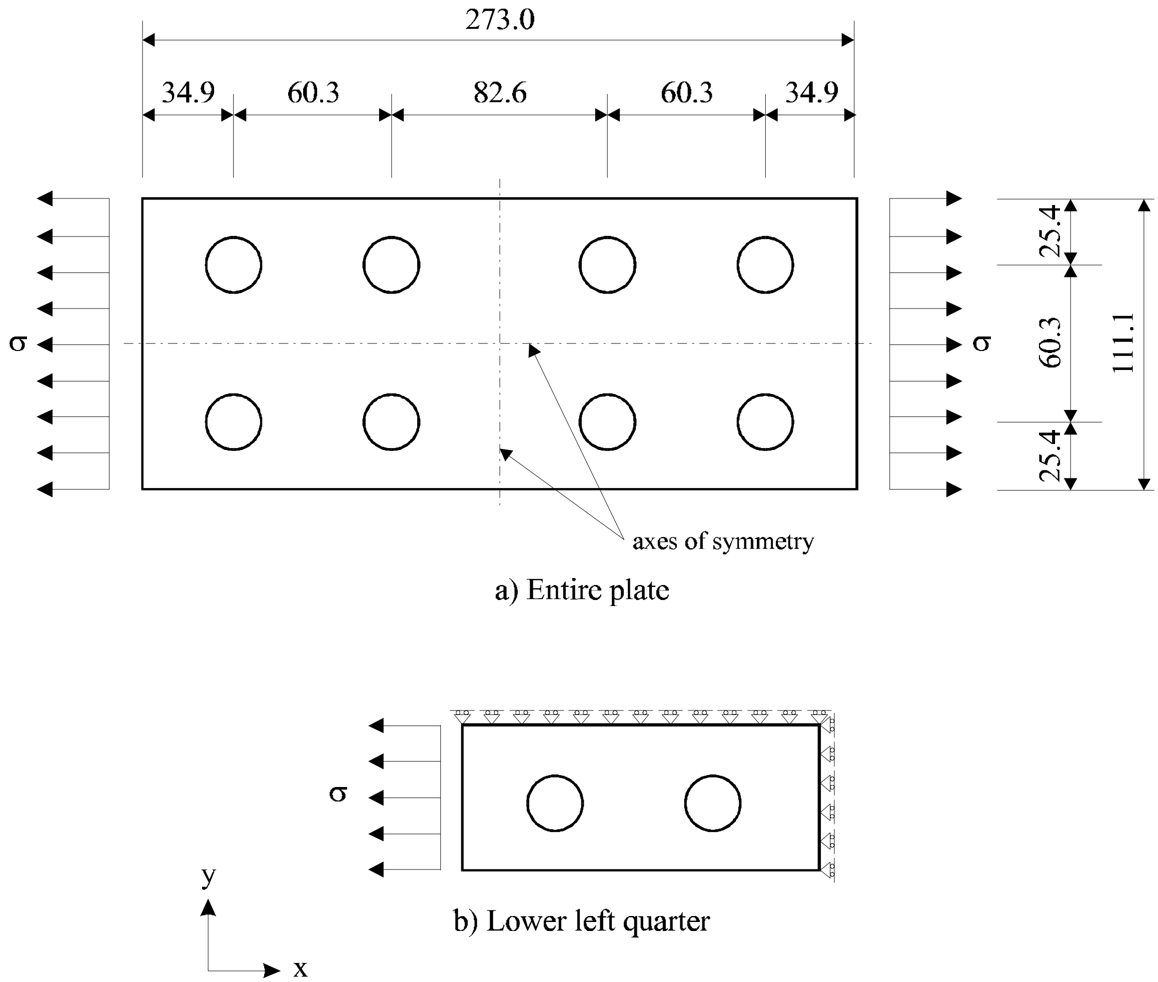

Figure 3.3 – Doubly symmetric shear splice subjected to a uniform gross section stress σ.

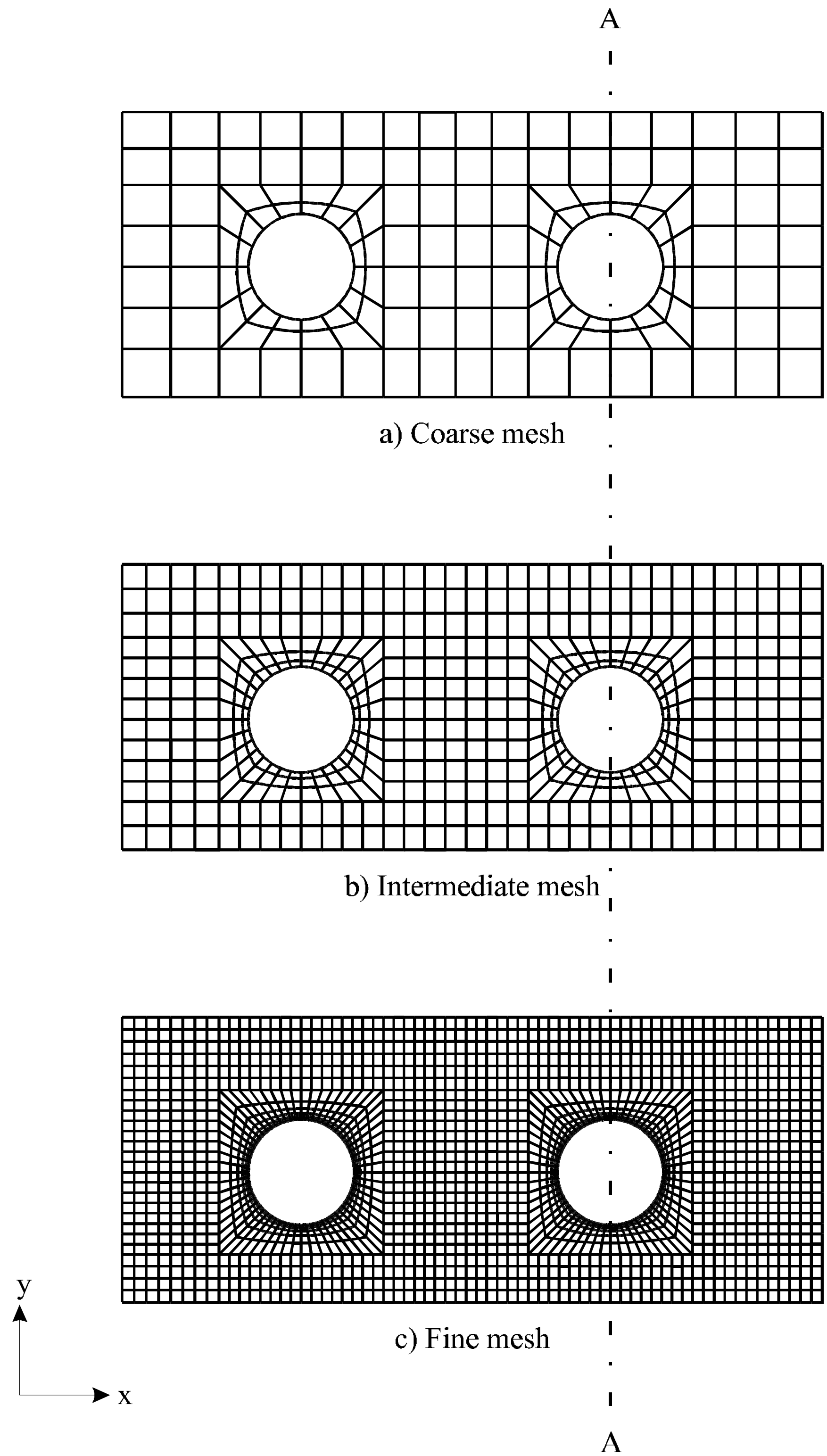

Figure 3.4 – Meshes for one quarter of the doubly symmetrical shear splice.

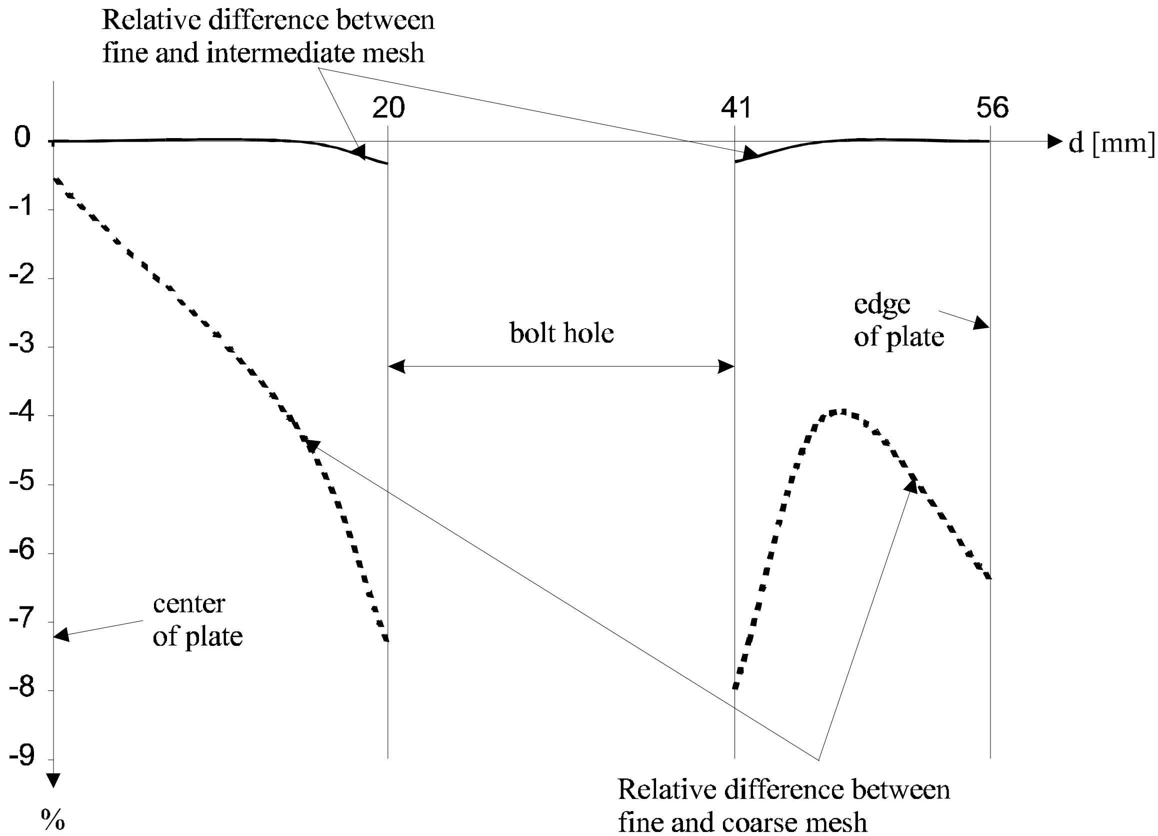

Figure 3.5 – Relative difference in stresses along a section through a bolt hole (with d = distance between center and outside edge of plate).

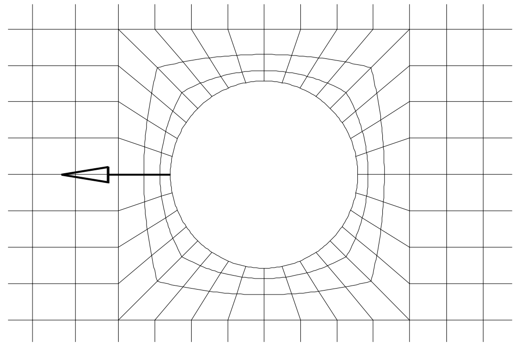

a) Single nodal load

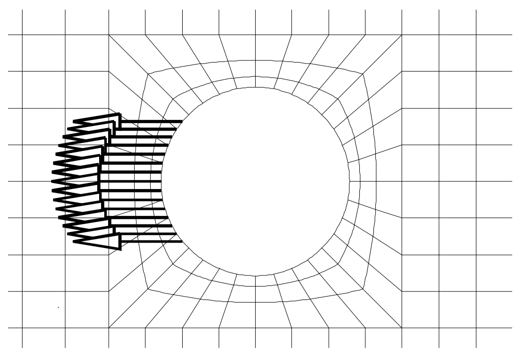

b) 15 equal nodal loads

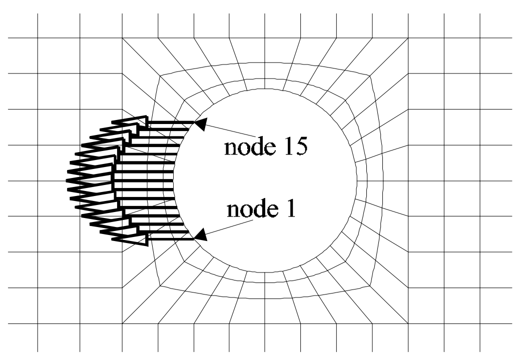

c) 15 projected nodal loads

Figure 3.6 – Possible load models.

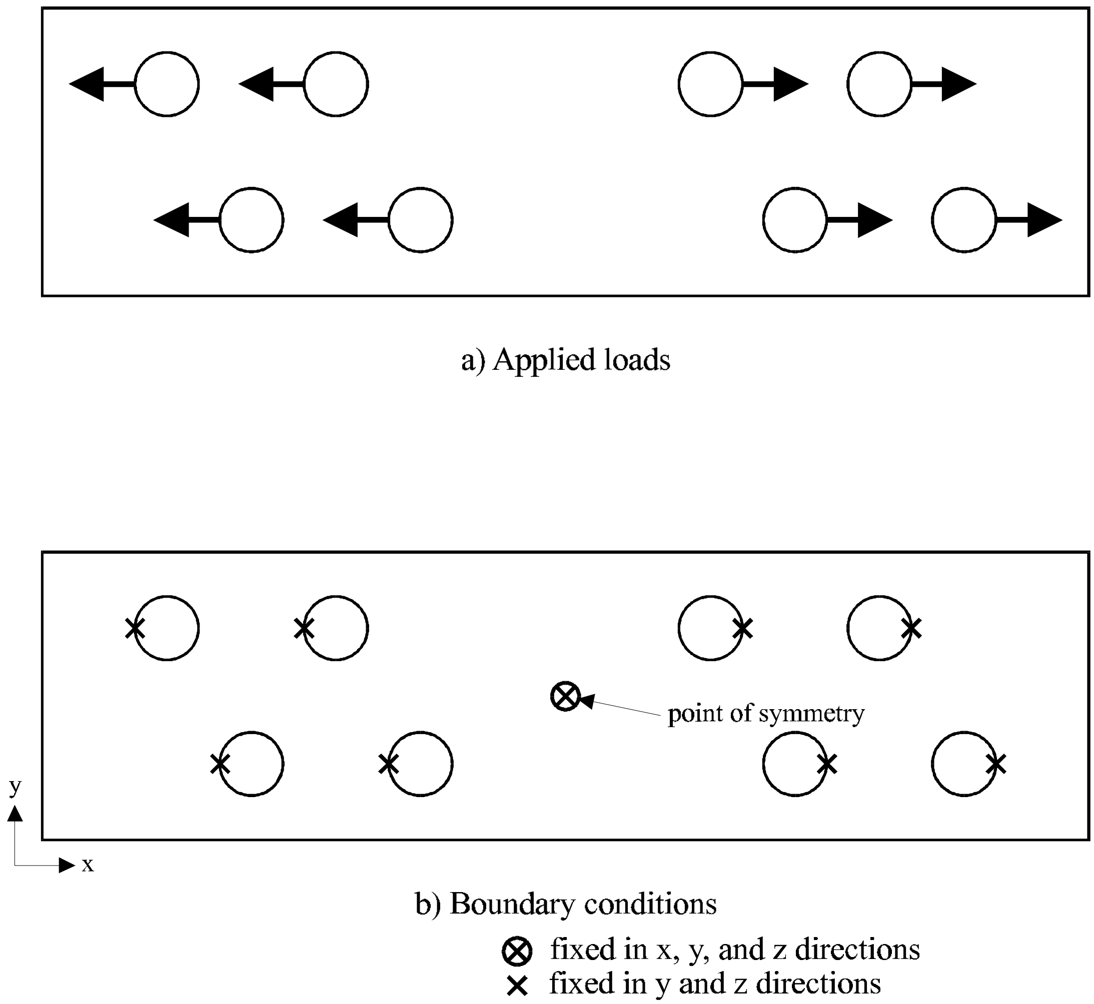

Figure 3.7 – Applied loads and boundary conditions for plate with staggered holes.

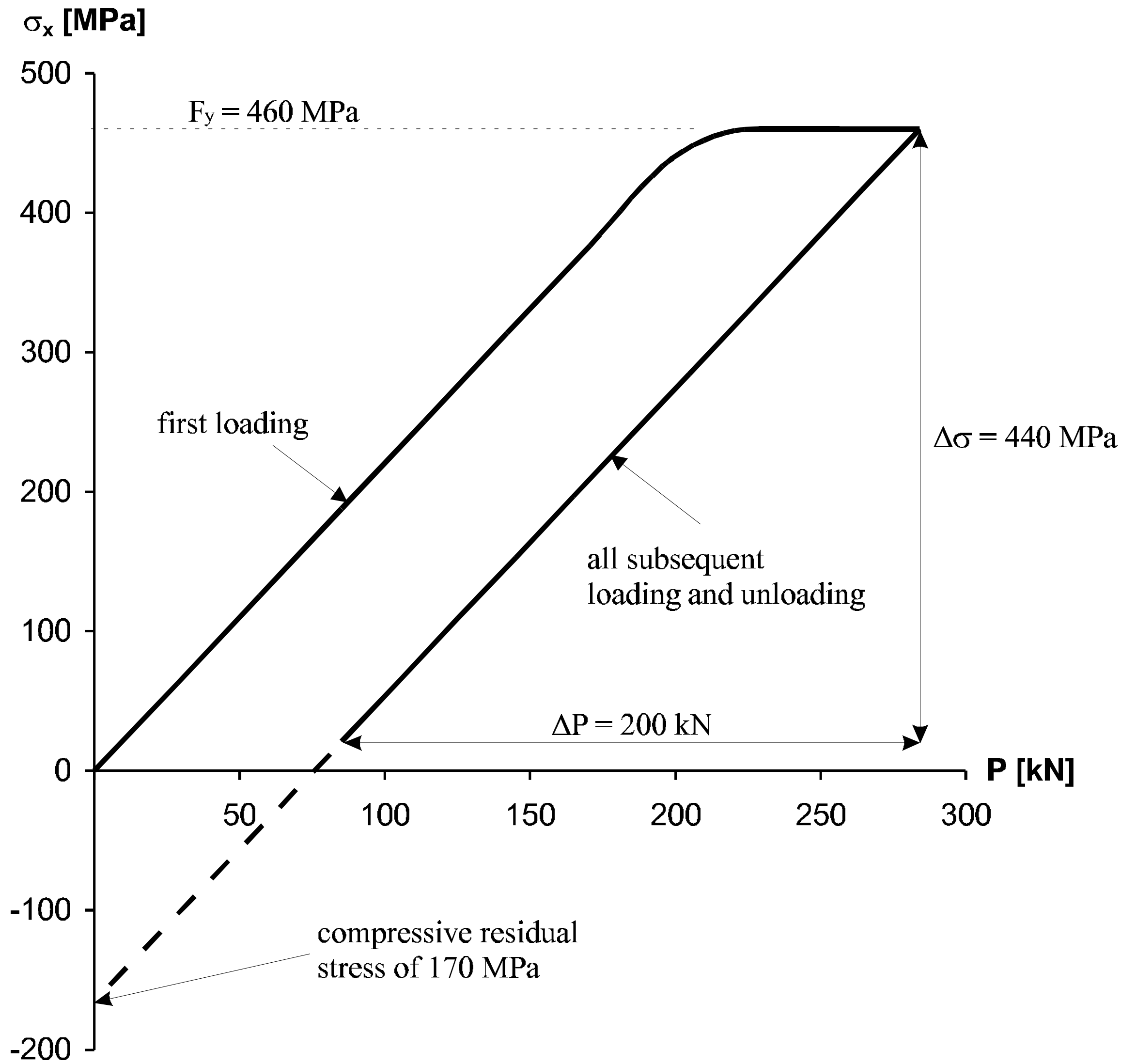

Figure 3.8 – Normal stress, s_x, at the highest stressed point around a bolt hole as a function of the applied load, P, for inelastic cyclic analysis.

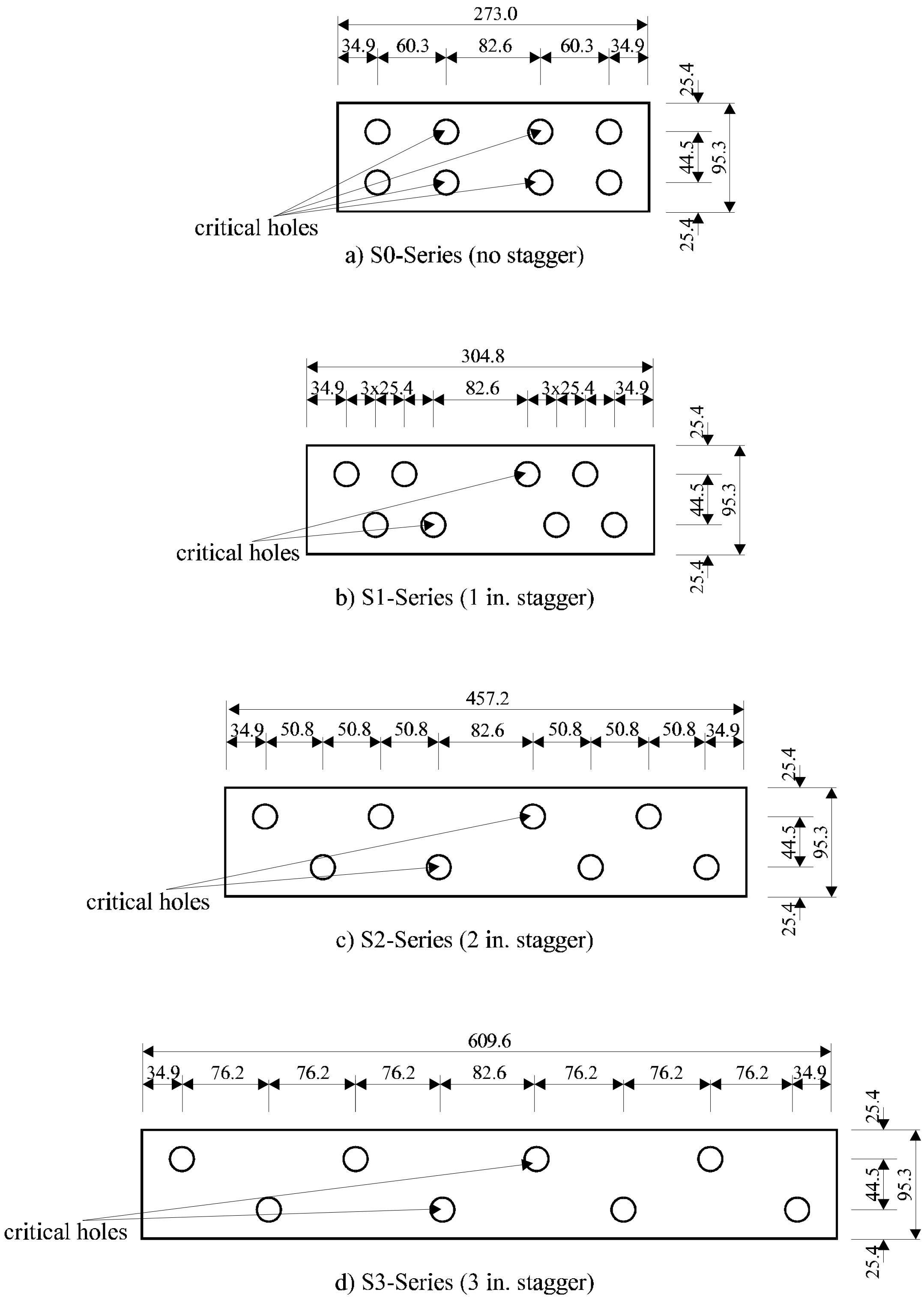

Figure 3.9 – Geometry of the four splice plates of the basic series (in mm).

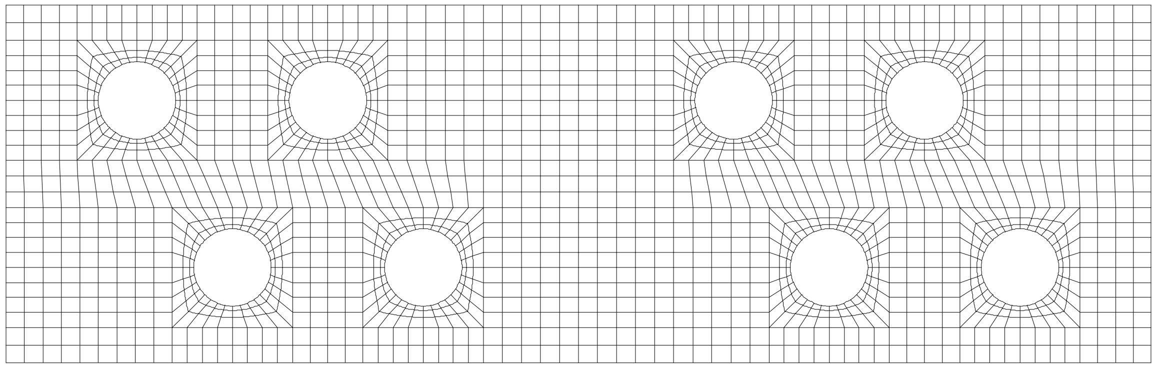

Figure 3.10 – Mesh used for the splice plates.

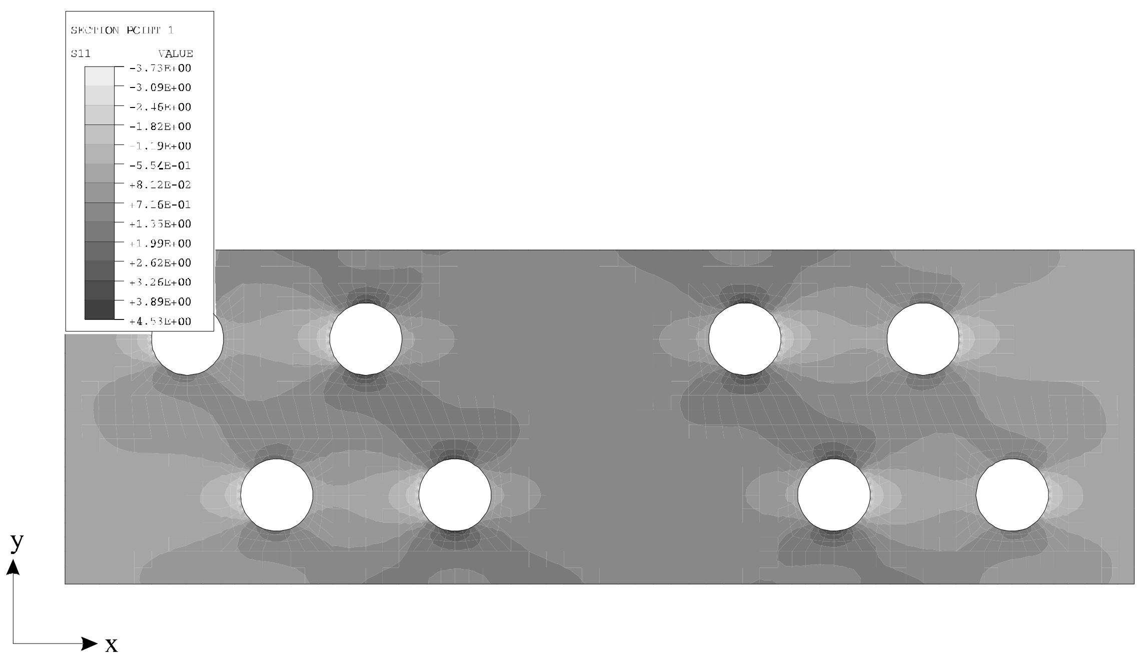

Figure 3.11 – Stress contour for normal stress, σ_x, in plate with hole stagger of 25.4 mm.

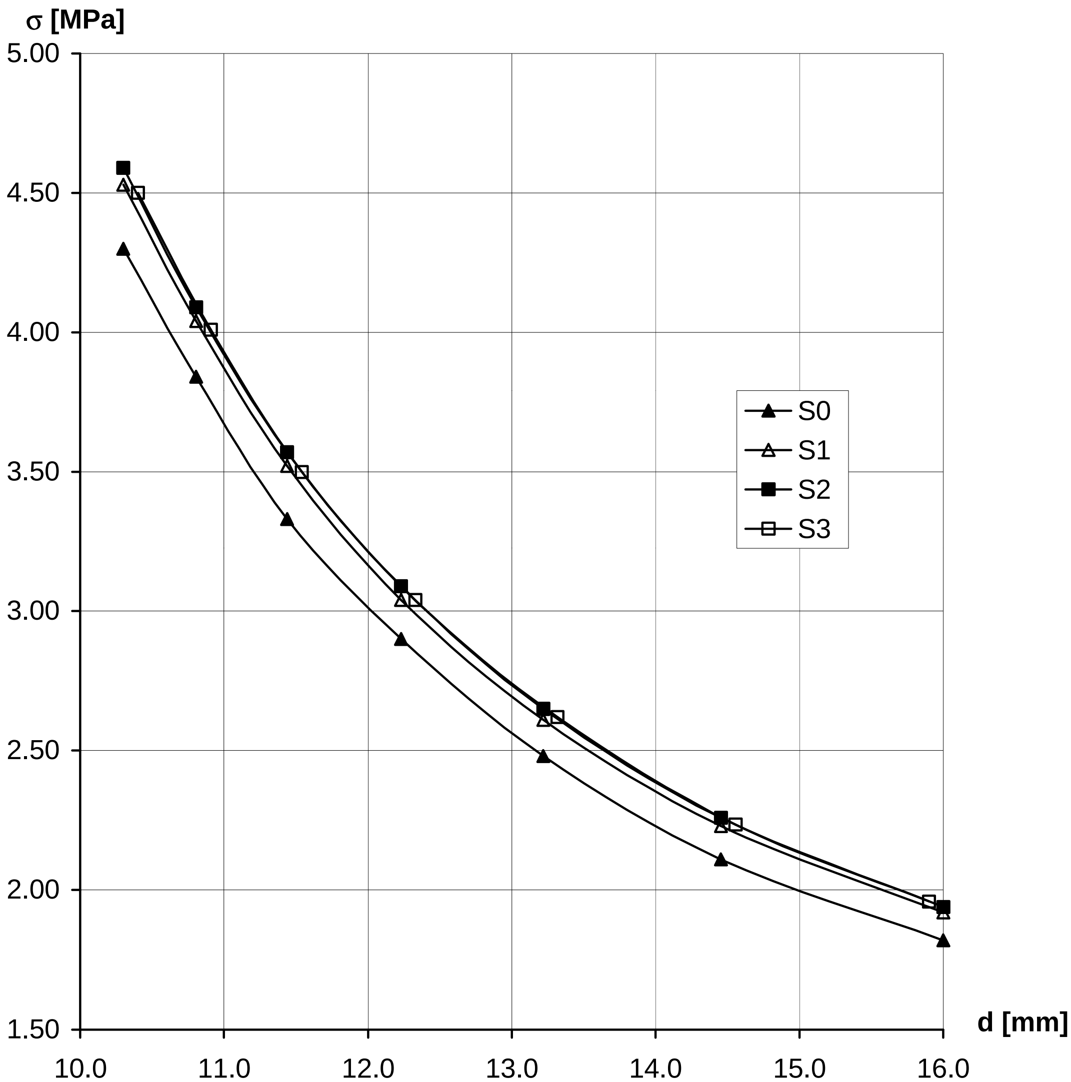

Figure 3.12 – Normal stress distribution, s_x, within edge distance of plate for different bolt staggers (d = distance from center of hole to closest edge of plate).

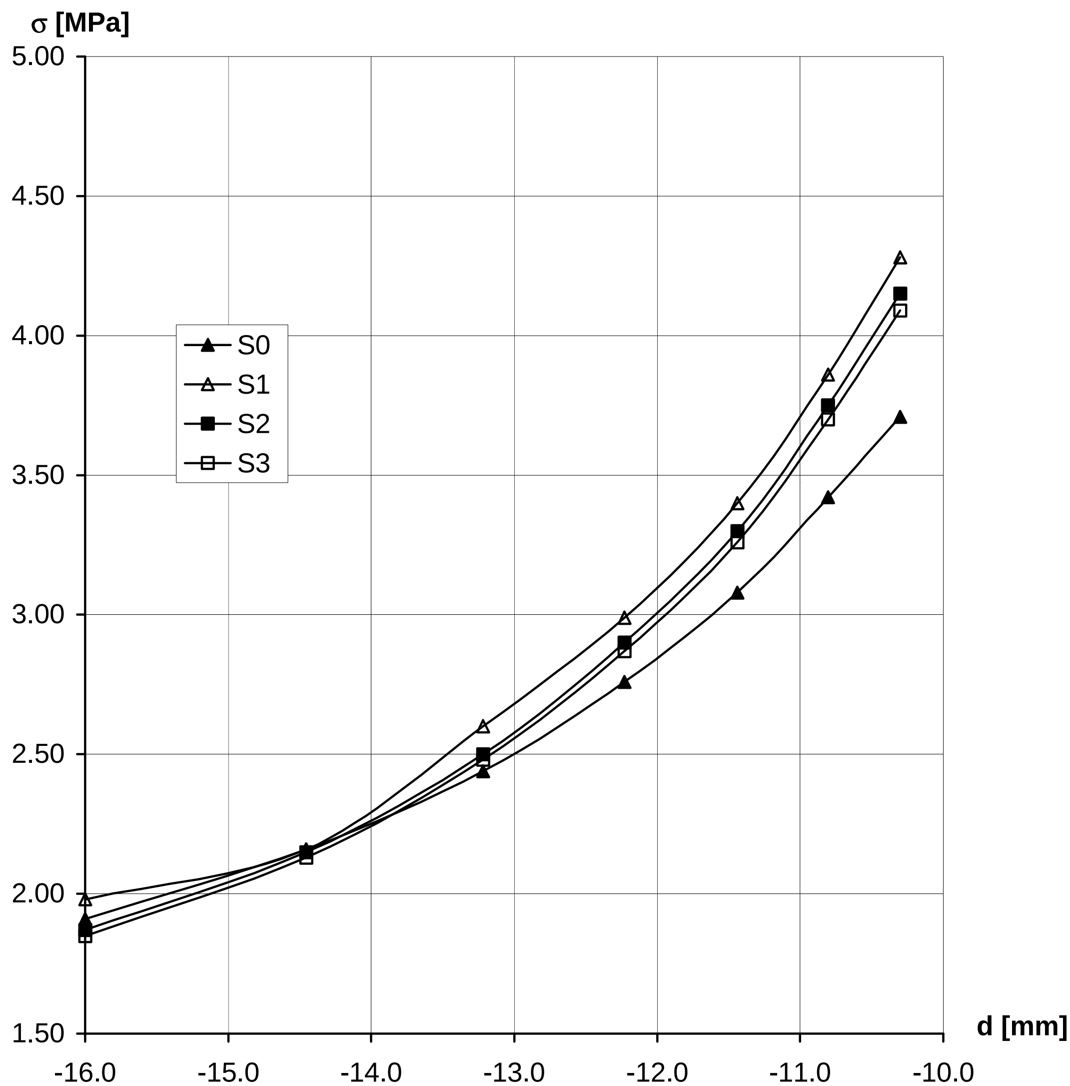

Figure 3.13 – Normal stress distribution, s_x, in center portion of plate for different bolt staggers (d = distance from center of hole to center of plate).

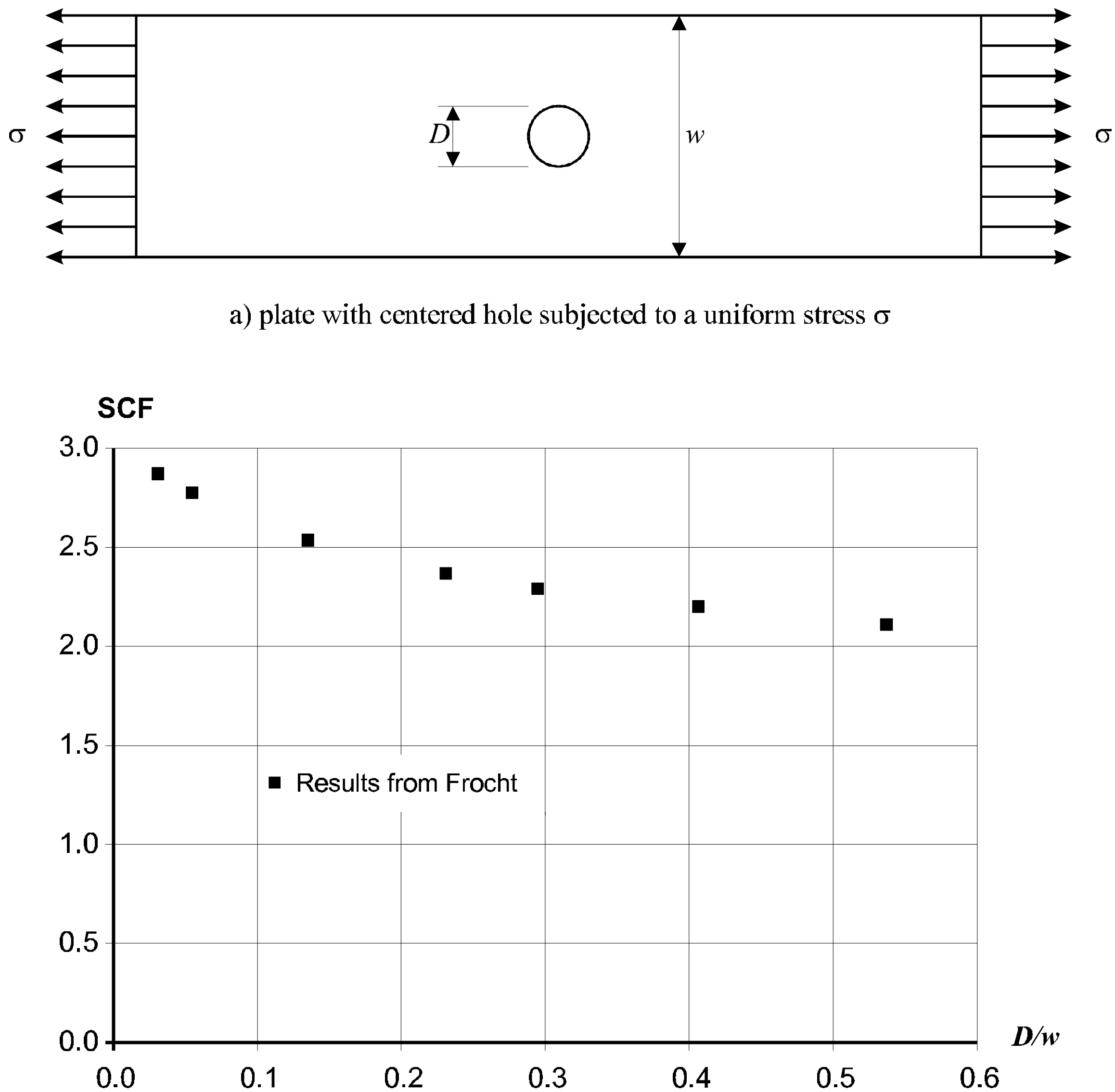

a) plate with centered hole subjected to a uniform stress σ

b) Stress concentration factor, *SCF*, as a function of *D/w*

Figure 3.14 – Stress concentration factor for plate with centered hole according to Frocht [3.4].

4. EXPERIMENTAL PROGRAM

a. Introduction

The experimental program on bearing-type shear splices described in this chapter was based on the analytical work presented in Chapter 3. The objectives of the tests were to verify the conclusions drawn from the analytical work and to help establish rules for the design and evaluation of bearing-type shear splices with staggered holes subjected to fatigue loading. In addition to a description of the test specimens, the results and observations from static and fatigue tests are presented.

b. Description of the Test Specimens

4.2.1 Geometry

In order to be able to verify the findings of the analytical investigation presented in Chapter 3, the geometry of the test specimens was the same as used in the analytical program. The general configuration of the splice plates used in the analytical and experimental investigations is shown in Figure 4.1. Three series of test specimens with different hole staggers, s, were tested. These were $s = 25.4$ mm (S1), $s = 50.8$ mm (S2), and $s = 76.2$ mm (S3). The width of these test specimens was 95 mm, which was selected because it is the width of the grip in the testing machine. The distance from the beginning of the grip to the first bolt holes, l, was kept constant for all specimens. The stress distribution in the main plates in front of the first bolt holes was therefore expected to be the same in all tests. The distance l was limited to 397 mm due to the overall length of the longest specimen (S3) that could be placed in the testing machine. In addition to the S1, S2, and S3 Series, a preliminary test (see Figure 4.2), a series of test specimens with non-staggered holes (S0 Series, see Figure 4.3), and a series with an increased gage width and hole stagger of 25.4 mm (G Series, see Figure 4.4) were tested. The width of the test specimens in these three series exceeded the width of the grips, requiring that the main plates be tapered, as shown in Figures 4.2 to 4.4.

The edge distance, e, was kept constant at 25 mm for all the test specimens. The thickness of all the splice plates, t_s, was 9.5 mm, and the thickness of the main plates, t_m, was 25 mm. The combined thickness of the two splice plates was therefore only 76 percent of the main plate thickness, and this made the splice plates the critical elements of the test specimens. ASTM A325 3/4 in. (19 mm) bolts were used in all the test specimens. The bolt length was selected as 83 mm in order to exclude the bolt threads from the shear planes.

4.2.2 Material Properties

Riveted connections designed in the first half of this century used so-called “mild steel,” which had a specified minimum yield strength of 190 MPa [4.1]. In the 1940’s, mild steel was gradually replaced by medium strength steel with a yield strength of 230 MPa. In the 1960’s, steel mills in North America introduced many new structural steels. These steels were characterized by higher yield strengths, up to about 450 MPa. Nowadays, only these higher strength structural steels are commonly available. Although the effect of yield strength upon fatigue life is generally considered to be secondary [2.28], a review of the literature revealed that a lower fatigue strength may result in bolted connections with lower strength material. Therefore it was decided to use the lowest steel grade commonly used for structural applications—CAN/CSA G40.21 [4.2] 300W steel—for all the plates of the test specimens. Steel of grade 300W has a specified minimum yield strength of 300 MPa and, depending on the plate thickness, an ultimate tensile strength of between 450 and 600 MPa.

In order to carry out the inelastic analysis of the splice plates presented in Chapter 3, the actual stress–strain behavior for the plate material had to be determined. Three tension coupons from the splice plate material were tested prior to the fatigue study. The tension coupons were prepared in accordance with the requirements of ASTM A 370-94 [4.3], with a gage length of 50 mm and a reduced section width of 12.5 mm. The material tests were conducted at a strain rate of about 15 $\mu\varepsilon$/sec in the elastic range and at about 50 $\mu\varepsilon$/sec in the plastic range. Strains in the first tested coupon were measured using two electrical resistance strain gages and a clip-on extensometer. After verifying that the average strains measured with the strain gages corresponded to the strains measured with the extensometer, only the extensometer was used for the subsequent tests. Four static stress values—two in the yield stress plateau, one near the ultimate stress, and one near the failure stress—were obtained for each test.

The tension coupon tests showed that the splice plates had an average elastic modulus of 212 000 MPa. The static and dynamic yield stresses were found to be 420 MPa and 460 MPa, respectively. The static and dynamic ultimate strengths are about 480 MPa and 500 MPa, respectively. Specific results from each of the tension coupon tests are tabulated in Appendix A.

4.2.3 Preparation of the Test Specimens

With the exception of the first test specimen, all the test specimens were fabricated by one steel fabricator. The splice plates were sheared and the main plates were flame cut to size. Bolt holes of 21 mm diameter were match drilled and the plate surfaces were left undisturbed; i.e., the mill scale was left on. Because of the limited height available in the testing machine, the butt splice connections were assembled in the testing machine. The bolts were first loosely clenched and, after having applied a static tensile load of about 150 kN to the connection, which increased the probability of having all bolts in bearing, the bolts were tightened with a calibrated wrench to introduce a tensile stress of about 100 MPa in each bolt. This value corresponds to the average stress introduced in a 19 mm bolt when snug-tightened [1.2].

In order to confirm that the load was introduced uniformly across the width of the test specimens, three electrical resistance strain gages were placed on each side of the two main plates at some distance from the bolt holes of specimen S0a. The strains measured during a static test confirmed that the stress was uniform across the width of the plate at a reasonable distance from the bolt holes. In order to facilitate the visual detection of fatigue cracks, the splice plates were coated with a whitewash just prior to the start of the fatigue tests.

c. Test Characteristics and Results

The following parameters were investigated in order to assess their effect on the fatigue behavior of bearing-type shear splices:

- stress range
- bolt stagger
- gage dimension.

The characteristics of each test series (geometry, load and net section stress range, number of test specimens) are summarized in Table 4.1. The net cross-sectional area was calculated deducting two holes from the gross section for the preliminary test and the S0 Series and deducting one hole for all other specimens. In order to assess variability in the test results, each test was repeated three times, except for the preliminary test, which was repeated only once.

4.3.1 Designation of Fatigue Crack Locations

In order to facilitate the description of the fatigue crack locations, each bolt hole on the splice plates is referred to by a designation consisting of two letters (for staggered holes) or three letters (for non-staggered holes) followed by one number, as illustrated in Figure 4.5. The first letter designates either the bottom (B) or the top (T) half of the test specimen, the second letter designates either the north (N) or the south (S) splice plate, and the third letter, used for non-staggered holes, designates either the east (E) or west (W) line of holes. The number varies from 1 (most critical hole) to 4 (the least critical hole).

A critical hole is defined as the hole where the net section stress range is the maximum. (Calculation of the stress range is discussed in Section 4.3.3.) This corresponds to the holes closest to the center of the splice plates. The holes become less critical with increasing distance from the center of the joint. Although the probability of crack initiation is highest at a critical hole, it is possible that cracks start at non-critical holes if, for example, initial imperfections are more severe or bearing pressures are higher at a non-critical hole.

Fatigue cracks can initiate at a bolt hole either toward the edge distance of the plate or toward the center of the plate. As illustrated in Figure 4.6, the former case is referred to as a crack initiating at the "outside" of a hole and the latter as a crack initiating at the

4.3.2 Test Procedure

All tests were carried out in the universal servo-hydraulic testing machine shown in Figure 4.7 with an installed specimen. The cyclic load pattern was generated by a microprofiler, and it followed a sine wave function. The load cycles were counted by a microconsole. The same console monitored and controlled the maximum and minimum loads applied to the specimens as well as the corresponding strokes of the testing machine. An automatic shutdown took place when the load or stroke passed predefined upper or lower limits. Visual inspection of the specimens was usually done at least twice a day until appearance of a crack, and more often thereafter depending on the crack propagation stage. Since the test specimens were inspected visually, it was impossible to detect cracks before they had emerged from under the bolt head or washer. The automatic shutoff of the testing machine at the upper stroke limit often preceded the visual detection of a crack and was therefore a useful tool for crack detection.

4.3.3 Test Conditions

Calculation of the Stress Range

A review of the literature indicated that the stress range for bearing-type connections should be based on the net cross-section (see Chapter 2). For all non-staggered specimens the net cross-section corresponds to the gross cross-section minus the cross-sectional area of all holes in one line. Since drilled holes were used, the deduction simply corresponded to the size of the hole. For the largest stagger investigated (76.2 mm), the net section according to the Cochrane rule [2.20] corresponds to a transverse section that passed through one bolt hole only. Because the numerical results reported in Chapter 3 showed no marked difference in elastic stress concentrations between the different staggers, the net section for the other two staggers (25.4 mm and 50.8 mm) was also defined as that on an orthogonal line passing through one hole.

__Preliminary Test__

A preliminary test (specimen P) was conducted in order to check at what combinations of load level, load range, and loading frequency tests could be carried out conveniently. The geometry of the preliminary test specimen is shown in Figure 4.2. All plates for this specimen were flame-cut and drilled at the University of Alberta. The gage width, $g = 61$ mm, and the edge distance, $e = 25$ mm, were selected based on the minimum allowed by CAN/CSA S16.1 [2.30] for 3/4 in. (19 mm) bolts. The net section stress range was chosen at 180 MPa. Although the effect of mean stress is considered to be secondary and will not be investigated in this study, a relatively high stress ratio, $R = 0.3$ was selected. This should result in a safe estimate of the fatigue life (cf. Section 2.4). The test conditions were considered to be an upper bound of stress condition for the test program. The resulting load range, $\Delta P = 240$ kN, required six bolts to transfer the load from the main plates into the splice plates [2.4]. The test was started at a frequency of 5.0 Hertz. After 460,000 cycles of testing the frequency was increased to 6.0 Hertz, which demonstrated that fatigue tests could be conducted at reasonable frequencies even at high load ranges. The result of this test is presented in Section 4.3.4.

__S Series Tests__

The main objectives of this series of tests were to substantiate the observations made in the analytical investigation and to form a database of test results for bearing-type connections with staggered holes. Four different bolt patterns with four different staggers (S0, S1, S2, and S3) were tested[1].

S0 Series

In order to assess the effect of bolt stagger on the fatigue strength of bearing-type connections above the probable constant amplitude fatigue limit, it was desirable to restrict the number of runouts (tests that do not develop cracks even after a large number of load cycles, usually exceeding ten million). The fatigue strength of bearing-type shear splices at two million cycles is, according to CAN/CSA S16.1 for a fatigue category B detail [2.30], approximately 125 MPa on the net cross-section. However, this value represents a low probability of failure and a higher fatigue strength can therefore be expected in a test. The stress range for specimens S0a, S0b1, and S0b2[2] (see Figure 4.3 for the geometry of the specimens) was therefore selected at 140 MPa. It was expected that this stress range would lead to a failure of the specimens at more than two million cycles and thus should be representative of fatigue lives encountered in practice. The three remaining specimens of the S0 Series (S0c1, S0c2, and S0d) were tested at an

[1] Specimens S3 were tested before S1 and S2.
[2] The specimen designation S0b2 means that a second set of splice plates were used with the same main plates as for specimen S0b1.

increased stress range, namely, 180 MPa. The literature review suggested that the fatigue strength of bolted shear splices might decrease with an increase in the stress ratio, $R = s_{min}/s_{max}$. A relatively high stress ratio, $R = 0.3$, was therefore chosen. The resulting maximum applied net section stresses was still below the yield strength of the plates, however. The S0 Series tests were conducted at frequencies of about 10.0 Hertz.

S1 Series

The geometry of the specimens in the S1 Series is shown in Figure 4.1, where $s = 25.4$ mm. In order to compare the test results from the S1 Series with those of the S3 Series, which was tested before the S1 Series, the net section stress range for the first three specimens (S1a1, S1a2, and S1b) was fixed at the same stress range as the first three specimens of the S3 Series (140 MPa). Because a runout was obtained in one of the specimens from the S3 tests (at 90 MPa), the remaining specimens of the S1 Series (S1c1, S1c2, and S1d) were tested at a net section stress range of 110 MPa. The stress ratio for all six specimens of this series was fixed at $R = 0.3$. The tests were conducted at frequencies between 8.0 and 12.0 Hertz.

S2 Series

The geometry of the specimens from the S2 Series was the same as for the S1 Series with the exception of the stagger, which was set at 50.8 mm. In order to compare the S2 Series with the S1 and S3 tests, the net section stress range for the first three specimens (S2a1, S2a2, and S2b) was also fixed at 140 MPa. The stress range for the other three specimens (S2c1, S2c2, and S2d) was identical to the one for the last three specimens from the S1 Series, namely, 110 MPa. All six test specimens were tested at a stress ratio $R = 0.3$. The tests were conducted at frequencies between 8.0 and 12.0 Hertz.

S3 Series

The geometry of the specimens from the S3 Series was the same as for the S1 Series and S2 Series with the exception of the stagger, which was set at 76.2 mm. Based on the results from test specimens of the S0 Series, the net cross-section stress range for the first three specimens (S3a1, S3a2, and S3b) of the S3 Series was also fixed at 140 MPa. However, these three specimens failed at a relatively low number of cycles, and the net section stress range for the three remaining specimens of this series (S3c1, S3c2, and S3d) was reduced to 90 MPa. All six specimens were tested at a stress ratio $R = 0.3$. The tests were conducted at frequencies between 6.0 and 10.0 Hertz.

G Series Tests

The analytical investigation showed that an increase in the net-to-gross cross-sectional area ratio, A_n/A_g, resulted in a slight increase of the maximum stress around a bolt hole for a given net section stress. It was therefore hypothesized that an increase in gage width, while keeping all other geometrical properties constant, should result in a slight reduction of fatigue life. To verify this hypothesis, six tests with a gage width $g = 60.3$ mm (the gage width for the S Series was 44.5 mm) were carried out. The net section area for these test specimens was 1725 mm^2. The hole stagger of 25.4 mm and the net section stress ranges, Δs_n, were the same as for the S1 Series, i.e., three tests were run at $\Delta s_n = 140$ MPa and three at $\Delta s_n = 110$ MPa. These stress ranges correspond to load ranges of 240 kN and 190 kN. These are identical to the load ranges used for the S0 Series, and this then allows a direct comparison between the G Series and the S0 Series. Again, all the tests were conducted at a stress ratio $R = 0.3$ and at frequencies between 7.0 and 10.0 Hertz.

4.3.4 Test Results

The results of all the tests are presented in Table 4.2 . In addition to the identification of the specimens (stagger, s, applied net section stress range, Δs_n, and load range, ΔP), three cycle counts are reported. The first, N_d, corresponds to number of cycles at which a crack was first detected. The second, N_e, corresponds to the number of cycles at which the crack reached the edge of the plate. Often, the first and second numbers of cycles are identical because a crack was detected only after it had reached the edge of a plate. The third cycle count, N_f, corresponds to the end of a test, which was stopped either when a specimen could no longer carry the maximum load or one of the two splice plates was completely severed. Observations on three tests, which were run until rupture of the specimens, showed that the two criteria to stop the tests were within a very small range of load cycles. Table 4.2 also identifies the location of crack initiation.

d. Examination of the Test Specimens

4.4.1 Location of Cracks

A total of 31 fatigue tests were carried out. Specimen S3d had not developed a fatigue crack when the test was stopped at 16 million cycles, specimen S3c2 failed in the main plate, and specimen S2a1 failed in the gross cross-section of a splice plate. The other 28 test specimens failed as a result of cracks that started in the net cross-section of one of the splice plates. In 20 of these 28 specimens the location of the first crack was at a critical hole. In the other eight specimens the cracks started at the second-most critical hole.

Twenty-four tests failed as a result of cracks that started at the outside of a hole. Sixteen cracks started on the north side and twelve on the south side of the test specimens[1].

All six fracture surfaces from the S1 Series and the fracture surface from specimen S0b2, which had a much lower fatigue life than the other replicate specimens, were examined under an optical microscope at a maximum magnification of 50X in order to determine the origin of the fatigue fractures. (Unfortunately, the fracture surfaces of specimens S2a1 (gross cross-section failure) and S3c2 (main plate failure) were inadvertently damaged after testing and their fracture surface could not be examined under the microscope.) It was observed that crack initiation occurred at random locations around the bolt hole or, in one case, between the hole and the edge of the plate (S1c2). The cracks either started at some mechanical damage that existed before testing or as a result of fretting due to the contact between the bolt head, washer or main plate with the surface of the splice plate. After the preliminary examination under the optical microscope, three of the seven specimens were further investigated with a scanning electron microscope at a magnification of up to 4000X. Examination of specimen S1c1, which was representative of most of the test specimens, confirmed that the crack started due to fretting. The examination of specimen S1c2 showed that the crack started between the edge of the hole and the edge of the plate due to a mechanical defect, which was most likely caused by grinding of a particle on the surface. A rather large surface imperfection (about 60 μm in size) resulting from mechanical damage, as shown in Figure 4.8, was found to be the most likely cause of the early fatigue failure of specimen S0b2. The examination under the scanning electron microscope did not reveal any other irregularities in the microstructure or the chemical composition of the fracture surfaces. In some locations striations and secondary cracks, both of which are typical of fatigue fracture surfaces, could be detected easily, as shown in Figure 4.9 for specimen S1c2.

4.4.2 Crack Pattern

With the exception of some cracks that initiated at a non-critical hole in plates with 25.4 mm stagger, all the cracks propagated more or less on a straight line perpendicular to the applied load, as shown in Figure 4.10 for specimens S2a2 and Gb. This crack propagation pattern is similar to that observed in other tests carried out on riveted tension connections with staggered holes [2.54, 2.55]. All the cracks of the S1 Series and G Series that initiated at a non-critical hole also started out perpendicular to the applied load. However, because of the proximity of the critical hole, they then became inclined and eventually joined the critical hole, as shown in Figure 4.11 for specimen Ga2.

---

[1] In all specimens the bolt head was on the north side and the nut was put on the south. Washers were used under the nut only.

4.4.3 Examination of Bolts

After disassembling the specimens, the bolts were visually examined. All 252 bolts showed clear marks in the unthreaded portion confirming that they were in bearing and that the shear planes never intersected the threads. None of the bolts had any visible fatigue cracks.

e. Conclusions

A total of 31 bearing-type shear splices were tested in fatigue. The parameters investigated were stress range, hole stagger, and hole gage. A total of 28 out of 31 test specimens failed as a result of cracks that started in the net cross-section of one of the splice plates. As expected from the analytical investigation carried out in Chapter 3, most of the cracks began at the outside of a critical hole. The crack initiation occurred at random locations and was due to either fretting or pre-existing mechanical damage. With the exception of cracks starting at non-critical bolt holes in plates with a stagger of 25.4 mm, all the cracks propagated more or less on a straight line perpendicular to the main stress field, confirming observations made by other investigators. Although all the bolts were in bearing during the tests, none of the bolts themselves suffered any fatigue damage.

Table 4.1 – Characteristics of the test series.

Test Series	s [mm]	g [mm]	A_g [mm^2]	A_n [mm^2]	ΔP [kN]	Δs_n [MPa]	**Number of Tests**
Preliminary	0.0	60.3	2120	1330	240	180	1
S0	0.0	60.3	2120	1330	240 190	180 140	3 3
S1	25.4	44.5	1810	1420	200 160	140 110	3 3
S2	50.8	44.5	1810	1420	200 160	140 110	3 3
S3	76.2	44.5	1810	1420	200 130	140 90	3 3
G	25.4	60.3	2120	1720	240 190	140 110	3 3

Table 4.2 – Results of all the tests.

Test Specimen	***s*** **[mm]**	Δs_n **[MPa]**	ΔP **[kN]**	N_d $\times 10^6$	N_e $\times 10^6$	N_f $\times 10^6$	**Location of first crack (Fig. 4.5)**
P	0.0	180	240	0.569	0.569	0.571	Hole BNW1, outside
S0a	0.0	140	190	2.167	2.167	6.250[1)]	Hole BNE1, outside
S0b1	0.0	140	190	5.720	5.800	8.150	Hole TSW2, outside
S0b2	0.0	140	190	0.767	0.767	0.829	Hole TNE1, outside
S0c1	0.0	180	240	0.355	0.355	0.419	Hole BNE1, outside
S0c2	0.0	180	240	0.620	0.620	0.726	Hole TNE1, outside
S0d	0.0	180	240	0.578	0.581	0.621	Hole BNE1, outside
S1a1	25.4	140	200	0.255	0.255	0.269	Hole BN1, outside
S1a2	25.4	140	200	0.303	0.303	0.31	Hole BS2, outside
S1b	25.4	140	200	1.558	1.558	1.603	Hole TS1, outside
S1c1	25.4	110	160	2.827	2.827	3.073	Hole TS1, outside
S1c2	25.4	110	160	2.900	2.900	3.111	Hole BN1, outside
S1d	25.4	110	160	8.520	8.520	8.625	Hole BS2, outside
S2a1	50.8	140	200	1.062	1.062	1.100	In gross section
S2a2	50.8	140	200	0.307	0.307	0.443	Hole BS2, outside
S2b	50.8	140	200	0.649	0.649	0.761	Hole TS1, outside
S2c1	50.8	110	160	3.801	3.816	3.820	Hole BN1, inside
S2c2	50.8	110	160	1.497	1.518	1.530	Hole BN1, inside
S2d	50.8	110	160	2.650	2.662	2.730	Hole BN1, outside
S3a1	76.2	140	200	0.675	0.685	0.747	Hole TS1, outside
S3a2	76.2	140	200	0.695	0.695	0.731	Hole TN1, outside
S3b	76.2	140	200	0.515	0.515	0.540	Hole BN1, outside
S3c1	76.2	90	130	3.562	3.562	3.953	Hole BN1, outside
S3c2	76.2	65[2)]	130	13.673	13.673	13.711	Main plate failure
S3d	76.2	90	130	-	-	-	No failure[3)]

1) Four bolts on the cracked half were fully preloaded after detection of crack
2) Net section stress in main plate
3) Test was stopped with no cracks after 16 Mio cycles

Table 4.2 –Results of all the tests (cont'd).

Test Specimen	s [mm]	Δs_n [MPa]	ΔP [kN]	N_d $\times 10^6$	N_e $\times 10^6$	N_f $\times 10^6$	Location of first crack (Fig. 4.5)
Ga1	25.4	140	240	0.518	0.518	0.575	Hole BS2, outside
Ga2	25.4	140	240	0.295	0.295	0.334	Hole BS2, outside
Gb	25.4	140	240	0.318	0.318	0.349	Hole TS1, outside
Gc1	25.4	110	190	1.915	1.915	2.421	Hole TN2, outside
Gc2	25.4	110	190	2.838	2.894	2.937	Hole TS1, inside
Gd	25.4	110	190	1.000	1.000	1.121	Hole TN2, outside

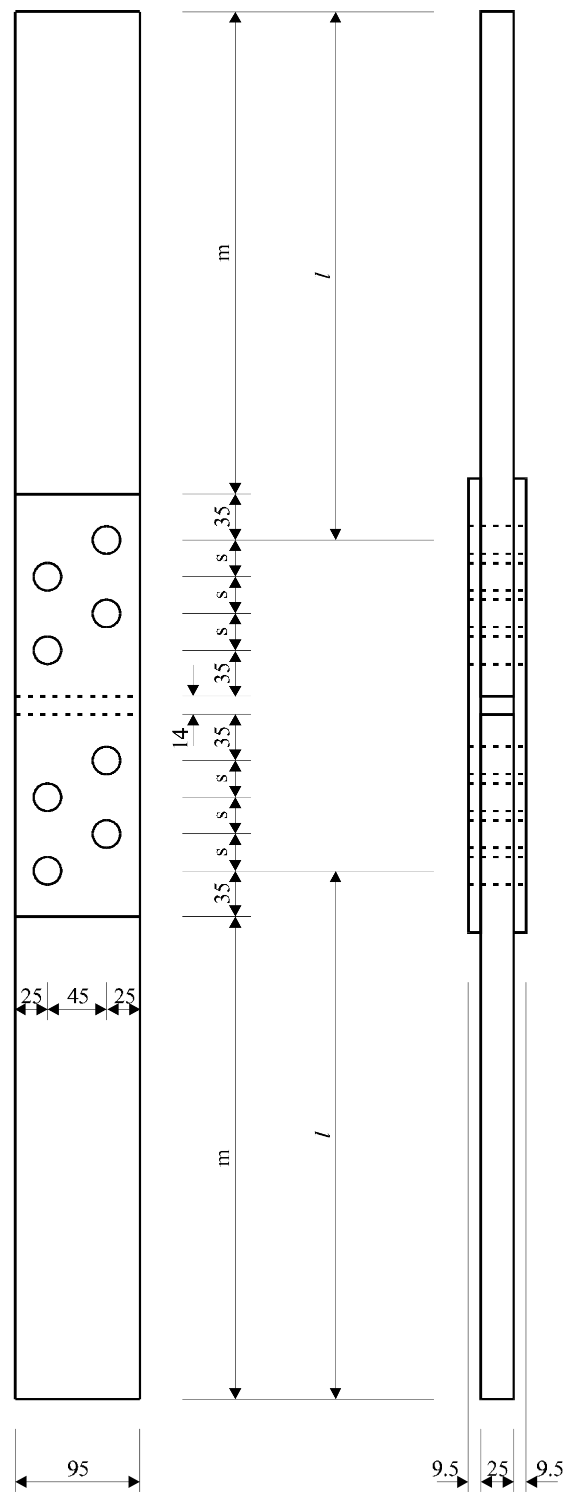

Figure 4.1 – Butt splice specimen with staggered holes.

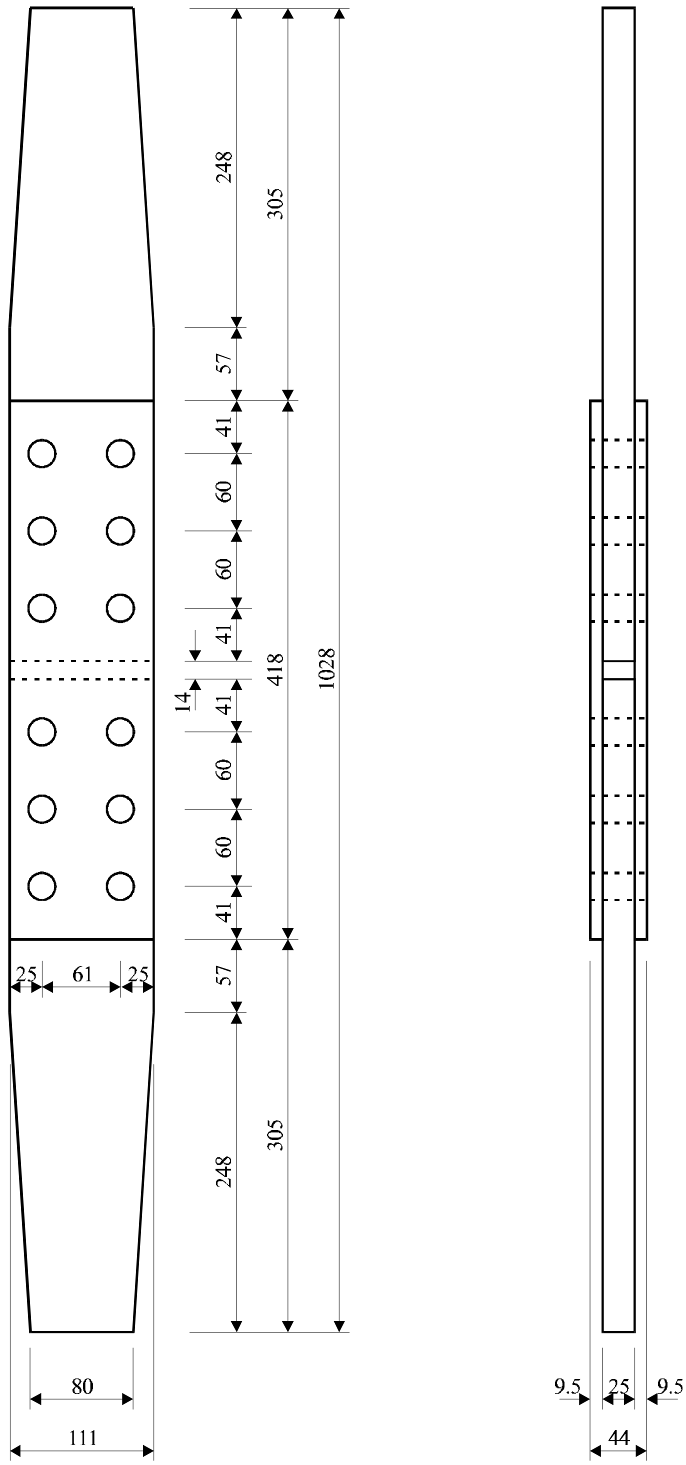

Figure 4.2 – Preliminary test specimen.

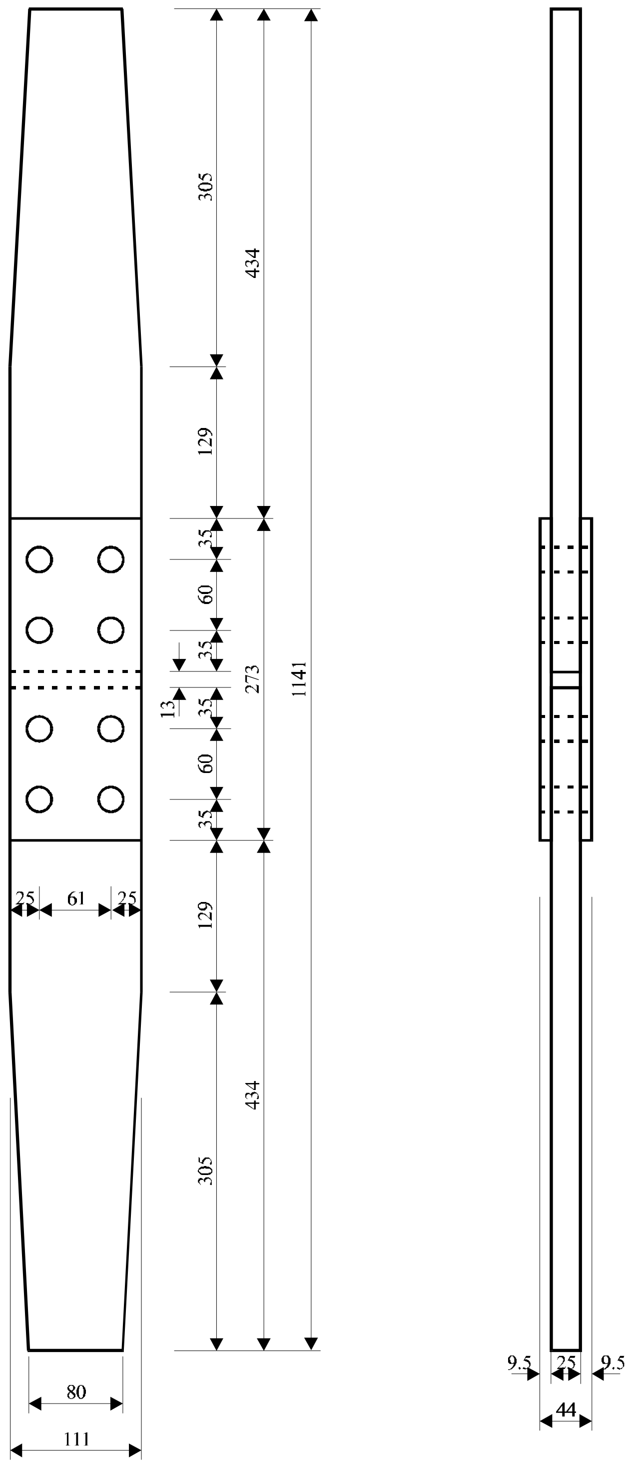

Figure 4.3 –S0 test specimen.

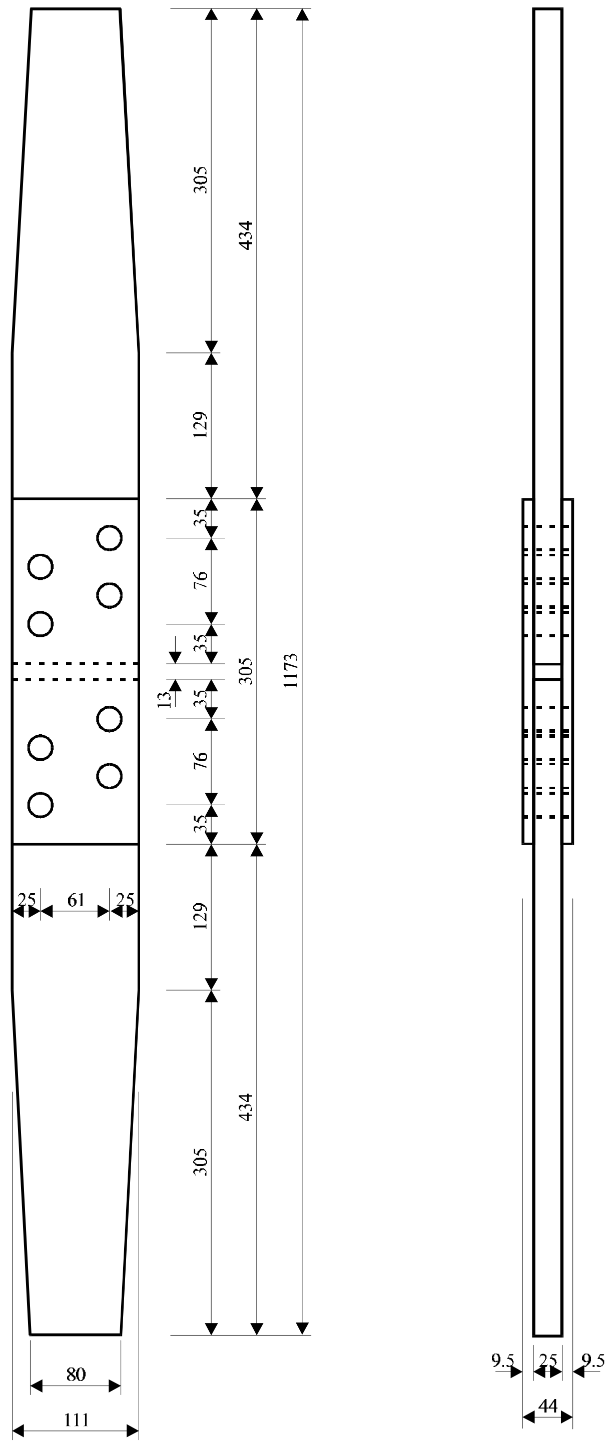

Figure 4.4 – G test specimen.

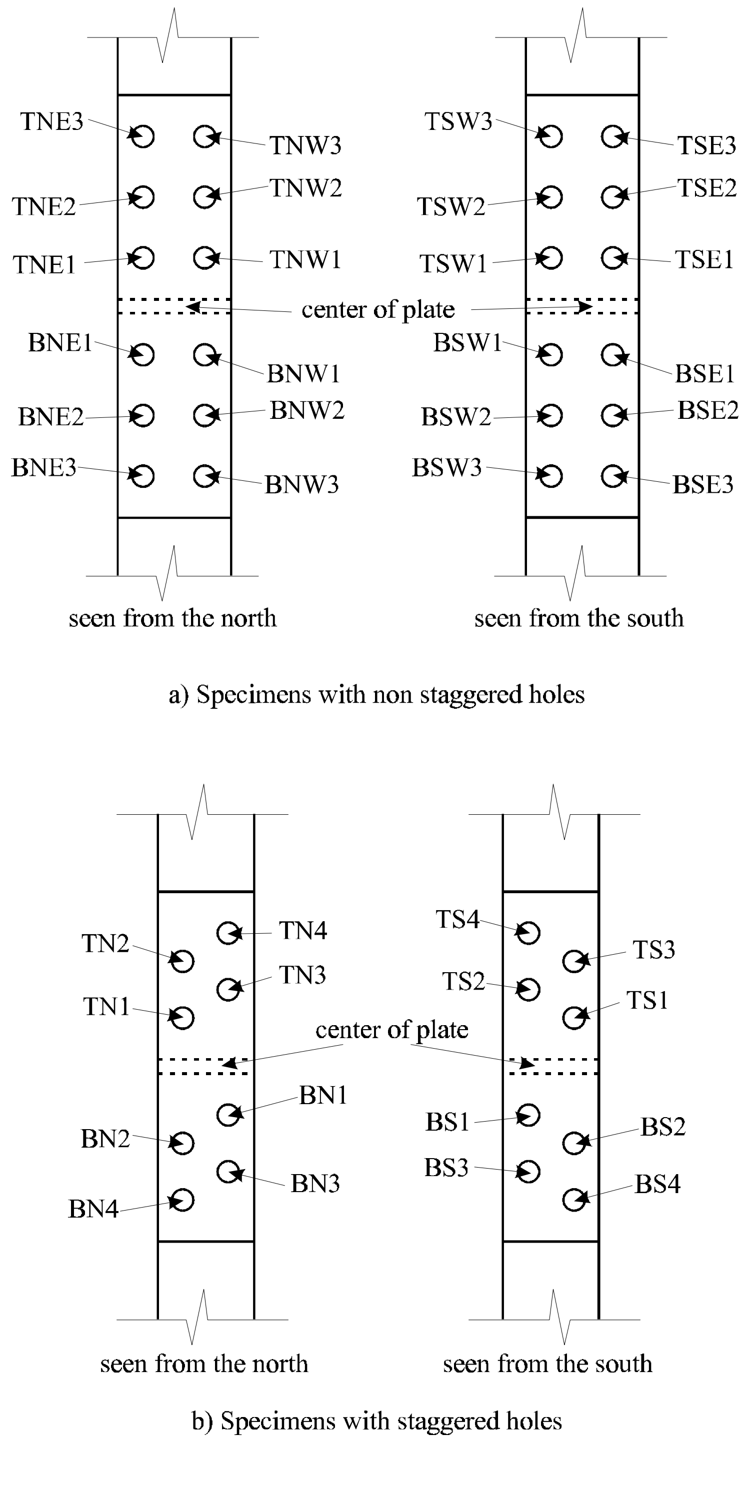

Figure 4.5 – Definition of the holes in the splice plates.

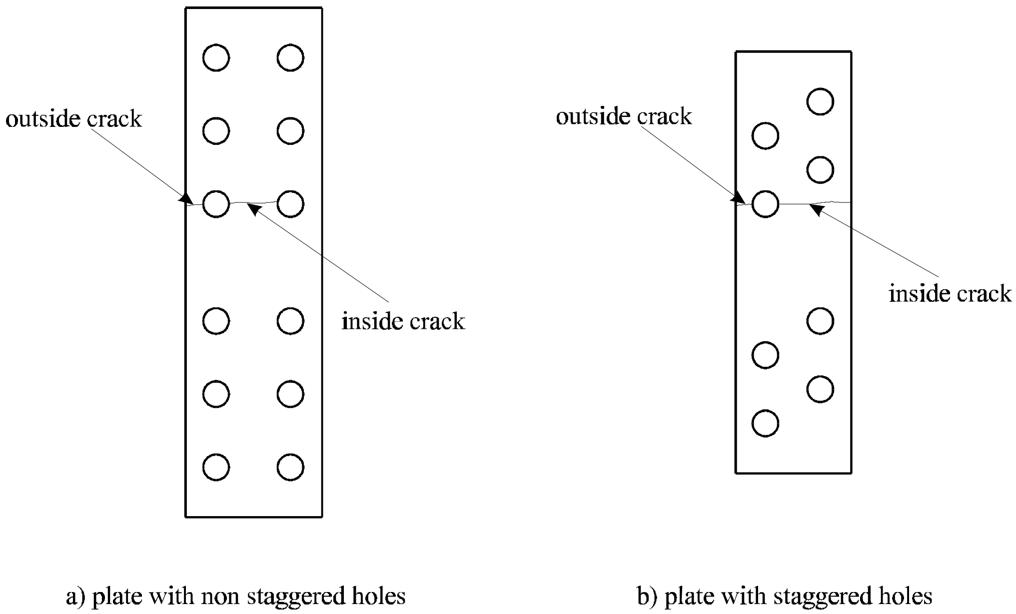

Figure 4.6 – Definition “inside” and “outside” cracks.

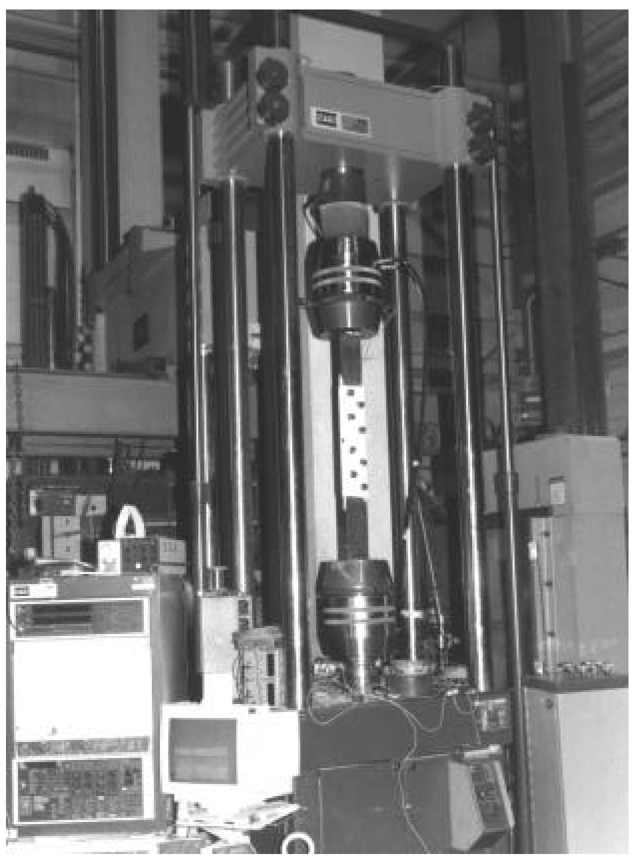

Figure 4.7 – Fatigue test specimen in testing machine.

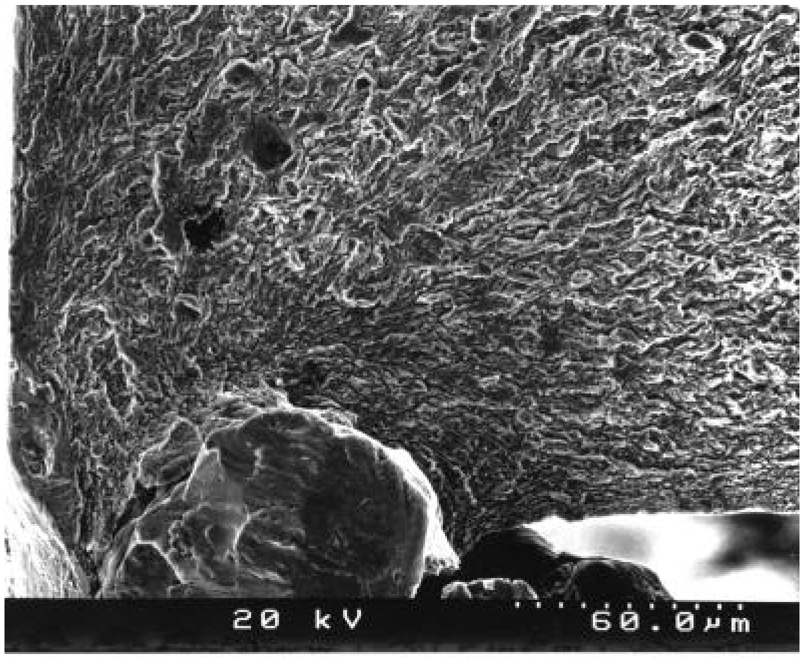

Figure 4.8 – Fracture surface of specimen S0d2 with important surface imperfection at lower left corner (magnification 500X).

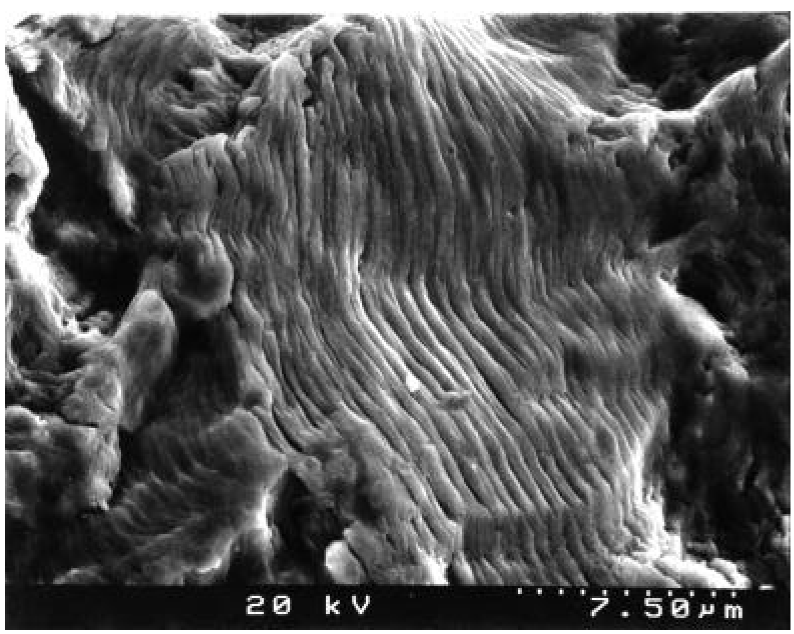

Figure 4.9 – Fatigue striations and secondary cracks in specimen S1c2 (magnification 4000X).

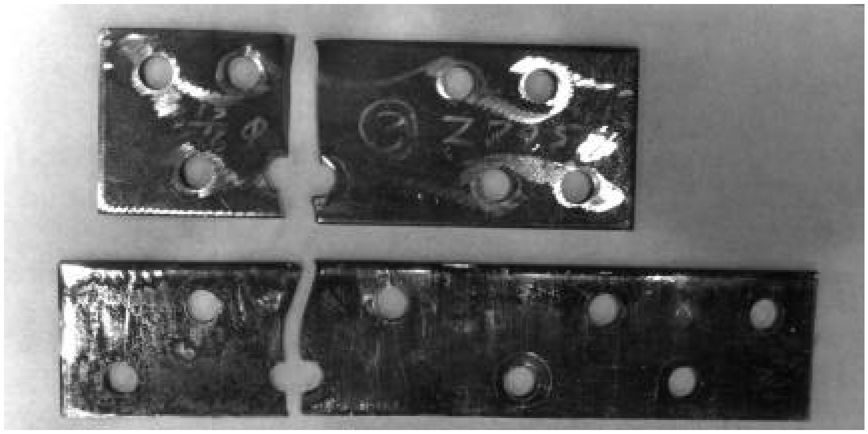

Figure 4.10 – Fatigue crack patterns for specimens Gb (top) and S2a2 (bottom).

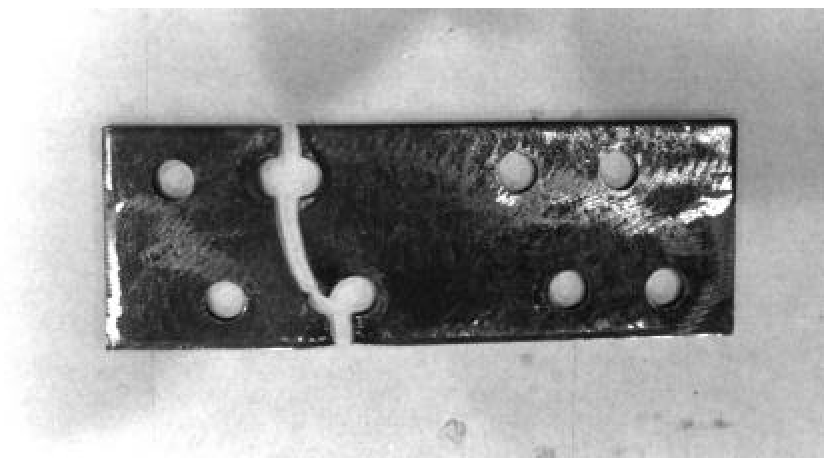

Figure 4.11 – Fatigue crack pattern for specimen Ga2.

5. DISCUSSION OF RESULTS

5.1 Introduction

Twenty-eight fatigue tests were conducted on bearing-type shear splices. The tests were designed to investigate the effect of stress range, bolt stagger, and gage distance on the fatigue life of bearing-type shear splices. Because of the large scatter usually observed in fatigue test results, each test was repeated three times in order to provide a quantitative measure of the scatter in the test results. This chapter presents a statistical analysis of the test results carried out in order to assess the effect of the parameters investigated in the experimental program.

In Chapter 3 a finite element analysis of the test specimens was presented in which the elastic stress concentration factor for each test specimen was determined. The purpose of Chapter 5 is to provide a comparison between the test results and the results of the finite element analysis. The goal is to establish a stress parameter that relates the test results to the results of the finite element analysis. Recommendations are made for a fatigue design approach for bearing-type shear splices. These are based on a stress range correction factor derived from the finite element analysis results and a fatigue curve obtained from a regression analysis of the test results.

5.2 Assessment of the Test Parameters

5.2.1 Analysis of Test Results and Failure Criterion

The test specimens (Chapter 4) were designed to assess the effect of the magnitude of bolt stagger and gage width on the fatigue resistance of bearing-type shear splices. The significance of the test parameters on fatigue life can now be assessed using a statistical analysis. The statistical tests used to compare sets of test data are the t test and the F test [5.1]. The t test is commonly used to compare the mean of two normally distributed samples. The t test is based on the assumption that the variance of both samples is the same, however. An F test is used to check the validity of this assumption.

In order to be able to conduct a statistical analysis of the test results, a failure criterion is required so that the test results can be compared on a common basis. The test results presented in Tables 4.1 and 4.2 show that by the time a crack has reached the edge of the plate from 85% to almost 100% of the fatigue life has been expended. In some of these tests it was possible to measure the life between the time of first detection of a crack from under the bolt head or washer to propagation of the crack to the edge of the plate. These tests indicated that the difference between the number of loading cycles at first detection and when the crack reached the edge was less than about 2% of the fatigue life of the specimen. Thus, the failure criterion used in this study, i.e., the propagation of a crack to the edge of the plate, is reasonable.

Since fatigue test results generally follow a log–normal distribution [5.2], all the subsequent statistical analyses are performed on the logarithm of the fatigue life, log (*N*), and stress range, log ($\Delta\sigma$). Table 5.1 presents the number of cycles corresponding to the failure criterion defined above and their logarithm. The mean value of the log of the fatigue life, $\bar{y}_i$, for each group of replicated tests and their standard deviation, $s_{y,i}$, are also tabulated. The results of the F and t tests for the different comparisons between sets of test results are shown in Table 5.2. (Details of the statistical tests are presented in Appendix B.) The calculated t values are compared to the tabulated value of the t distribution for a 95 percent confidence interval ($t_{\mathrm{lim}} = 2.776$). Similarly, the calculated F values are compared to the tabulated F value for the same confidence interval ($F_{\mathrm{lim}} = 19.0$) [5.3]. (A confidence interval of 95 percent means that there is a 5 percent probability of concluding that there is a real difference between the two samples when in fact the observed difference is due to chance only [5.1].) If the calculated values of t and F are smaller than the limiting values tabulated in standard statistical tables, the difference between the two means and variances can be assumed to be insignificant at the selected confidence level. The last column of Table 5.2 states whether the difference between Set 1 and Set 2, listed in the first two columns of the table, is significant.

5.2.2 Influence of the Magnitude of Stagger

Test series S1, S2, and S3 was used to investigate the influence of bolt stagger on the fatigue life of bearing-type shear splices. In each component of the program, tests were conducted at a load range of 200 kN. In addition, tests in Series S1 and S2 were conducted at a load range of 160 kN. The test results presented in Table 5.1 show that there was a slight increase in fatigue life with increased stagger at a load range of 200 kN and a slight decrease in fatigue life with increased stagger at a load range of 160 kN. However, Table 5.2 indicates that this increase in fatigue life is statistically insignificant. It can therefore be concluded that the magnitude of stagger does not significantly affect the fatigue behavior. This conclusion is also supported by earlier observations made from the results of the finite element investigation of the splice plates. Therefore, all the test results from the S1, S2, and S3 Series can be combined to find the appropriate fatigue strength (cf. Section 5.4) of this kind of detail.

5.2.3 Influence of Gage Dimension

The effect of gage dimension was assessed using a comparison between the S1 Series and the G Series test specimens. The statistical analysis of the test results (Table 5.2) indicates that the gage dimension has no significant effect on the fatigue life. The mean value of the log of fatigue life presented in Table 5.1 indicates, however, that there is a decrease in fatigue life with an increase in gage dimension. This was expected from the results of the finite element analysis presented in Chapter 3, which indicated that the peak stress increased with the gage dimension. However, this increase is too moderate to result in a significant difference between the two gage dimensions when the scatter in the test results is accounted for, as is done in the statistical comparison conducted using the *t* test. It can be concluded, therefore, that a variation in the gage distance from 44 mm to 60 mm has a negligible effect on the fatigue behavior, and that test results from the G Series can be combined with the results from the S1, S2, and S3 Series.

5.2.4 Presence or Absence of Stagger

The presence or absence of stagger on the fatigue resistance of bearing-type shear splices was investigated using the specimens from the S0 and G Series. Both series had the same plate width and edge distance and were tested at the same load range. The S0 Series specimens had no stagger and the G Series specimens had a stagger of 25 mm. The statistical analysis of the test results in Table 5.2 indicates that the presence or absence of stagger has no significant effect on the fatigue life of these two groups. However, the mean value of the log of fatigue life presented in Table 5.1 indicates that there is a decrease in fatigue life within the staggered series (G Series) itself. This was expected from the results of the finite element analysis presented in Chapter 3, which indicated that the peak stress increased when stagger was present. However, when the scatter in the test results is taken into account the difference in test results between shear splices with stagger and shear splices without stagger is not significant. Therefore, test results from the S0 Series can be combined with all the other results.

5.2.5 Conclusions

The finite element analysis carried out in Chapter 3 indicated that the difference in stress concentration factor for splice plates with different staggers is very small. This observation was supported by the results of fatigue tests. They showed that there is no significant difference in fatigue life with varying magnitudes of stagger. The finite element analysis also indicated potential for a slight reduction in fatigue life with an increase in gage width. Although the difference was found to be statistically insignificant, the mean value of the test results confirmed this trend. (It is not surprising that the slight differences in stress concentration did not translate into significant differences in fatigue life, considering the scatter of the test results.) A similar observation was made about the effect of the presence of stagger. Therefore, based on the observed trends, it can be concluded that the concept that the fatigue life is a function of the stress concentration around the highest stressed hole is supported by the test results.

5.3 Stress Range Calculation

5.3.1 General

The analysis did not show any significant difference in fatigue life between the S and the G Series and between the S0 and all other specimens from the S Series. Consequently, the effective area used to calculate the stress range should lead to the same stress range for all the test series that showed insignificant difference in fatigue life. It is not clear, however, which area can be used for this purpose. The following areas will first be considered:

- gross cross-section, A_g
- net cross-section deducting one bolt hole, $A_{n,1}$
- net cross-section deducting two bolt holes, $A_{n,2}$
- net cross-section using the Cochrane rule, $A_{n,C}$

5.3.2 Effective Cross-Section

Since the failure path in almost all of the test specimens went through the net cross-section of the splice plates, it is not appropriate to base the stress range on the gross cross-section, A_g. Furthermore, it is not logical to deduct only one hole for the non-staggered cases and, therefore, the use of $A_{n,1}$ cannot be justified. Since no significant difference between the staggered and non-staggered cases was observed, the use of $A_{n,2}$ as the effective cross-section seems to be a valid alternative. The validity of this observation to a broader range of joint geometry is questionable, however. Knowing that the magnitude of the stagger, s, does not influence the fatigue behavior of the shear splices investigated in this study, the use of the Cochrane rule cannot be justified either.

Assuming that the fatigue life is a function of the peak stress range, a more quantitative comparison of the various effective areas proposed above can be made by calculating the stress concentration factor, SCF_i, in terms of the proposed areas for each test specimen. The stress concentration factor is defined as:

$$SCF_i = \frac{\sigma_{peak}}{\sigma_i} \tag{5.1}$$

where,

σ_{peak} : peak stress in a plate with holes obtained using the analysis presented in Chapter 3.

s_i : stress obtained using one of the cross-sectional areas A_i defined above.

Since it has been argued that all the test results can be combined into one set of data, the use of the correct effective cross-sectional area to define the stress concentration factor should result in a constant, or close to constant, stress concentration factor for all the splice plates investigated.

The SCF_i for each plate geometry and effective cross-section defined above are presented in Table 5.3. The ratio, r_i, between the largest and smallest values of SCF_i for each effective cross-section is also presented in Table 5.3. The closer this ratio is to unity, the more accurately the effective cross-section reflects the stress concentration. The following observations can be made from Table 5.3:

- None of the cross-sections defined above result in a constant value of SCF .
- The gross section and the cross-sectional areas based on deduction of one or two bolt holes all lead to a similar ratio r_i.
- The cross-sectional area based on the Cochrane rule leads to the largest range of *SCF*.

It is therefore concluded that none of the effective cross-section definitions proposed above is adequate to calculate the effective stress range of bearing-type shear splices with staggered holes. A different approach is required.

5.3.3 Proposed Stress Range Calculation Based on Stress Concentration

The comparison of the experimental results presented in Section 5.2 supports the idea presented in Chapter 4 that the fatigue life of bearing-type shear splices is a function of the stress concentration at the critical hole. An approach that accounts for stress concentration in the calculation of the stress range is therefore proposed. This approach is summarized as follows:

- The stress concentration factor in plates with various bolt hole patterns will be normalized with respect to the bolt hole pattern used in the *S0* Series test specimens.
- The stress concentration factor of the reference pattern (*S0* Series pattern) is calculated with respect to the gross section[1] ($SCF_{S0} = \dfrac{\sigma_{peak,S0}}{\sigma_{g,S0}} = 3.95$)

---

[1] Since no adequate definition of a net section is possible, the stress range is defined using the gross sections.

- The stress concentration factor for any plate geometry k is calculated with respect to the gross section ($SCF = \frac{\sigma_{peak,k}}{\sigma_{g,k}}$)
- The stress concentration factor for the plate of geometry k is normalized with respect to *S0*. The normalized stress concentration will be used as a stress range correction factor, $F_{sc} = \frac{SCF_k}{SCF_{S0}}$
- The gross section stress range, Δs_g, for any plate geometry k is multiplied by the stress range correction factor, F_{sc}, to obtain the corrected stress range $\Delta s_{sc} = F_{sc} \Delta s_g$

The maximum and gross cross-section stresses used to calculate the stress concentration factor, *SCF*, as well as the corresponding stress range correction factor, F_{sc}, and the corrected stress range, $\Delta\sigma_{sc}$, for each splice plate and stress range used in the test program are presented in Table 5.4. The test results obtained with these corrected stress ranges along with the corresponding mean regression line are shown in Figure 5.1. (See Appendix B for more details on the regression analysis.) The test results from the specimens that did not fail in the net cross-section of the splice plate (S2a1 and S3c2) are not included in Figure 5.1 because they do not reflect the behavior observed in all the other test specimens. For the specimen that did not fail (S3d), the total number of cycles applied to the specimen was used for the regression analysis. This provides a conservative estimate of the fatigue strength of this test specimen. The goodness of fit of the mean regression line is measured using the correlation coefficient, r [5.1]. An r value of zero indicates that y is not linearly predicted in any useful way by x, and an r value of 1.0 indicates that y is linearly predicted perfectly by x.

The correlation coefficient for the test results plotted in Figure 5.1 is equal to 0.85. This correlation coefficient can now be compared to correlation coefficients of mean regression lines obtained with different stress range calculations, which are based on the following alternative cross-sectional areas:

- Alternative 1: The net section is obtained by deducting two holes for the plates with non-staggered holes and one hole for the plates with staggered holes. The test results expressed in terms of these net section stress ranges, $\Delta\sigma_{n,12}$, along with the corresponding mean regression line are shown in Figure 5.2. The correlation coefficient in this case is equal to 0.69.
- Alternative 2: The net section is obtained by deducting two holes for all the plates. The test results expressed in terms of these net section stress ranges, $\Delta\sigma_{n,2}$, along with the corresponding mean regression line are shown in Figure 5.3. The correlation coefficient in this case is equal to 0.78.

- Alternative 3: The net section is obtained according to the Cochrane rule. The test results expressed in terms of these net section stress ranges, $\Delta\sigma_{n,C}$, along with the corresponding mean regression line are shown in Figure 5.4. The correlation coefficient in this case is equal to 0.71.

A comparison of the correlation coefficients indicates that the test results are best predicted in terms of the corrected stress range. Consequently, it is proposed that the corrected stress range, $\Delta\sigma_{sc}$, be used to calculate the fatigue life of bearing-type shear splices.

5.4 Fatigue Design Curve

5.4.1 General

The mean regression line for the test results expressed in terms of the corrected stress range, $\Delta\sigma_{sc}$, is defined as follows (see Figure 5.1 and Appendix B)

$$\log(N) = 20.0 - 6.95 \log(\Delta s_{sc}) \tag{5.2}$$

Since this is the mean regression line, by definition 50% of all test results can be expected to fall below this curve. For the design and evaluation of the fatigue strength of bearing-type shear splices a smaller probability of failure is desirable, however. This can be achieved using different approaches. One approach consists of plotting the test results and comparing the test results to existing fatigue curves (in the following this is referred to the "existing curve" approach). This approach is straightforward, but does not indicate the level of reliability and is inconsistent with probabilistic approaches used in most modern structural design codes. An alternative procedure consists of defining confidence limits on the regression curve, thus defining a probability of failure. These confidence limits can either be compared to existing fatigue curves or they can be used directly for design. The lower confidence limit is generally found by subtracting a certain number of the standard error of estimate, s_e, from a reference value [5.4]. This results in a $\Delta s - N$ curve parallel to the mean regression curve. It is customary to take the lower confidence limit two standard errors of estimate below the mean regression line [1.4]. In the following, this method is referred to the "two standard deviation" approach. The design fatigue curve obtained in this way represents (approximately) a 97.5% probability of survival for an infinitely large number of normally distributed test results [5.5]. Because the sample size in this test program is sufficiently large, the distribution of the test results can be approximated by a normal distribution and alternative statistical analyses, such as the use of a Student's *t* distribution as proposed in reference [5.6], is not necessary.

5.4.2 "Existing Curve" Approach

Figure 5.5 shows a comparison between the test results and the detail categories B, C, D, and E curves defined in the AASHTO Specifications. For all the test results to lie above one of the AASHTO detail categories, the E curve would have to be selected. However, the use of this curve would lead to very conservative fatigue life predictions for the lower stress ranges. Furthermore, the statistical analysis carried out in Appendix B shows that the slope of the regression line of the test results ($m = 6.95$) is significantly different from the value $m = 3$ used in the AASHTO Specifications. Therefore, it seems clear that existing curves are not appropriate for fatigue life prediction of bearing-type shear splices.

5.4.3 "Two Standard Deviation" Approach

A simplified confidence interval of about 95 percent for the regression curve can be obtained by subtracting two standard error of estimate, s_e, from the mean value of $\log(N)$ [5.5]. If the slope of the regression line is rounded to 7.0 from the value 6.95 determined in the regression analysis, the intercept *a* and the standard error of estimate, s_e, are 20.1 and 0.255, respectively. The lower 95 percent confidence limit obtained is given by Equation 5.3. (For details see Appendix B.)

$$\log(N) = 19.6 - 7\log(\Delta s_{sc}) \tag{5.3}$$

Alternatively, Equation (5.3) can be written in the following form:

$$N = 3.98 \times 10^{19}\ \Delta\sigma_{sc}^{-7} \tag{5.4}$$

The proposed curve gives an excellent lower bound of the test results, as shown in Figure 5.6. Because only one runout was obtained in the experimental program, the definition of a constant amplitude fatigue limit is not possible. It is suggested that equation (5.4) be used for all stress ranges, $\Delta\sigma_{sc}$. This produces conservative predictions of the fatigue life for the lower stress ranges.

5.5 Calculation of Stress Range Correction Factors

5.5.1 General

In order to apply the approach presented in Section 5.3.3 in conjunction with the fatigue curve defined in the previous section, stress range correction factors, F_{sc}, for more general cases than the ones investigated in Chapters 3 and 4 were obtained using the finite element models presented in Chapter 3. Only flat plates with two, three or four lines of bolts (n_l = 2, 3, or 4 in Figure 5.7) and two rows of bolts (n_r = 2 in Figure 5.7) were considered. Although other shapes are used in structural engineering, the flat plates investigated here cover a large number of applications. The case with two rows of bolts leads to conservative stress range correction factors for plates with $n_r > 2$. The geometric parameters that were investigated are stagger, s, gage, g, and edge distance, e. In order for the approach to be used with any bolt hole diameter, D, these parameters were non-dimensionalized with respect to D. For practical reasons, the following limitations were imposed:

- $g \le 3D$
- $1.2D \le e \le 2.0D$

The limit imposed on the gage distance, g, is in accordance with the minimum bolt spacing allowed by S16.1. For values of $g > 3D$, staggering of the bolts is no longer required. The limits imposed on the edge distance, e, correspond to the majority of the cases encountered in practice.

5.5.2 Two Lines of Bolts

The stress concentration factor and the stress range correction factor, F_{sc}, for plates with two lines of bolts and varying stagger and gage and edge distances are presented in Table 5.5. A graphical representation of the effect of the gage distance, g, on F_{sc} is shown in Figure 5.8. The figure indicates that the gage distance has only a small effect on F_{sc}, and the most conservative results are obtained when g is maximum. The effect of the edge distance, e, on F_{sc} is shown in Figure 5.9. Based on the conclusions drawn from Figures 5.8 and 5.9, all further analyses are carried out for $g = 3D$ and varying edge distances. Table 5.6 presents values of F_{sc} for $g = 3D$, $1.2D \le e \le 2.0D$, and stagger values varying from 0.0 to about $4.5D$. These values are plotted in Figure 5.10 as a function of s/D for different e/D ratios.

5.5.3 Three and Four Lines of Bolts

The stress concentration factor and the stress range correction factor, F_{sc}, for three lines of bolts, $n_l = 3$, and stagger values varying from 0.0 to about $4.5D$, a gage distance of 3D, and edge distance varying from 1.2D to 2.0D are presented in Table 5.6. Because of the odd number of bolts perpendicular to the applied load, the two bolt configurations shown in Figure 5.11 have to be investigated. The configuration shown in Figure 5.11 (a) contains two bolt holes on the critical section (the edge holes) and the configuration shown in Figure 5.11 (b) contains only the center hole on the critical section. The results presented in Table 5.6 are shown graphically in Figure 5.12 for edge holes critical and in Figure 5.13 for center hole critical.

Table 5.6 presents the stress concentration factor, F_{sc}, for four lines of bolts, $n_l = 4$, and stagger values varying from zero to about $4.5D$, a gage distance of 3D, and edge distance varying from 1.2D to 2.0D. The results are also presented graphically in Figure 5.14.

5.5.4 Discussion

For design purposes the stress range correction factor, F_{sc}, can be obtained from Figures 5.10 and 5.12 to 5.14. It is desirable, however, to simplify these curves. Three levels of simplifications were investigated, namely,

- Use of a different upper bound curve for each of Figures 5.10 and 5.12 to 5.14 (Simplification 1).
- Use of a common upper bound curve for all the cases presented in the above figures (Simplification 2).
- Use of a constant stress range correction factor of 1.09, which corresponds to the maximum value in Table 5.6, no matter what the stagger, s, or the number of bolts, n_t, perpendicular to the applied load is (Simplification 3).

Although the differences in F_{sc} using these simplifications might first appear to be small, because of the shallow slope of the design fatigue curve they can have an important effect on the fatigue life calculations. In order to assess the effect of these various proposed simplifications, the ratio of the fatigue life predicted using the calculated stress correction factor and the approximate value based on the proposed simplifications have been calculated. This ratio of predicted fatigue life can be expressed as follows:

$$p_n = 100\left(\frac{F_{sc}}{F'_{sc}}\right)^7 \quad (5.5)$$

where

p_n : fatigue life using the simplified stress range correction factor, F'_{sc}, expressed as a percentage of the fatigue life calculated with the exact stress range correction factor, F_{sc}

Figure 5.15 illustrates the three simplifications outlined above for plates with two lines of bolts. Figures 5.16 to 5.18 show the percentage of the fatigue life, p_n, as a function of the stagger for the analyzed cases having two lines of bolts ($n_l = 2$) and for the three different simplifications shown in Figure 5.15. Similar results were obtained for three and four lines of bolts, but these are not presented herein. Although Simplification 1 is the least conservative of all the simplifications, it still results in very conservative predictions of the fatigue life for many different geometries. In view of the significant degree of conservatism in prediction of the fatigue life that may result from the use of any one of the three simplifications, it is recommended that Table 5.6 with the appropriate interpolations be used.

5.6 Comparison with other Test Results

From the over 500 tests on bolted shear splices that were reviewed in Chapter 2, only six—all of them investigated by Graf [2.43]—were carried out on specimens that had more or less snug-tightened bolts. Two of the Graf tests consisted of "loosely clenched" bolts (Series 0) and four tests used bolts that had a pretension of approximately 150 MPa (Series 11). Although this pretension is about 50% higher than the pretension applied to the bolts used in this study, it is only about 30% of the full pretension value appropriate for bolts of the grade used by Graf.

The geometry of the specimens tested by Graf is shown in Figure 5.19. The stress range correction factor, F_{sc}, for this geometry (determined using ABAQUS), the corrected stress range, $\Delta\sigma_{sc}$, and the number of cycles to failure, N, reported by Graf are presented in Table 5.7. The test results are plotted in Figure 5.20, which also shows the mean regression line for the test results presented in Section 5.3.3 with the corresponding 95% confidence interval. It can be observed that the Graf test results follow a slope consistent with the one established in this study. Furthermore, both of the test results from the specimens with loosely clenched bolts (Series 0 in Figure 5.20) fall within the 95 percent confidence interval. The four test results from Series 11 all fall above the upper 95 percent confidence limit. This is not surprising considering that the pretension in these specimens was higher than that present in the specimens investigated in this study. This higher pretension should, theoretically, result in more moderate bearing pressures and therefore in a smaller stress range correction factor, F_{sc}, than calculated for bearing-type splices.

The only fatigue test results on bearing-type shear splices with staggered holes that can be compared to the regression lines proposed in this study were obtained by DiBattista and Kulak [2.53]. Riveted diagonal members were taken from a dismantled bridge, and the component tested was the end connections (bottom and top chord attachments). The critical element was an angle, and it had staggered holes in two planes. Constant amplitude fatigue loading was used. Figure 5.21 shows the test results for the bottom (BD Series) and the top chord attachments (TD Series) using a net section orthogonal to the direction of the load to calculate the stress range, as proposed by DiBattista and

Kulak. The stress range correction factor, F_{sc}, for the two series, as well as the corrected stress range, $\Delta\sigma_{sc}$, and the number of cycles to failure, *N*, are presented in Table 5.8. The stress range correction factors were determined using Table 5.6 . Since the critical member of the specimens consisted of angle sections and not flat plates, it cannot be necessarily expected that the correction factors developed for flat plates will apply. The test results are plotted in terms of the corrected stress range in Figure 5.22. The following observations can be made:

- The test results follow a slope similar to the one established in this study.
- Using the corrected stress ranges, as shown in Figure 5.22, gives more consistent results for the two series (BD and TD) compared to the results presented with the stress range calculated based on an orthogonal net section, as shown in Figure 5.21.
- All test results obtained by DiBattista and Kulak fall well below the lower 95 percent confidence limit established in Section 5.3.3.

The last observation is in contradiction with the expectation that, because of clamping forces that might be present in riveted connections, the stress concentration should be more moderate than in a truly bearing-type connection. As a result, a riveted connection should have a longer fatigue life than a bearing-type bolted one. The following reasons might have contributed to these lower fatigue results:

- Approximate value of F_{sc}: The stress range correction factor developed for flat plates was used for angles. Even though both legs of the angles were connected, some shear lag might have been present, resulting in higher stress concentrations around the critical hole.
- Loading condition: The I-shaped diagonals consisted of four angle sections as flanges and a flat plate as the web. In the testing it was assumed that the stresses were uniformly distributed across the entire cross-section. However, it is possible that one of the angles was subjected to a higher load than the others, resulting in higher stress concentrations around the critical hole.
- Hole fabrication: The holes were sub-punched and reamed. If the reaming was not done carefully, then some of the microcracks caused by the punching of the holes might not have been eliminated entirely.
- Pre-existing damage: Calculations by DiBattista and Kulak showed that no pre-existing damage was present before the specimens were tested in the laboratory. The constant amplitude fatigue limit was assumed to be at 48 MPa, as proposed in the AREA Code [5.7], and the maximum stress range during the life of the bridge was around 40 MPa. However, both the constant amplitude fatigue limit as well as the maximum stress range are estimates, and it can not be stated with absolute certainty that no pre-existing fatigue damage was present.

- Corrosion: Corrosion can significantly affect the fatigue life of a structure (see for example reference [5.8]). DiBattista and Kulak noted that corrosion of the diagonals was light. Therefore it is unlikely that the difference between their test results and the fatigue curve established in this study can be explained solely by the effect of corrosion.

Table 5.1 – Summary of test results.

Set	Specimen Designation	Load Range [kN]	Fatigue Life	$y = \log(N)$	$\bar{y}$	s_y
$S0_{190}$	S0a	190	2 167 000	6.336	6.328	0.43937
	S0b1	190	5 800 000	6.763		
	S0b2	190	767 000	5.885		
$S0_{240}$	S0c1	240	355 000	5.550	5.702	0.13242
	S0c2	240	620 000	5.792		
	S0d	240	581 000	5.764		
$S1_{200}$	S1a1	200	255 000	5.407	5.694	0.43381
	S1a2	200	303 000	5.481		
	S1b	200	1 558 000	6.193		
$S1_{160}$	S1c1	160	2 827 000	6.451	6.615	0.27348
	S1c2	160	2 900 000	6.462		
	S1d	160	8 520 000	6.930		
$S2_{200}$	S2a1	200	1 062 000	6.026	5.775	0.2714
	S2a2	200	307 000	5.487		
	S2b	200	649 000	5.812		
$S2_{160}$	S2c1	160	3 816 000	6.582	6.396	0.20176
	S2c2	160	1 518 000	6.181		
	S2d	160	2 662 000	6.425		
$S3_{200}$	S3a1	200	685 000	5.836	5.796	0.07341
	S3a2	200	695 000	5.842		
	S3b	200	515 000	5.712		
G_{240}	Ga1	240	518 000	5.714	5.562	0.13276
	Ga2	240	295 000	5.470		
	Gb	240	318 000	5.502		
G_{190}	Gc1	190	1 915 000	6.282	6.248	0.23265
	Gc2	190	2 894 000	6.461		
	Gd	190	1 000 000	6.000		

Table 5.2 – Results of the F and t tests using a 95 percent confidence interval.

Set 1	Set 2	Parameter	F (calculated)	F_{lim} (tabulated)	t (calculated)	t_{lim} (tabulated)	Comment
$S1_{200}$	$S2_{200}$	Hole Stagger (25mm vs. 51mm)	2.56	19.0	0.2764	2.776	No significant difference
$S1_{200}$	$S3_{200}$	Hole Stagger (25mm vs. 76mm)	34.9	19.0	0.4054	2.776	No significant difference
$S2_{200}$	$S3_{200}$	Hole Stagger (51mm vs. 76mm)	13.7	19.0	0.1314	2.776	No significant difference
$S1_{160}$	$S2_{160}$	Hole Stagger (25mm vs. 51mm)	1.84	19.0	1.115	2.776	No significant difference
$S1_{200}$	G_{240}	Gage Width (44mm vs. 60mm)	10.7	19.0	0.5014	2.776	No significant difference
$S1_{160}$	G_{190}	Gage Width (44mm vs. 60mm)	1.38	19.0	1.770	2.776	No significant difference
G_{240}	$S0_{240}$	Presence or Absence of Stagger	1.01	19.0	1.294	2.776	No significant difference
G_{190}	$S0_{190}$	Presence or Absence of Stagger	3.57	19.0	0.2792	2.776	No significant difference

Table 5.3 – SCF_i for the investigated splice plates and considered cross-sections i.

Plate	σ_{peak} [MPa]	SCF_g	$SCF_{n,1}$	$SCF_{n,2}$	$SCF_{n,C}$
P	3.59	3.80	3.10	2.39	2.39
S0	3.73	3.95	3.22	2.48	2.48
S1	4.53	4.11	3.22	2.33	2.49
S2	4.59	4.17	3.26	2.36	3.00
S3	4.59	4.17	3.26	2.36	3.26
G	3.86	4.09	3.33	2.57	2.67
$\boldsymbol{r_i}$		1.10	1.08	1.10	1.37

$$r_i = \frac{\max(SCF_i)}{\min(SCF_i)}$$

Table 5.4 – Calculation of SFC , F_{sc} , and of Δs_{sc} for the test specimens.

Set of Tests	σ_{max} [MPa]	σ_g [MPa]	*SCF*	F_{sc}	ΔP [kN]	A_g [mm^2]	$\Delta\sigma_g$ [MPa]	$\Delta\sigma_{sc}$ [MPa]
P	3.59	0.94	3.80	0.96	240	2117	113	109
$S0_{240}$	3.73	0.94	3.95	1.00	240	2117	113	113
$S0_{190}$					190		90	90
$S1_{200}$	4.53	1.10	4.11	1.04	200	1815	110	115
$S1_{160}$					160		88	92
$S2_{200}$	4.59	1.10	4.17	1.06	200	1815	110	116
$S2_{160}$					160		88	93
$S3_{200}$	4.59	1.10	4.17	1.06	200	1815	110	116
$S3_{130}$					130		72	76
G_{240}	3.86	0.94	4.09	1.03	240	2117	113	117
G_{190}					190		90	93

$SCF = s_{max} / s_g$

$F_{sc} = SFC_i / SFC_{S0}$

$\Delta\sigma_{sc} = F_{sc}\,\Delta\sigma_g$

Table 5.5 – Calculation of F_{sc} for the test specimens and additional cases.

Specimen	n_r	n_l	***D***	***e/D***	***g/D***	***s/D***	$s_{max,o}$	A_g	***SCF***	F_{sc}
			[mm]				**[MPa]**	**[mm^2]**		
S0	2	2	20.6	1.23	2.93	0.0	3.73	2118	3.95	1.00
P	3	"	"	"	"	"	3.59	2118	3.80	0.96
S1	2	"	"	"	2.16	1.23	4.50	1815	4.08	1.03
S2	"	"	"	"	"	2.47	4.59	1815	4.17	1.05
S3	"	"	"	"	"	3.70	4.59	1815	4.17	1.05
	"	"	"	"	"	4.93	4.60	1815	4.18	1.06
	"	"	"	"	2.52	0.62	4.08	1958	4.00	1.01
	"	"	"	"	"	1.23	4.17	1958	4.08	1.03
	"	"	"	"	"	2.47	4.28	1958	4.19	1.06
	"	"	"	"	"	3.70	4.28	1958	4.19	1.06
	"	"	"	"	2.93	0.62	3.79	2118	4.01	1.02
G	"	"	"	"	"	1.23	3.86	2118	4.09	1.04
	"	"	"	"	"	2.47	3.97	2118	4.20	1.06
	"	"	"	"	"	3.70	4.00	2118	4.24	1.07
	"	"	"	1.85	2.16	1.23	3.43	2299	3.94	1.00
	"	"	"	2.16	"	"	3.18	2543	4.04	1.02
	"	"	"	2.47	"	"	3.00	2783	4.17	1.06
	"	"	"	1.85	"	2.47	3.48	2299	4.00	1.01
	"	"	"	2.16	"	"	3.18	2543	4.04	1.02
	"	"	"	2.47	"	"	2.96	2783	4.12	1.04
	"	"	"	1.85	"	3.70	3.47	2299	3.99	1.01
	"	"	"	2.16	"	"	3.17	2543	4.03	1.02
	"	"	"	2.47	"	"	2.95	2783	4.11	1.04

Table 5.6 –Stress range correction factor, F_{sc} .

e/D	***s/D***	$\boldsymbol{F_{sc}}$			
		$n_l = 2$	$n_l = 3$ (edge holes critical)	$n_l = 3$ (center hole critical)	$n_l = 4$
1.2	0.0	1.01	1.02	1.02	1.03
1.2	1.4	1.05	1.03	1.02	1.04
1.2	2.8	1.08	1.05	1.00	1.07
1.2	4.2	1.09	1.06	0.97	1.08
1.4	0.0	0.97	0.97	0.97	0.96
1.4	1.4	1.01	0.99	0.97	0.99
1.4	2.8	1.04	1.02	0.98	1.02
1.4	4.2	1.05	1.02	0.98	1.03
1.6	0.0	0.96	0.94	0.94	0.93
1.6	1.4	1.00	0.97	0.98	0.99
1.6	2.8	1.03	1.00	1.00	1.01
1.6	4.2	1.03	1.00	0.99	1.01
1.8	0.0	0.96	0.93	0.93	0.91
1.8	1.4	1.00	0.95	1.01	1.01
1.8	2.8	1.02	0.99	1.01	1.02
1.8	4.2	1.03	0.99	1.00	1.00
2.0	0.0	0.96	0.94	0.94	0.92
2.0	1.4	1.00	0.95	1.03	1.03
2.0	2.8	1.03	0.99	1.03	1.03
2.0	4.2	1.03	0.99	1.01	1.02

Table 5.7 – Results of Series 0 and Series 11 tested by Graf [2.43].

Series	Specimen	$\Delta\sigma_g$ [MPa]	F_{sg}	$\Delta\sigma_{sc}$ [MPa]	N
Series 0	4	125	1.067	133	372 000
	14	101	1.067	108	1 384 000
Series 11	7	195	1.067	208	78 000
	9	156	1.067	166	249 000
	12	140	1.067	149	517 000
	11	125	1.067	133	1 005 000 [1)]

1) Run-out

Table 5.8 – Results of BD and TD Series tested by DiBattista and Kulak [2.53].

Series	Specimen	$\Delta\sigma_g$ [MPa]	F_{sg}	$\Delta\sigma_{sc}$ [MPa]	N
BD-Series	BD1	59.2	0.94	56	2 401 580
	BD2	55.9	0.94	53	3 958 270
	BD3	59.2	0.94	56	2 849 000
	BD4	53.5	0.94	50	5 250 610
TD-Series	TD1	59.0	0.98	58	1 944 670
	TD2	57.1	0.98	56	2 415 840
	TD3	53.4	0.98	52	2 415 140

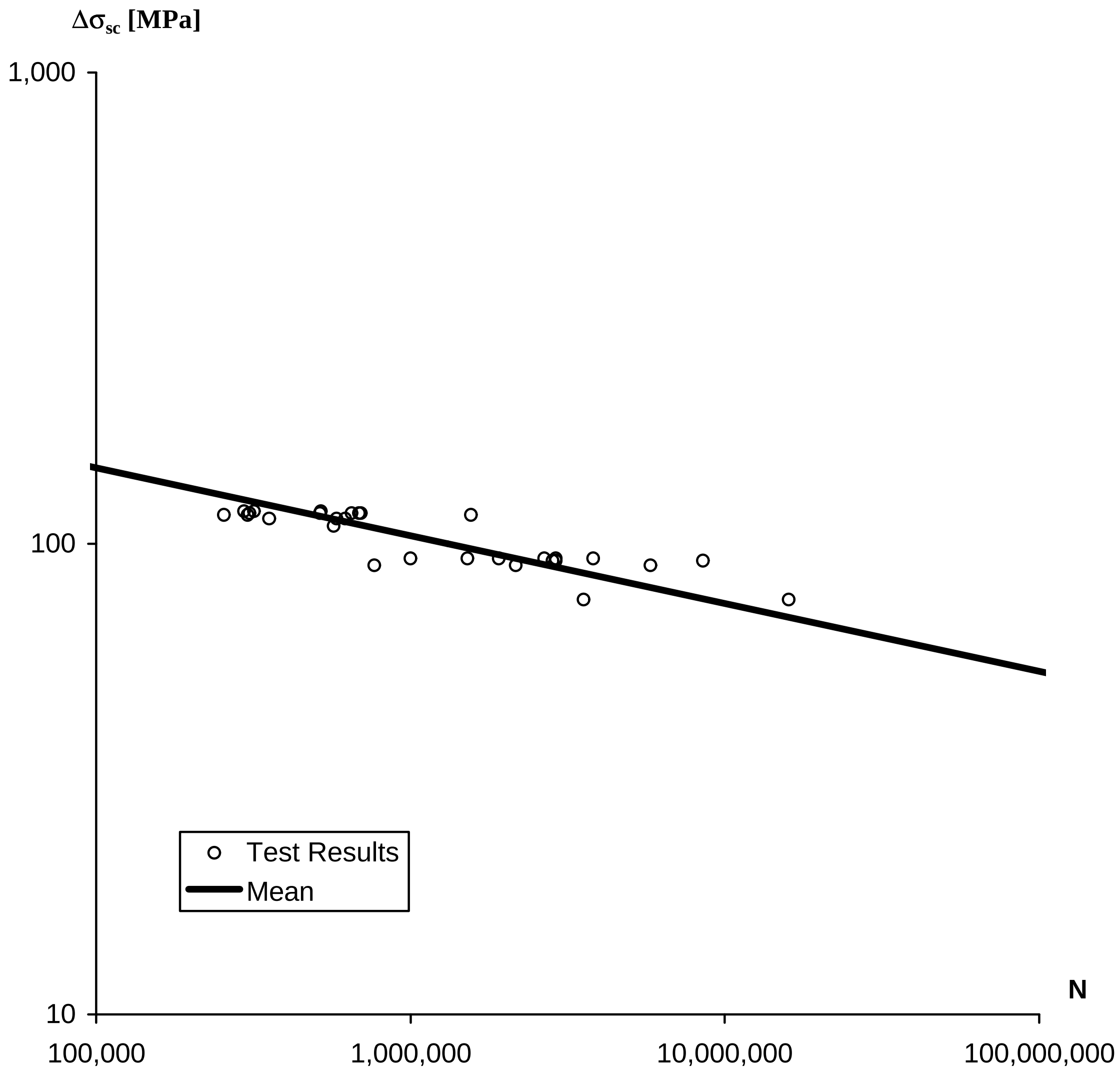

Figure 5.1 – Test results and mean regression line for the corrected stress range, $\Delta\sigma_{sc}$.

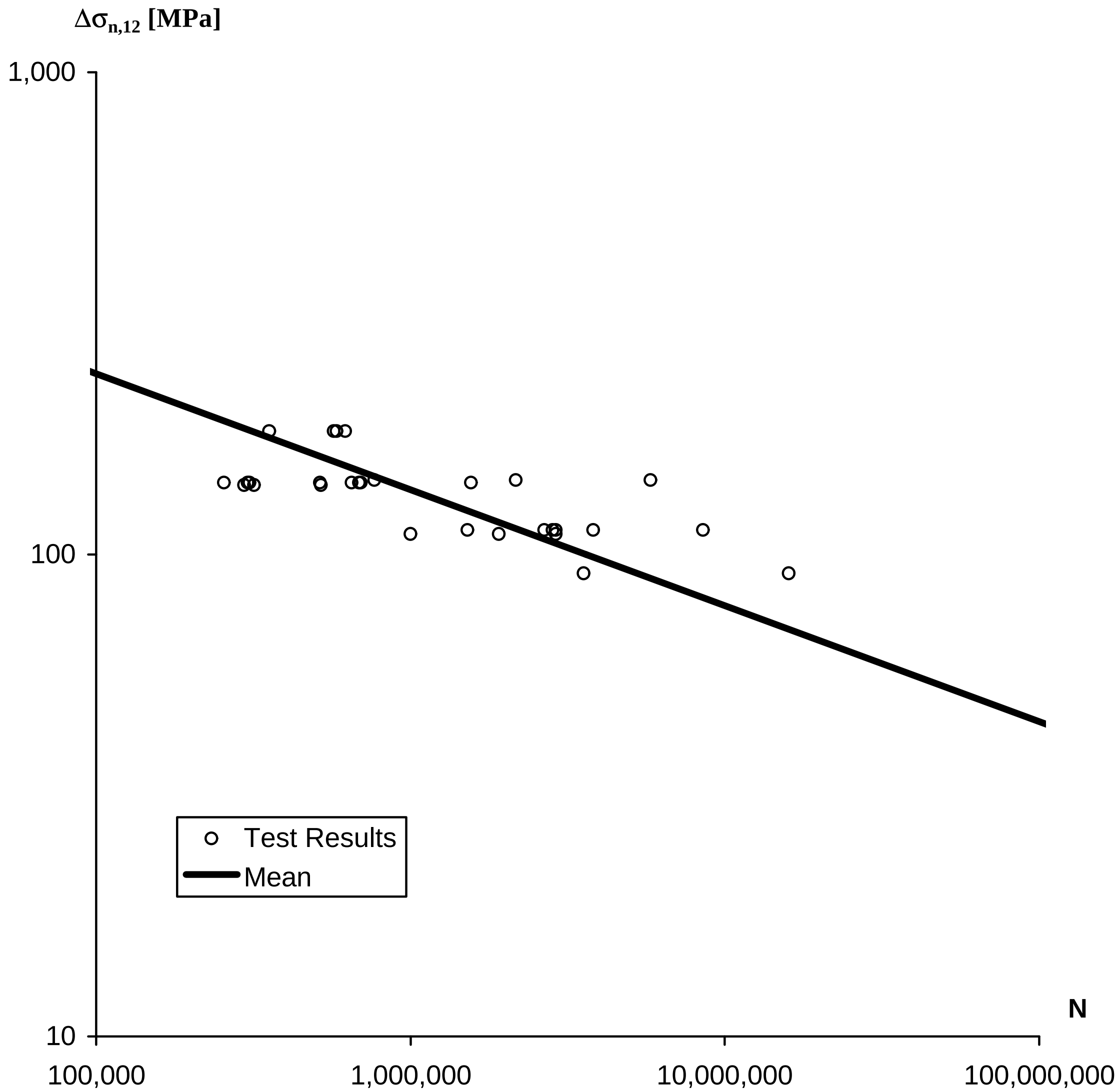

Figure 5.2 – Test results and mean regression line based on Alternative 1 to calculate the stress range.

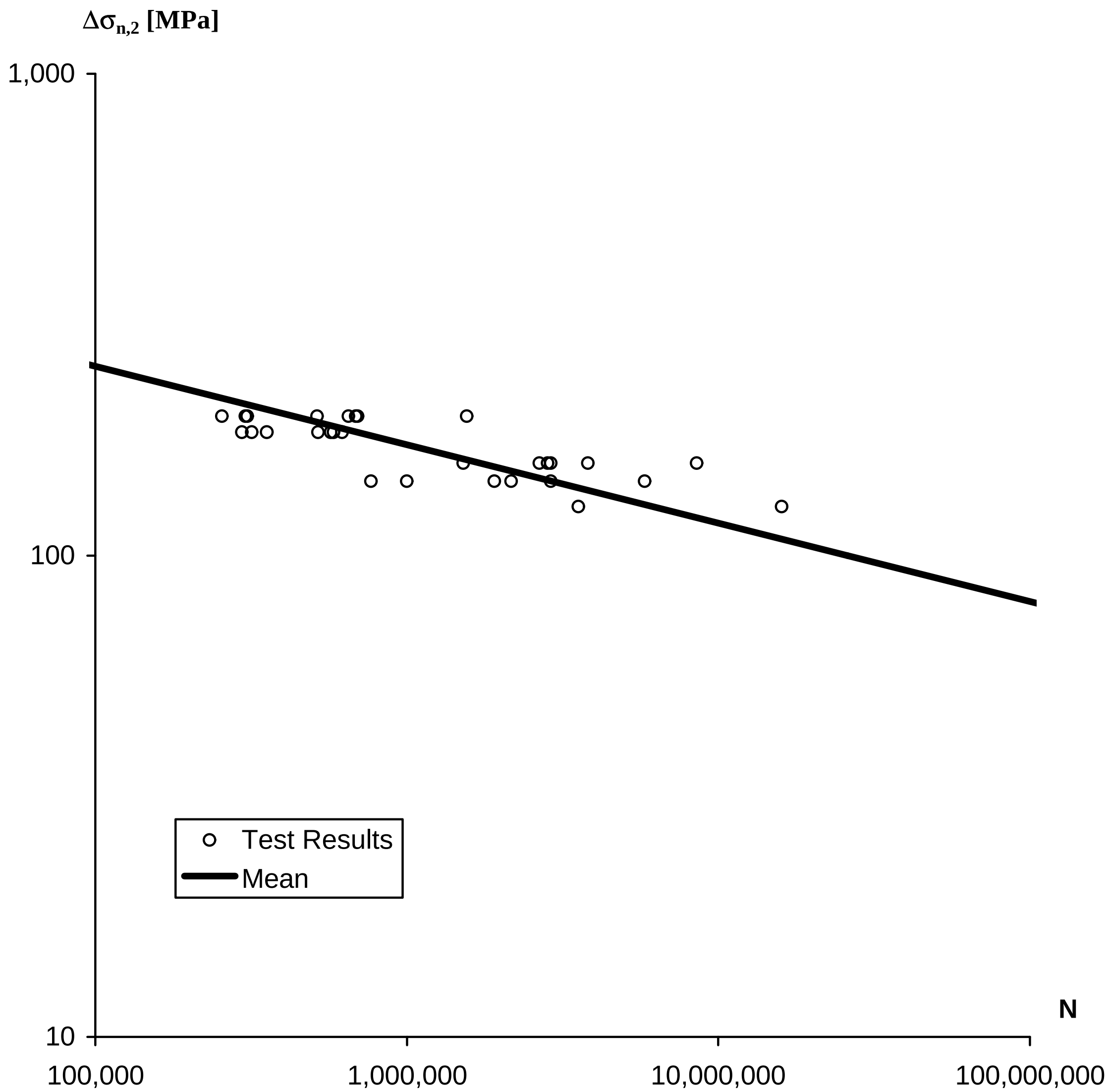

Figure 5.3 – Test results and mean regression line based on Alternative 2 to calculate the stress range.

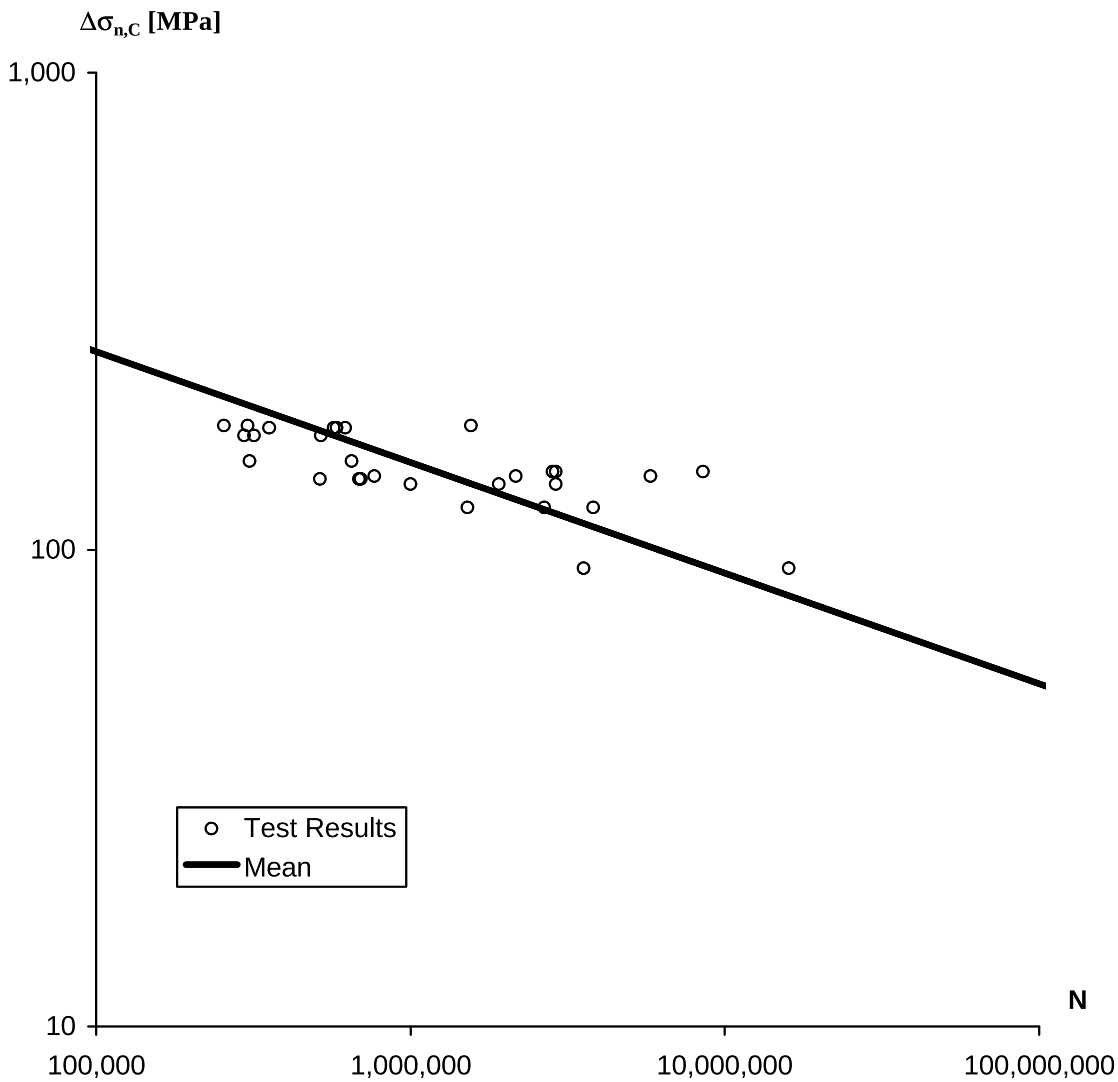

Figure 5.4 – Test results and mean regression line based on Alternative 3 (Cochrane's rule) to calculate the stress range.

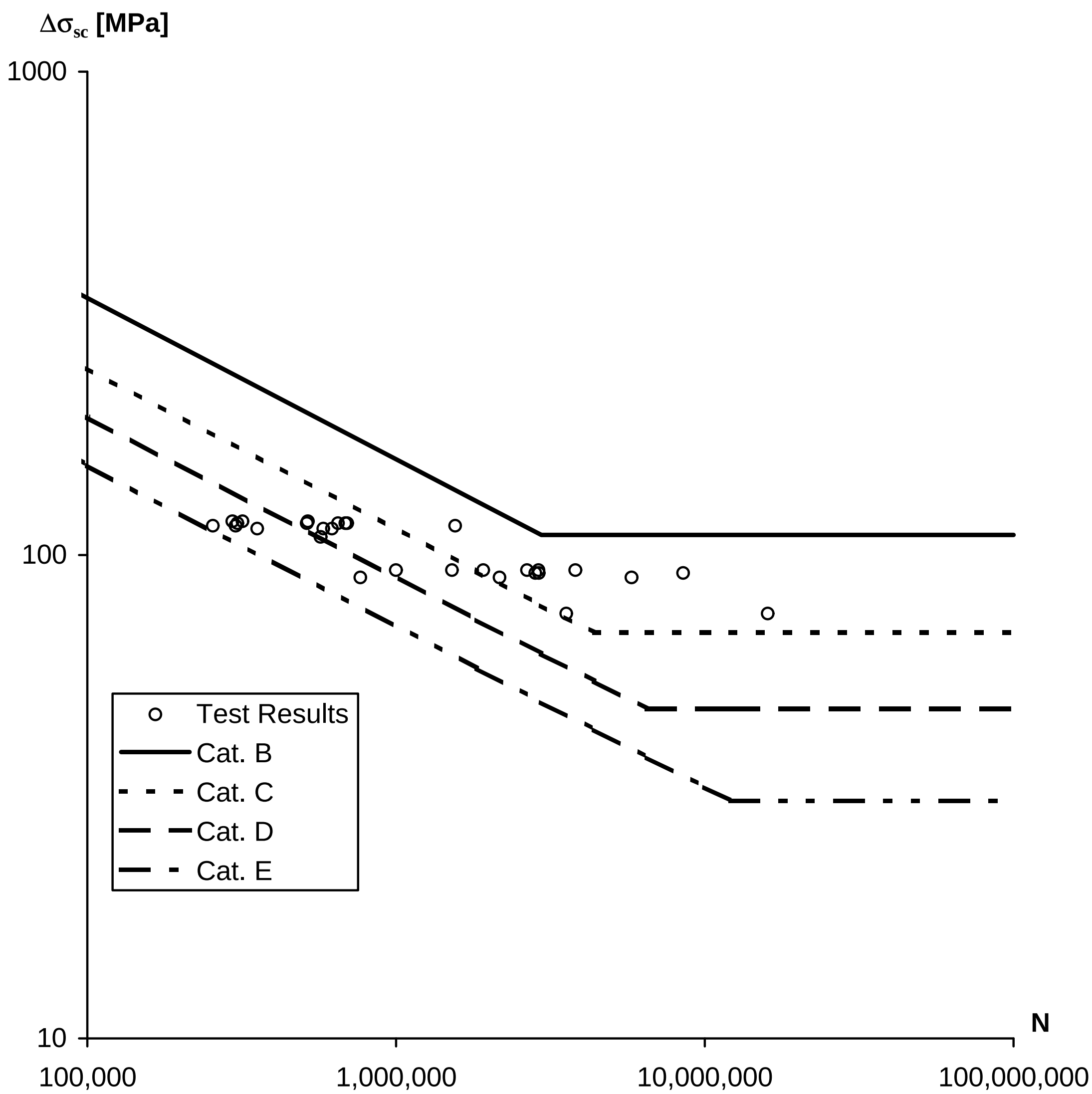

Figure 5.5 – Comparison of test results with existing fatigue curves.

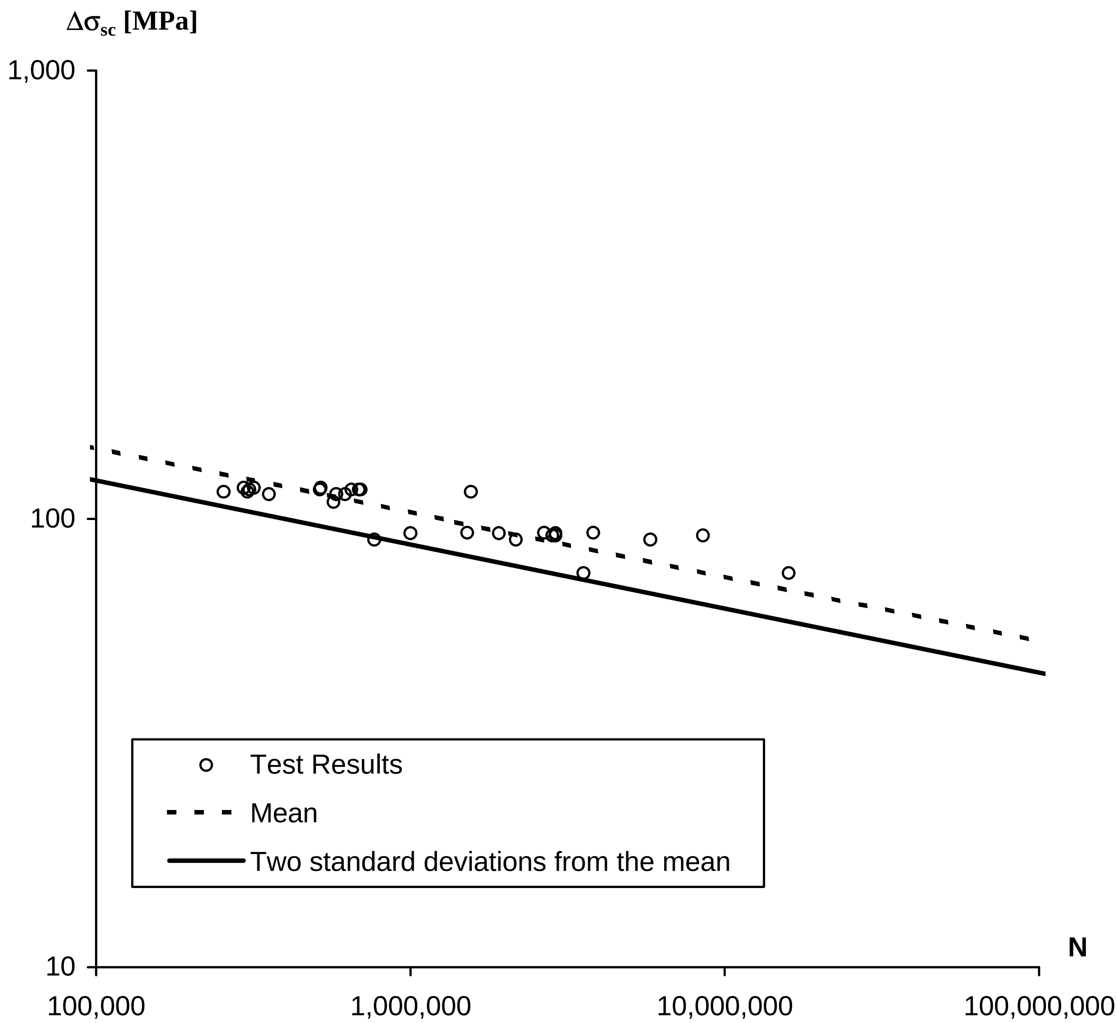

Figure 5.6 – Test results with regression and fatigue design curves.

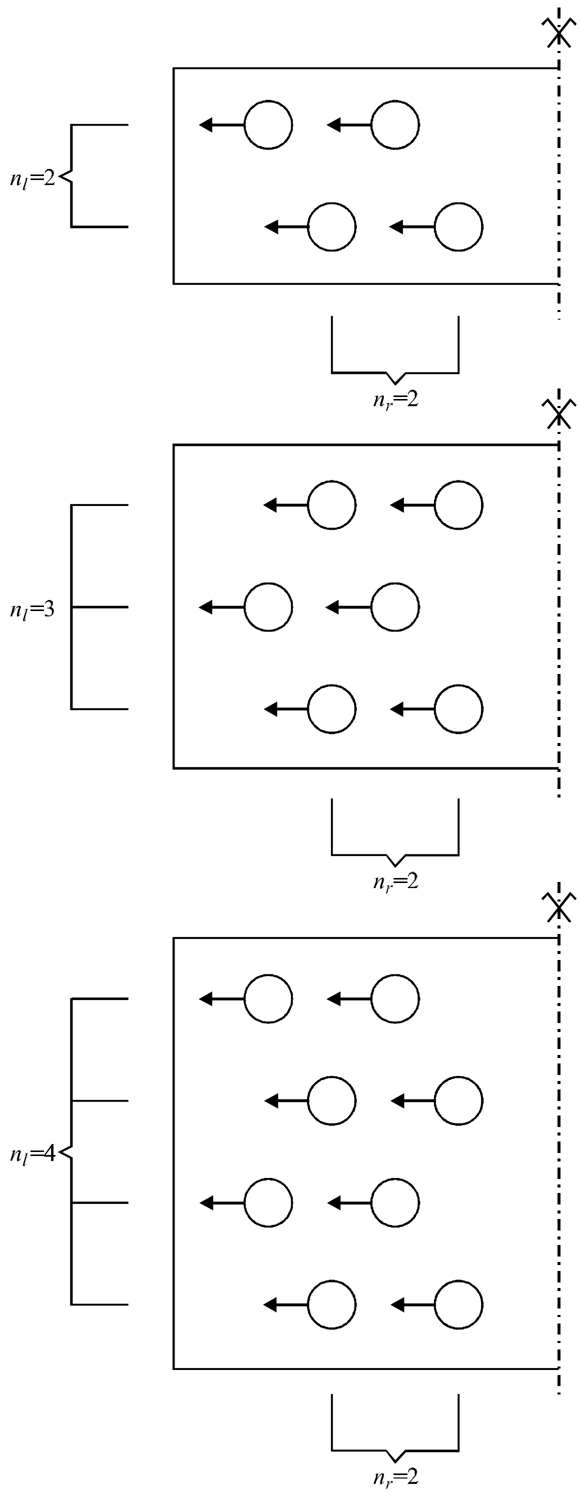

Figure 5.7 – Definition of lines of bolts, n_l , and rows of bolts, n_r .

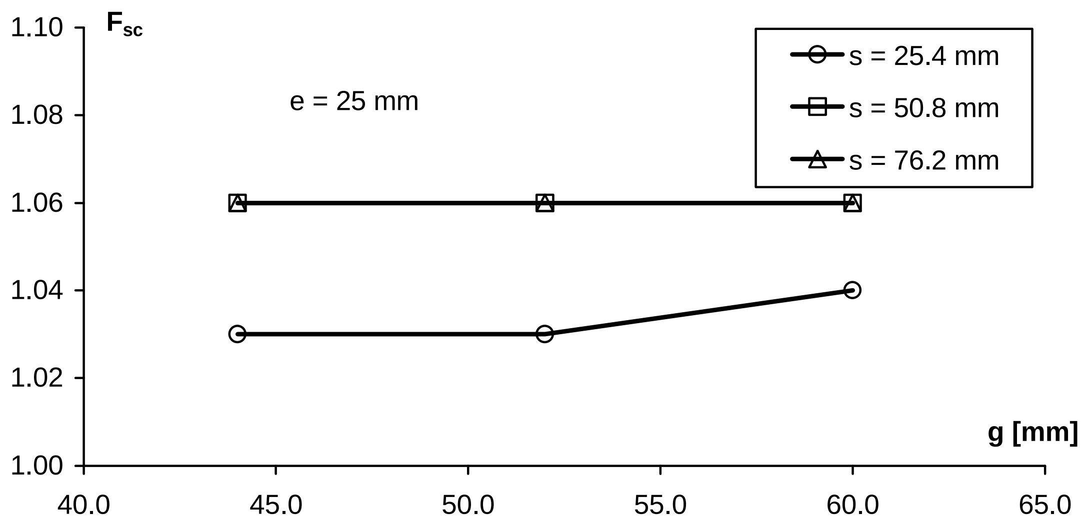

Figure 5.8 – F_{sc} as a function of gage distance, g.

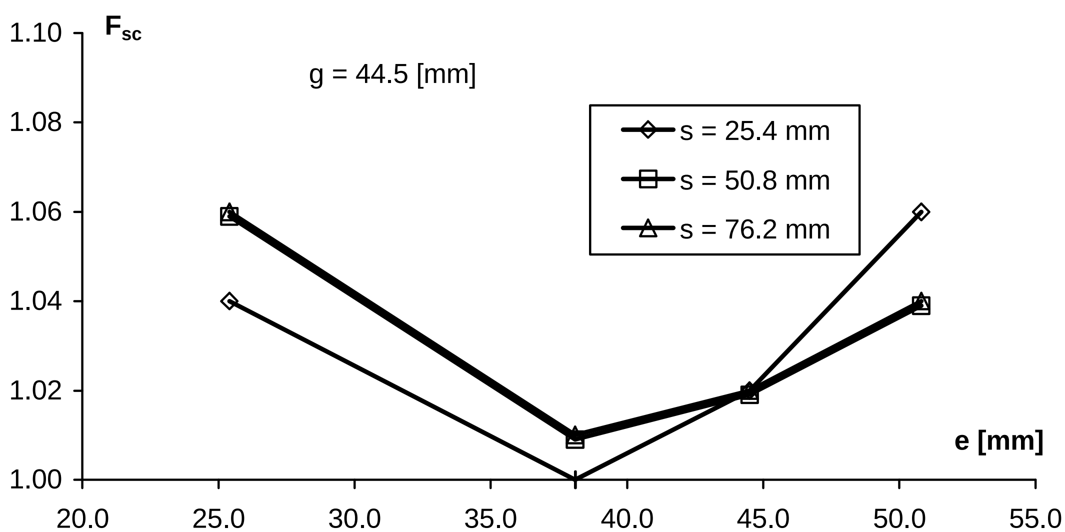

Figure 5.9 – F_{sc} as a function of edge distance, e.

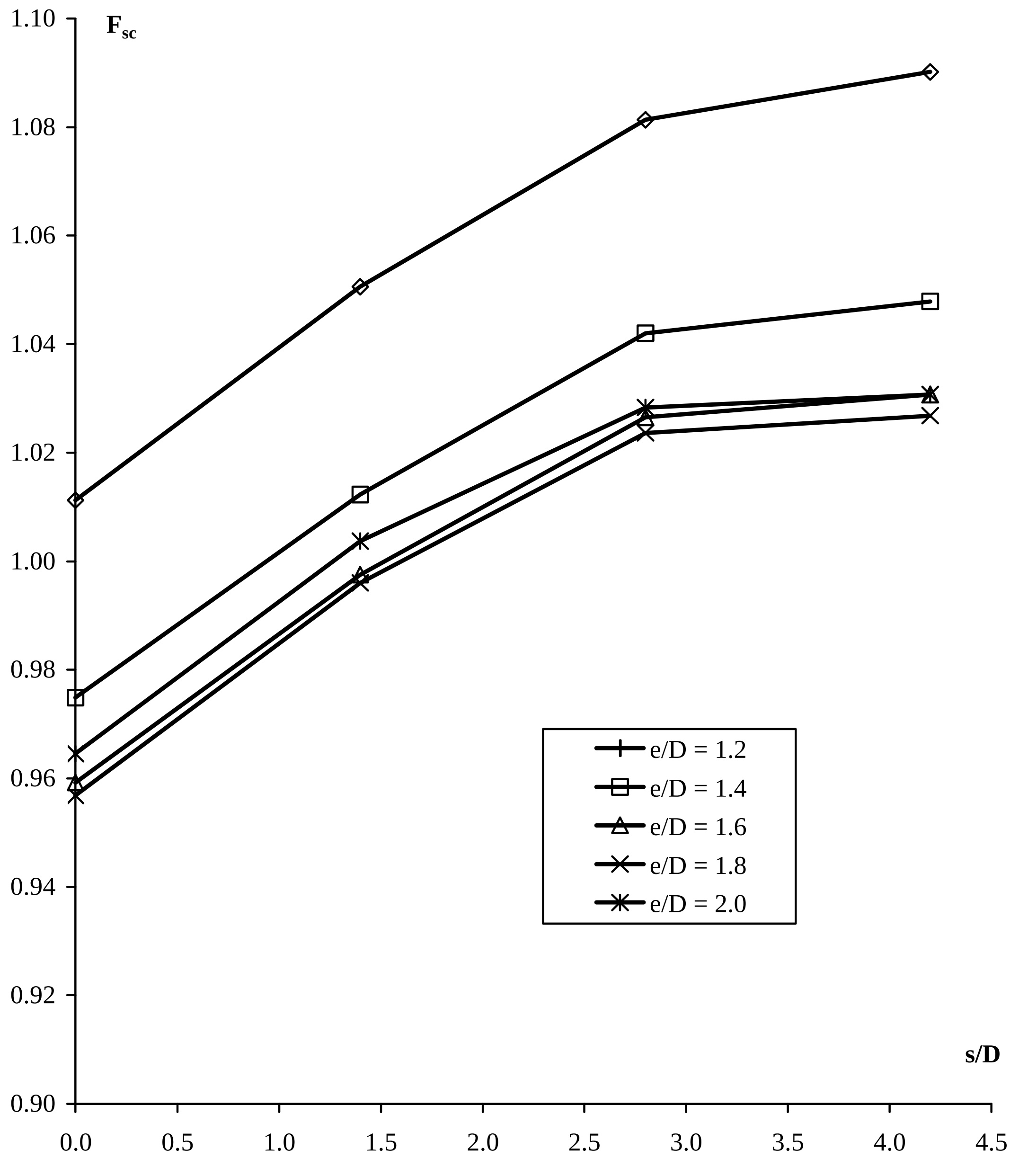

Figure 5.10 – F_{sc} as a function of stagger and edge distance for $n_l = 2$.

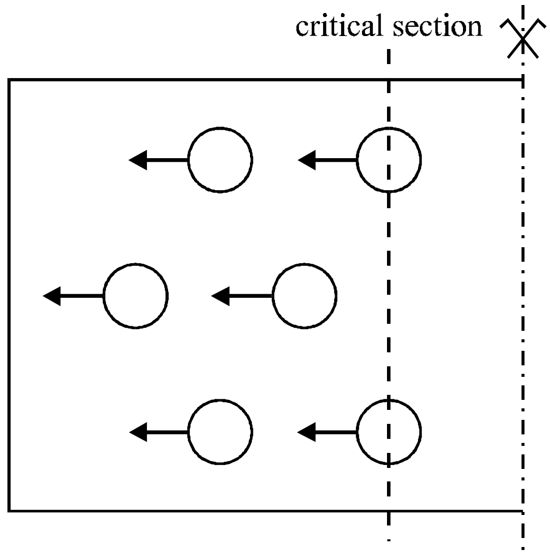

a) edge holes critical

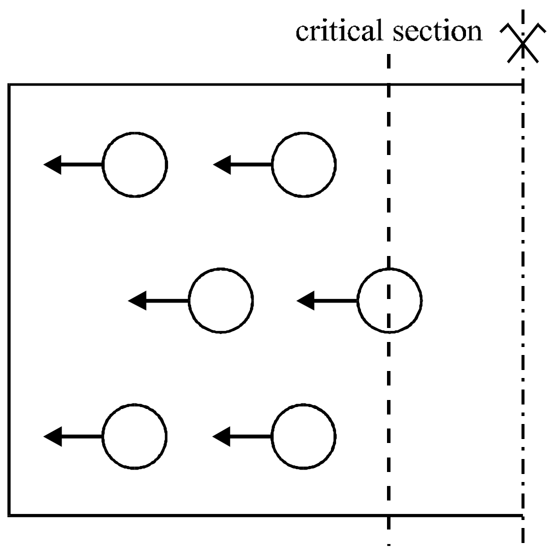

b) center hole critical

Figure 5.11 – Definition of critical holes for $n_l = 3$.

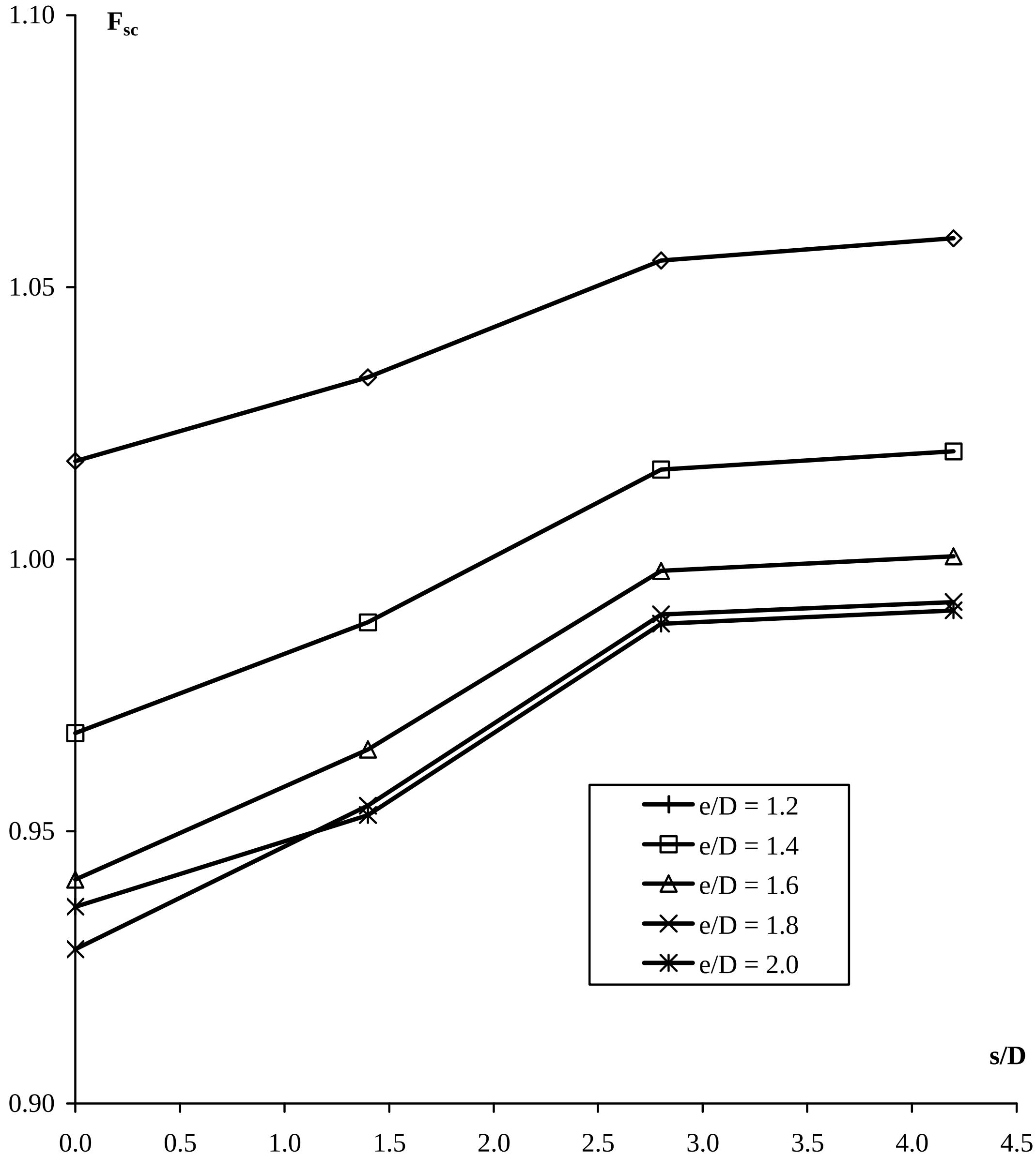

Figure 5.12 – F_{sc} as a function of stagger and edge distance for $n_l = 3$ (edge holes critical).

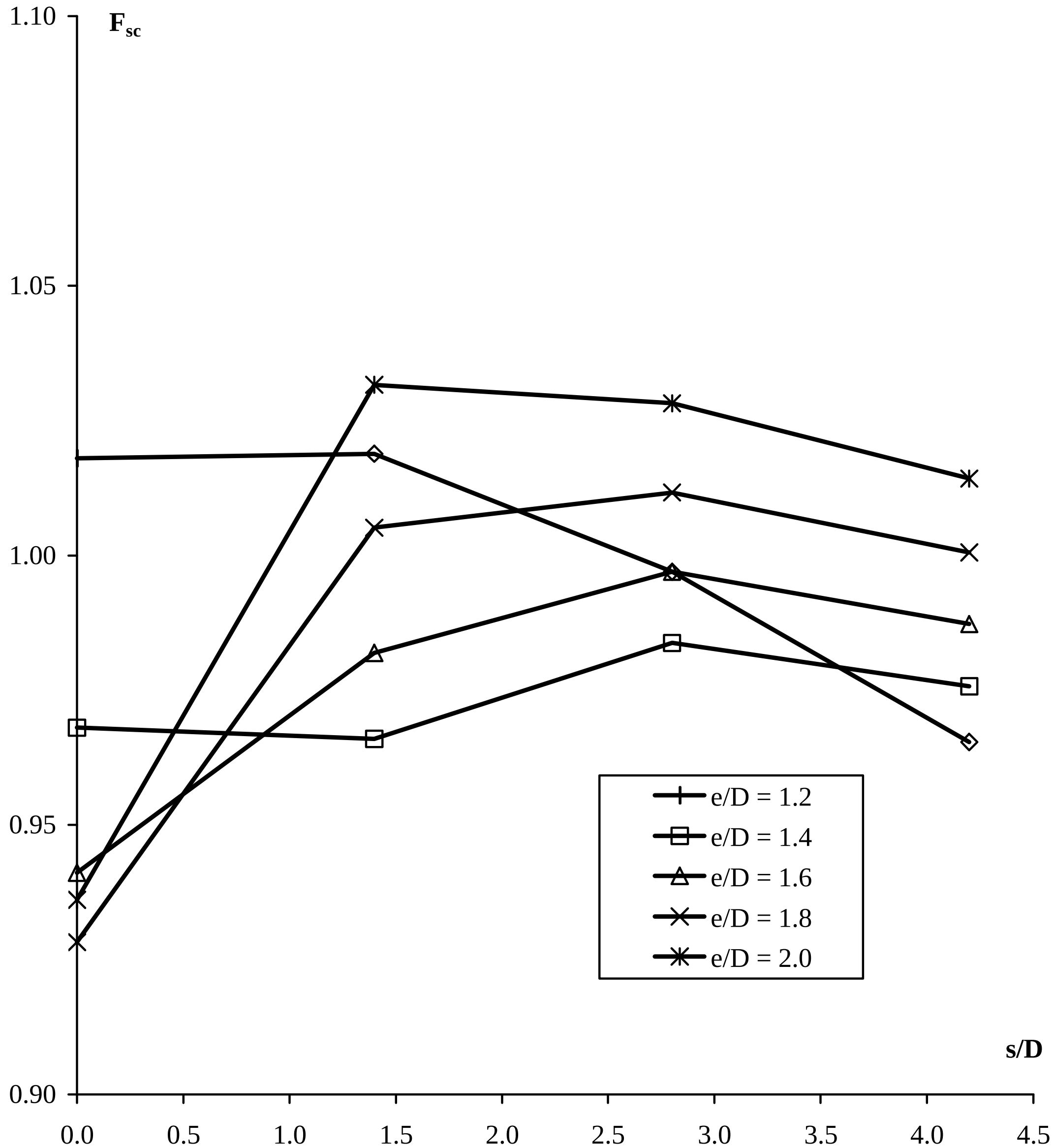

Figure 5.13 – F_{sc} as a function of stagger and edge distance for $n_l = 3$ (center hole critical).

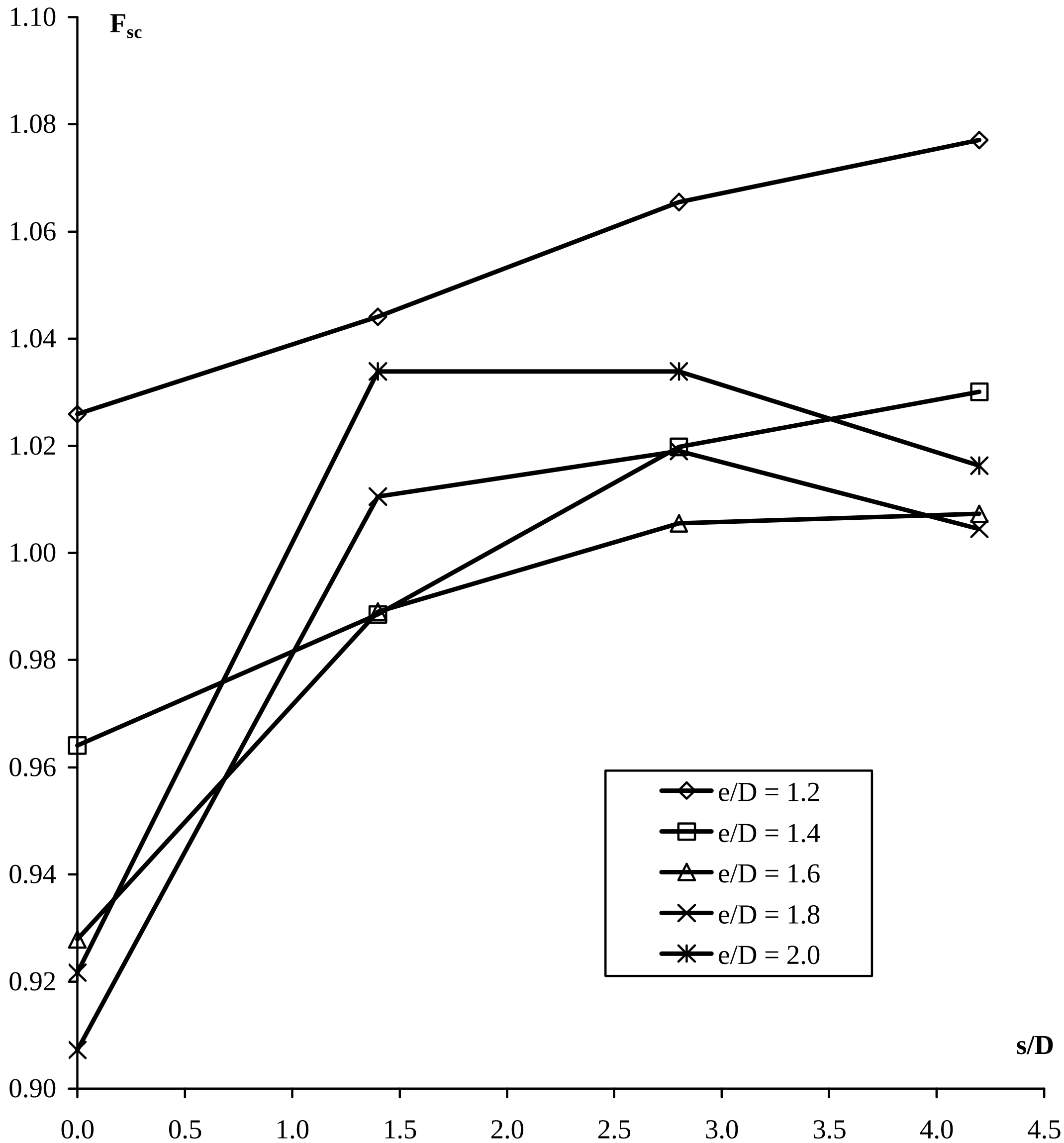

Figure 5.14 – F_{sc} as a function of stagger and edge distance for $n_l = 4$.

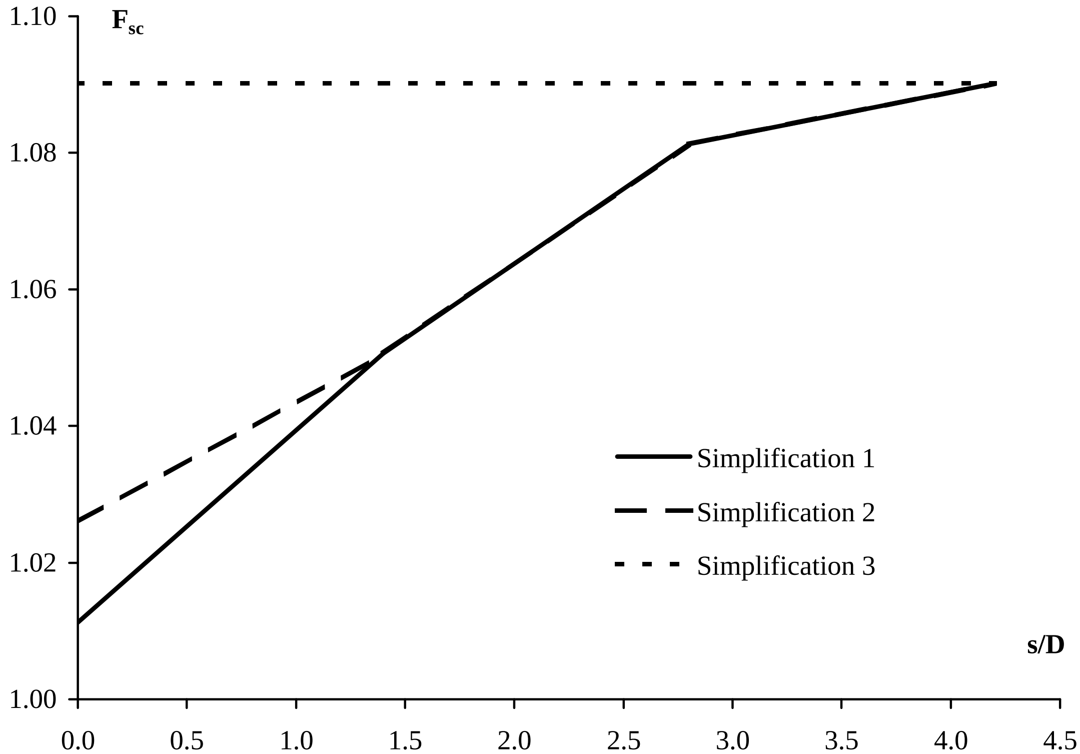

Figure 5.15 – Simplifications for the determination of F_{sc} $(n_l = 2)$.

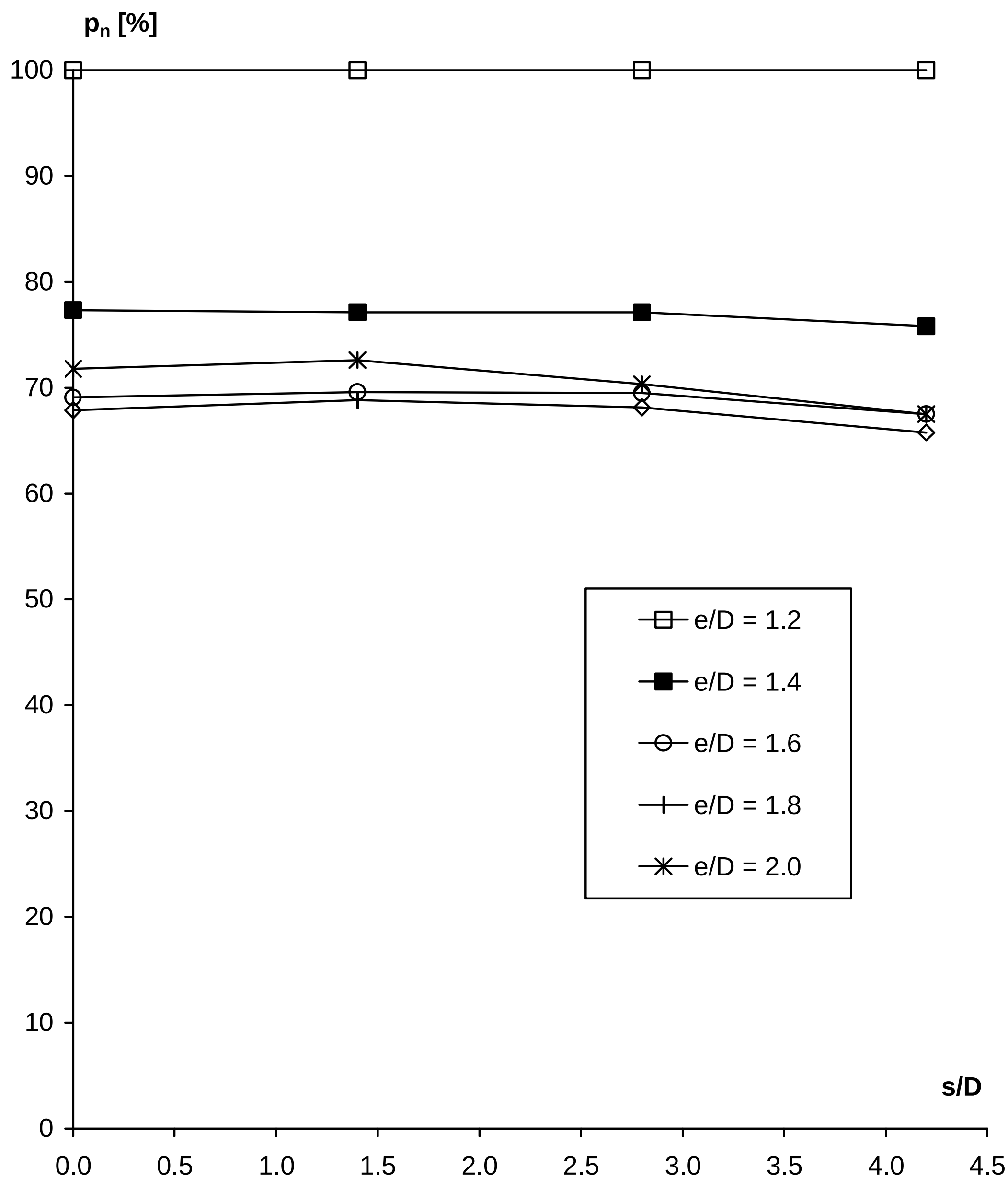

Figure 5.16 – Percentage of fatigue life, p_n, using simplification 1 for F_{sc} $(n_l = 2)$.

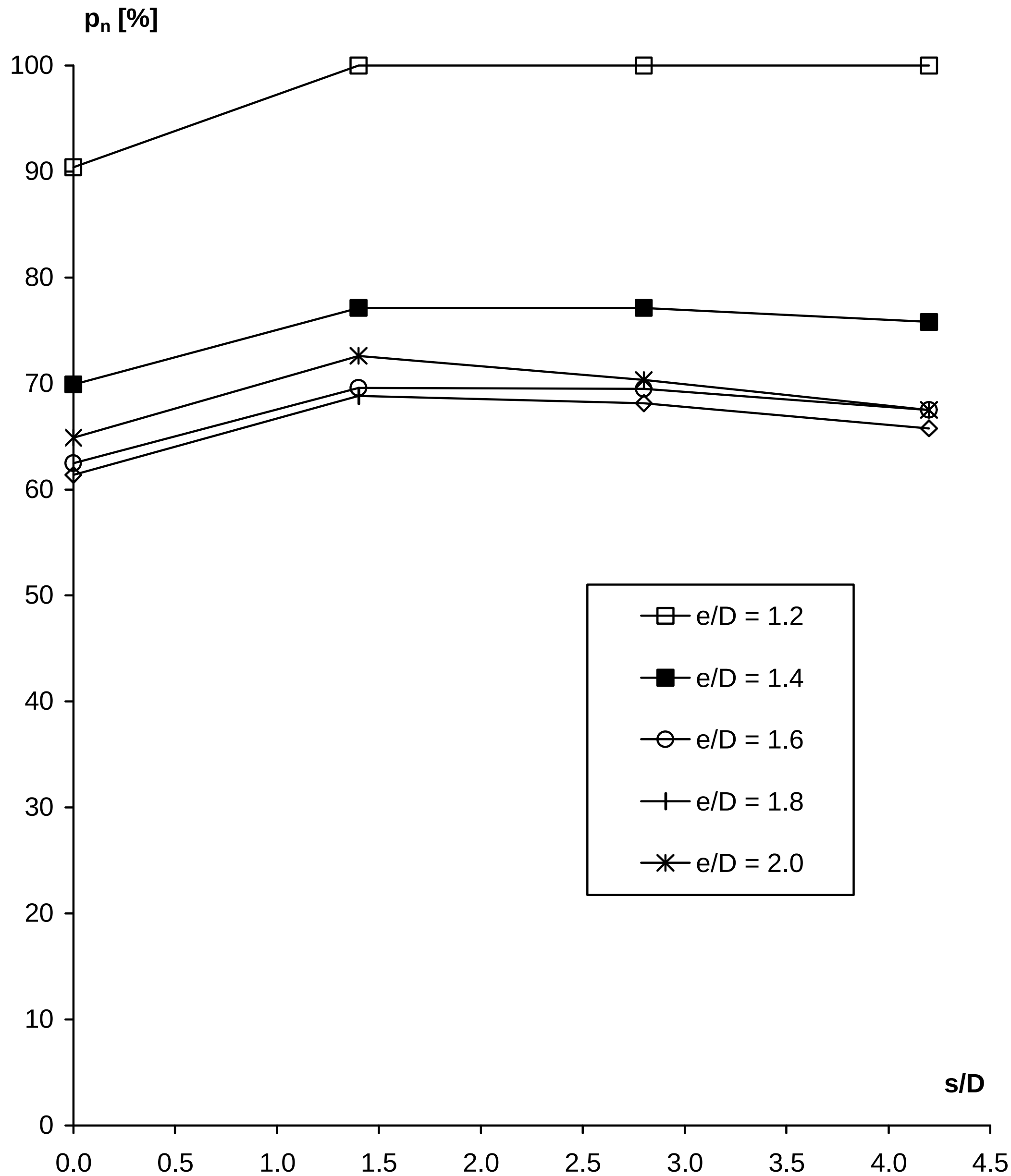

Figure 5.17 – Percentage of fatigue life, p_n, using simplification 2 for $F_{sc}(n_l = 2)$.

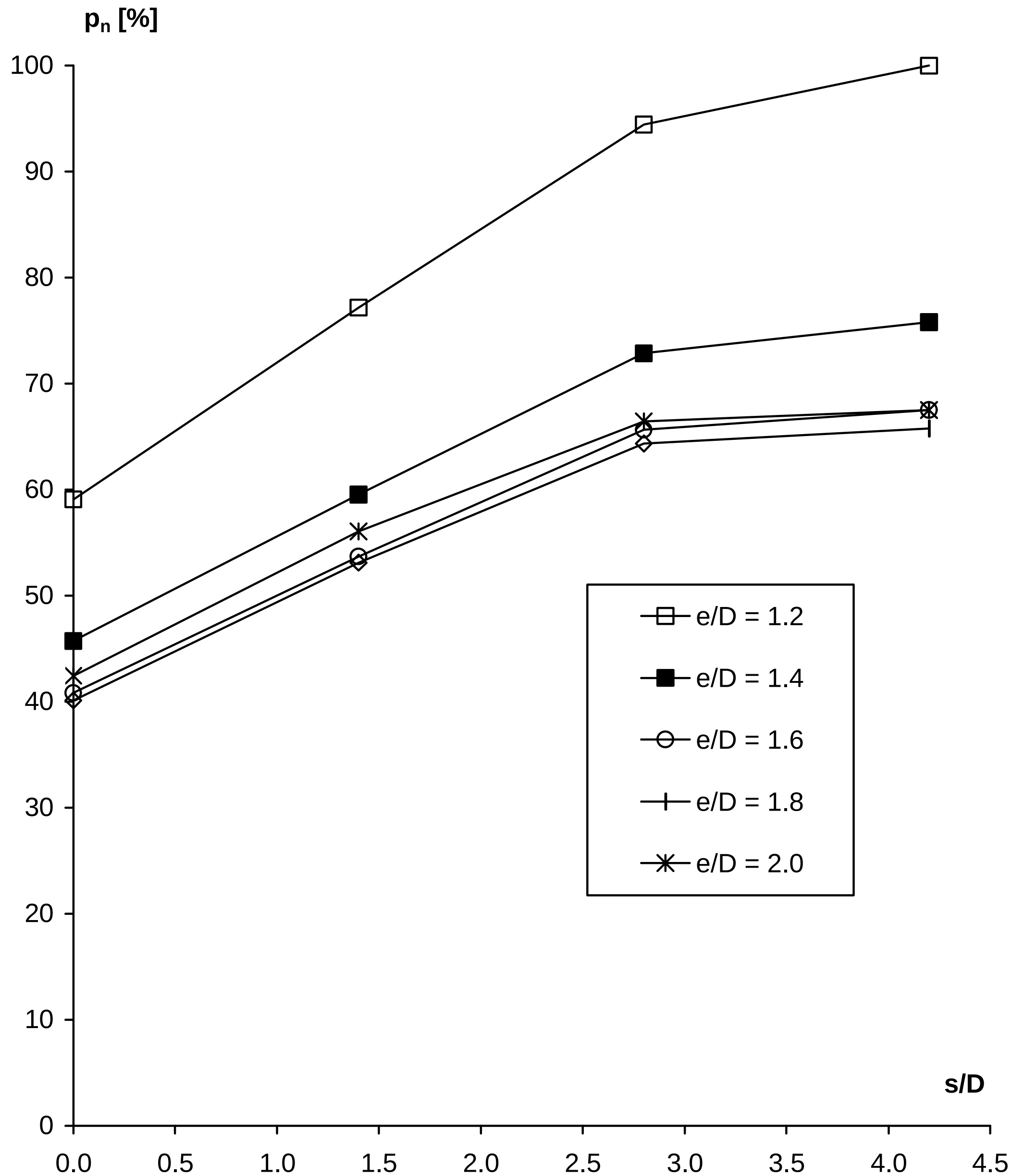

Figure 5.18 – Percentage of fatigue life, p_n, using simplification 3 for F_{sc} $(n_l = 2)$.

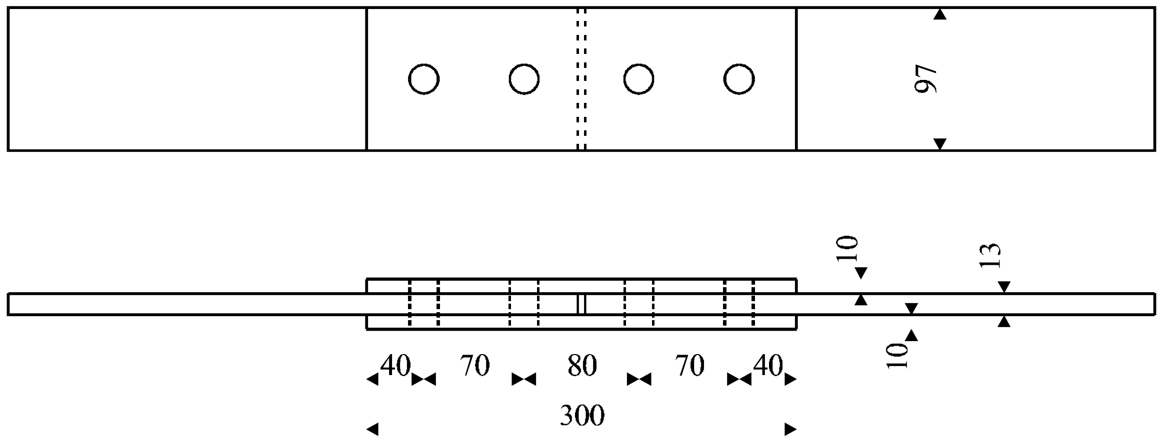

Figure 5.19 – Geometry of the specimens tested by Graf [2.43].

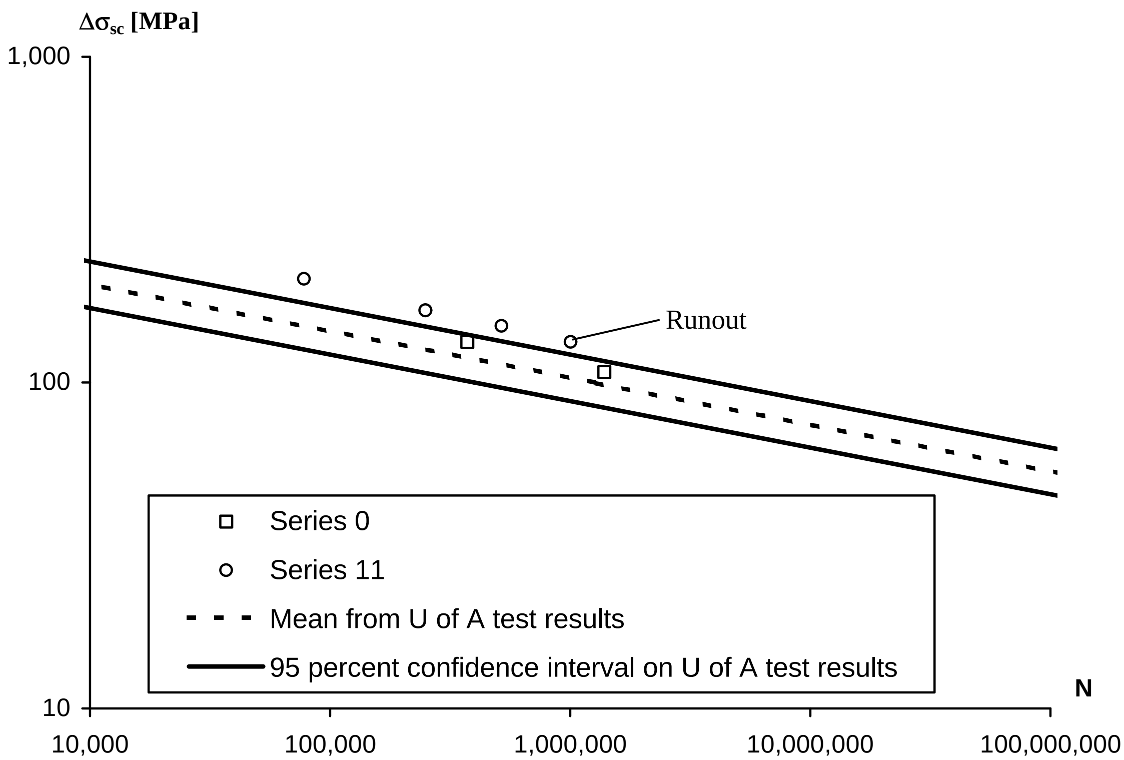

Figure 5.20 –Corrected test results from Graf [2.43] and regression lines from this study.

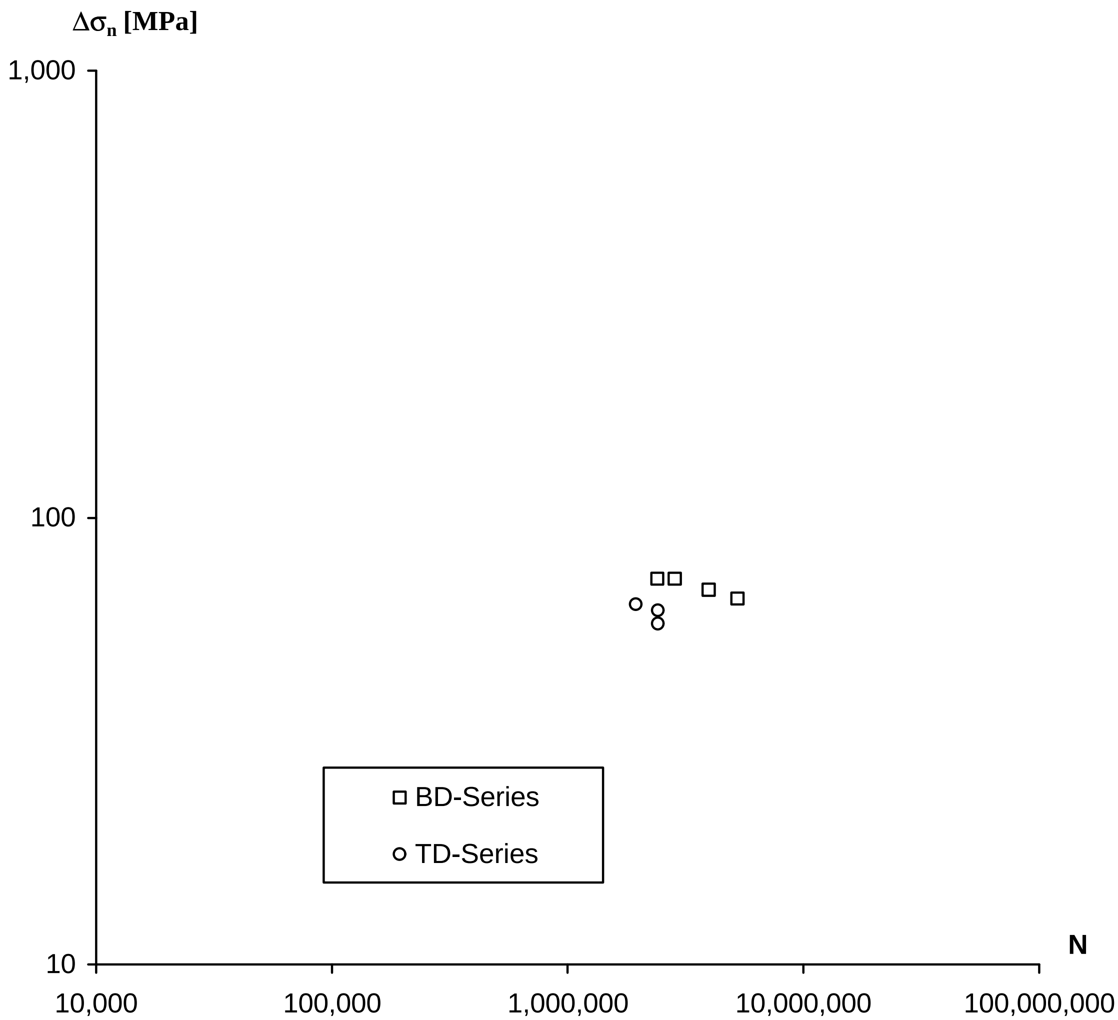

Figure 5.21 – Test results as presented by DiBattista and Kulak [2.53].

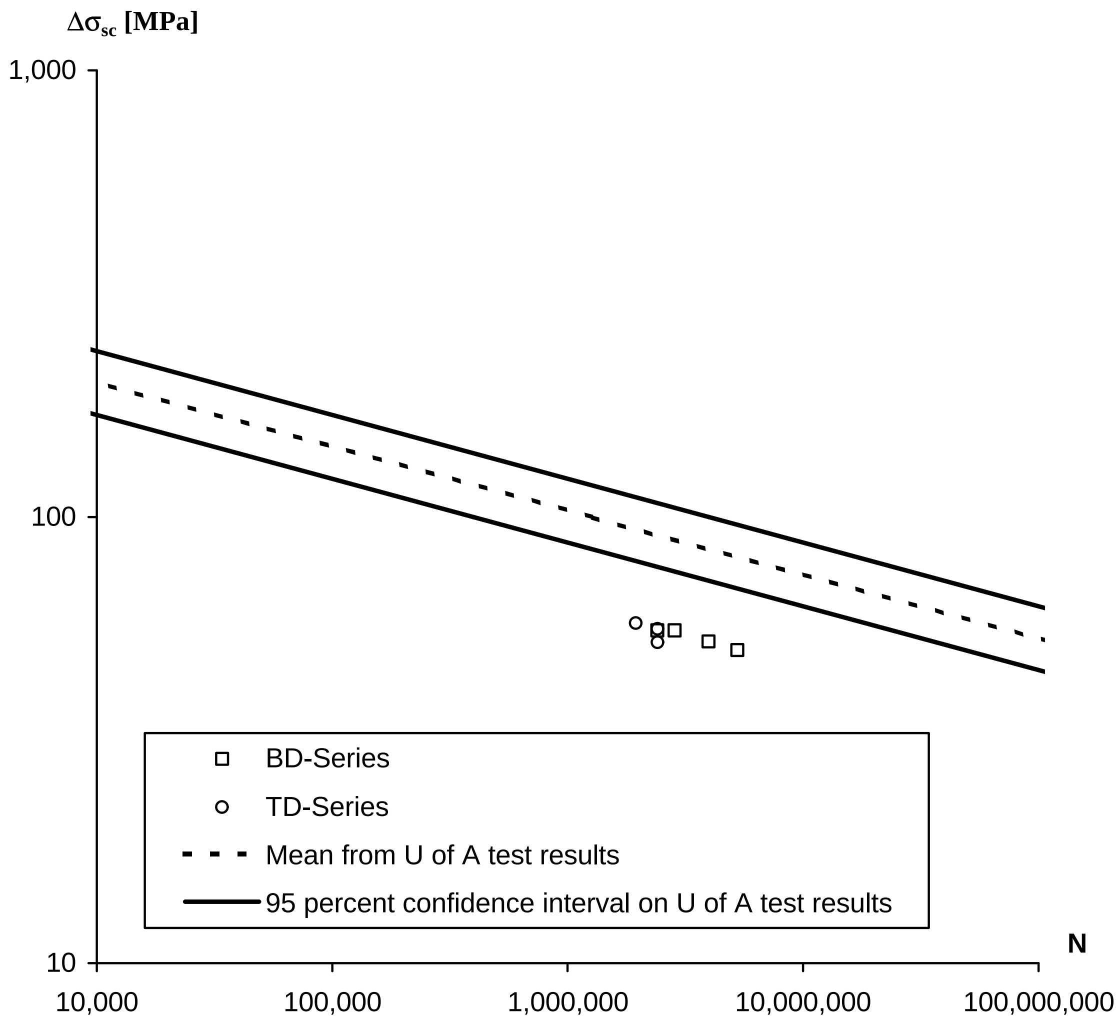

Figure 5.22 – Corrected test results from DiBattista and Kulak [2.53] and regression lines from this study.

6. SUMMARY, CONCLUSIONS, AND RECOMMENDATIONS

6.1 Summary

As the interest in the use of high strength bolts as structural fasteners grew in the late 1950s, many tests were carried out to assess the fatigue behavior of bolted connections. Based on the results of these tests, bolted shear splices were assigned to existing fatigue design curves using the average net cross-sectional stress for bearing-type connections. However, the use of the net section as the critical cross-section is controversial. The question about the critical cross-section for fatigue calculations becomes confusing in the presence of bearing-type connections with staggered holes. No special guidelines for a net section calculation for fatigue life assessment have been implemented in existing codes, and it is often assumed that the net section calculated according to Cochrane's rule (or other similar rules) can be used. Since the Cochrane rule is founded on the assumption that plastic deformation conditions are present over the entire width of a plate, it is doubtful that this definition of net section is adequate for load levels below the ultimate loads, as is the case for fatigue loading.

An analytical and experimental investigation of the fatigue resistance of bearing-type shear splices was conducted to assess the effect bolt hole pattern on fatigue resistance. Stress analysis on a variety of shear splices consisting of flat plates was conducted to investigate the effect of bolt hole stagger, gage dimension, and edge distance on the stress concentration around the bolt holes. Based on the findings of this analytical investigation, a test program was developed. Thirty-one fatigue tests on symmetrical bearing-type shear splices consisting of flat plates were carried out. Statistical analyses of the test results were used to compare the analytical and experimental results and to assess the fatigue strength of bearing-type shear splices.

6.2 Conclusions

The following conclusions can be drawn from the results of the work described above:

1. An increase in bolt hole stagger from 25 to 75 mm has a negligible effect on the stress concentration in the splice plates and their fatigue resistance.
2. By comparison with shear splices with no bolt hole stagger, the presence of stagger results in an increase in stress concentration. However, the increase is too moderate to significantly affect the fatigue life of the investigated shear splices.
3. Changes in plate geometry, such as varying the gage width, g, or the edge distance, e, affect the stress concentration. These differences, however, are

too small to significantly affect the fatigue life of the investigated shear splices.

4. Calculation of the stress range based on the Cochrane $s^2/4g$ rule, or any other commonly used cross-sectional area definition, was found to give poor correlation with the observed test results.
5. Corrected gross cross-section stress range, which accounts for the stress concentration in a bearing-type shear splice, was found to provide a good correlation with the test results. The correction of the gross cross-section stress range is performed with respect to a reference splice plate configuration by means of a stress range correction factor, F_{sc}. The stress range correction factor can be obtained using a linear elastic finite element analysis of the splice plate.
6. A regression analysis of the test results indicates that the slope of the fatigue curve for bearing-type shear splices ($m = 7$) is significantly different from the slope defined in modern codes for other fatigue details ($m = 3$). Therefore, the use of existing fatigue curves is not advisable.
7. Results consistent with the ones found in the experimental program are obtained when the concept of corrected stress range, $\Delta\sigma_{sc}$, is applied to test results on flat plate specimens tested by others. However, the limited evidence available indicates that the use of stress range correction factors, F_{sc}, developed for flat plates does not work well with shapes other than flat plates.

A new fatigue curve based on statistical analysis of the test results was defined in this study. In addition, the stress range correction factor, F_{sc}, has been derived for the most common cases of flat plates.

6.3 Recommendations

6.3.1 Design

The fatigue strength of bearing-type shear splices should be based on gross cross-section stress ranges. These stress ranges are corrected to account for the stress concentration present because of the bolt hole. The following fatigue life equation should be used for bolted bearing-type shear splices:

$$N = 4 \times 10^{19} \Delta\sigma_{sc}^{-7} \qquad (6.1)$$

where

N : fatigue life in cycles of loading

Δs_{sc} : stress range modified to account for stress concentration, $\Delta s_{sc} = F_{sc} \Delta s_g$

F_{sc} : stress range correction factor, $F_{sc} = \dfrac{SCF_k}{SCF_{S0}}$

SCF_k : stress concentration factor for plate *k*, $SCF_k = \dfrac{\sigma_{hole,k}}{\sigma_{g,k}}$

SCF_{S0} : stress concentration factor for the reference plate S0, $SCF_{S0} = 3.95$

$\sigma_{hole,k}$: peak stress in considered plate (plate *k*)

$\sigma_{g,k}$: gross section stress of considered plate (plate *k*)

Table 5.6 can be used to determine the stress range correction factor, F_{sc}, for flat plates having at least two rows of bolts, n_r, and a gage distance smaller or equal to three times the bolt hole diameter, $g \leq 3D$.

6.3.2 Future Research Needs

Although the approach proposed in this study is satisfactory for flat plates, more work is needed to validate the method for tension members of different shapes (e.g. angle sections). Additional research involving analytical investigations and experimental work should be carried out to verify that the approach proposed in this study can be used for other types of bolted bearing-type shear splices.

The number of test results obtained in this test program and other test programs on bearing-type shear splices is insufficient to establish with confidence a constant amplitude fatigue limit, CAFL, for this detail. More tests are required to establish the appropriate CAFL.

Rivets are used as fasteners in numerous existing bridges. A means of extrapolating the approach proposed in this study to riveted shear splices needs to be found.

LIST OF REFERENCES

[1.1] KAMINETZKY, D.: *Design and Construction Failures: Lessons From Forensic Investigations.* McGraw-Hill, New York, 1991.

[1.2] KULAK, G. L.; FISHER, J. W.; STRUIK, J.H.A.: *Guide to Design Criteria for Bolted and Riveted Joints.* Second Edition, John Wiley & Sons, New York, 1987.

[1.3] FISHER, J. W.: *Fatigue and Fracture in Steel Bridges.* John Wiley & Sons, New York, 1984.

[1.4] AASHTO: *AASHTO LRFD Bridge Design Specifications.* SI Units, 1st Edition, American Association of State Highway and Transportation Officials, Washington, D.C., 1994.

[1.5] ECCS: *Recommendations for the Fatigue Design of Steel Structures.* Publication No. 43, European Convention for Constructional Steelwork, Brussels, 1985.

[2.1] RCSC: *Load and Resistance Factor Design Specification for Structural Joints Using ASTM A325 or A490 Bolts.* Research Council on Structural Connections, 1994.

[2.2] BAKER, K. A.; KULAK, G. L.: *Fatigue Strength of Two Steel Details.* Structural Engineering Report No. 105, Department of Civil Engineering, University of Alberta, Edmonton, 1982.

[2.3] RESEARCH COUNCIL ON STRUCTURAL CONNECTIONS: *Load and Resistance Factor Design: Specification for Structural Joints Using ASTM A325 or A490 Bolts.* Edited by the American Institute of Steel Construction, Chicago, 1996.

[2.4] ECCS: *European Recommendations for Bolted Connections in Structural Steelwork.* Publication No. 38, European Convention for Constructional Steelwork, Brussels, 1985.

[2.5] HECHTMAN, R. A.; YOUNG, R. D.; CHIN, J. M.; SAVIKKO, J. M.: *Slip of Joints under Static Loads.* Proceedings of the American Society of Civil Engineers, Structural Division, Vol. 80, September, 1954, Separate No. 484.

[2.6] KULAK, G. L.; FISHER, J. W.: *Behavior of Slip-Resistant Bolted Joints.* IABSE Surveys S-32/85, IABSE Periodica 4, International Association for Bridge and Structural Engineering, Zurich, 1985, pp. 45-62.

[2.7] VASARHELYI, D. D.; CHIANG, K. C.: *Coefficient of Friction in Joints of Various Steels.* Journal of the Structural Division, ASCE, Vol. 93, ST4, 1967, pp. 227-243.

[2.8] YURA, J. A.; FRANK, K. H.; CAYES, L.: *Bolted Friction Connections with Weathering Steel.* Journal of the Structural Division, ASCE, Vol. 107, ST11, 1981, pp. 2071-2087.

[2.9] STERLING, G. H.; FISHER, J. W.: *A440 Steel Joints Connected by A490 Bolts.* Journal of the Structural Division, ASCE, Vol. 92, ST3, 1966, pp.101-118.

[2.10] LEE, J. H.; O'CONNOR, C.; FISHER, J. W.: *Effect of Surface Coatings and Exposure on Slip.* Journal of the Structural Division, ASCE, Vol. 95, ST11, 1969, pp. 2371-2383.

[2.11] BROOKHART, G. C.; SIDDIQI, I. H.; VASARHELYI, D. D.: *Surface Treatment of High-Strength Bolted Joints.* Journal of the Structural Division, ASCE, Vol. 94, ST3, 1968, pp. 671-681.

[2.12] FOUAD, F. H.: *Slip Behavior of Bolted Friction-Type Joints with Coated Contact Surfaces.* MS Thesis, The University of Texas at Austin, 1978.

[2.13] BOUWMAN, L. P.; PIRAPREZ, E.: *The Tightening of High-Strength Bolts in Europe.* Unpublished Paper, 1986.

[2.14] FISHER, J. W.; RUMPF, J. L.: *Analysis of Bolted Butt Joints.* Journal of the Structural Division, ASCE, Vol. 91, ST5, 1965, pp. 181-203.

[2.15] FISHER, J. W.; BEEDLE, L. S.: C*riteria for Designing Bearing-Type Bolted Joints.* Journal of the Structural Division, ASCE, Vol. 91, ST5, 1965, pp. 129-154.

[2.16] BENDIGO, R. A.; HANSEN, R. M.; RUMPF, J. L.: *Long Bolted Joints.* Journal of the Structural Division, ASCE, Vol. 89, ST6, 1963, pp. 187-213.

[2.17] KULAK, G. L.; FISHER, J. W.: *A514 Steel Joints Fastened by A490 Bolts.* Journal of the Structural Division, ASCE, Vol. 94, ST10, 1968, pp. 2303-2323.

[2.18] KULAK, G. L.: *The Behavior of A514 Steel Tension Members.* AISC Engineering Journal, Vol. 8, No. 1, 1971, pp. 1-5.

[2.19] FISHER, J. W.; KULAK, G. L.: *Tests of Bolted Butt Splices.* Journal of the Structural Division, ASCE, Vol. 94, ST11, 1968, pp. 2609-2619.

[2.20] COCHRANE, V. H.: *Rules for Rivet Hole Deductions in Tension Members.* Engineering News-Record, Vol. 89, November 16, 1922, pp. 847-848.

[2.21] HIRT, M. A.; BEZ, R.: *Construction métallique: notions fondamentales et méthodes de dimensionnement.* Traité de Génie Civil de l'EPFL, Vol. 10, Presses Polytechnique et Universitaire Romandes, Lausanne, 1994.

[2.22] SWISS SOCIETY OF ENGINEERS AND ARCHITECTS: *SIA Standard 161: Steel Structures (1979 Edition).* Schweizerischer Ingenieur- und Architektenverein, Zurich, 1979.

[2.23] YOUNG, C. R.: *True Net Sections of Riveted Tension Members.* Bulletin No. 2, School of Engineering Research, Faculty of Applied Science and Engineering, University of Toronto, 1921.

[2.24] McGUIRE, W.: *Steel Structures.* Prentice-Hall, Englewood Cliffs, N. J., 1968, pp. 308 ff.

[2.25] AMERICAN INSTITUTE OF STEEL CONSTRUCTION: *Bridge Fatigue Guide: Design and Details.* AISC, Chicago, 1977.

[2.26] GURNEY, T. R.: *Fatigue of Welded Structures.* 2nd Edition, Cambridge University Press, 1979.

[2.27] FUCHS, H. O.; STEPHENS, R. I.: *Metal Fatigue in Engineering.* John Wiley and Sons, New York, 1980.

[2.28] FISHER, J. W.; KULAK, G. L.; SMITH, I. F. C.: *A Fatigue Primer for Structural Engineers.* National Steel Bridge Alliance, American Institute of Steel Construction, Chicago, IL., 1998.

[2.29] BASQUIN, O. H.: *The Exponential Law of Endurance Tests.* Proceedings of the American Society for Testing and Materials, Vol. 10, 1910, pp. 625-630.

[2.30] CAN/CSA S16.1-94: *Limit States Design of Steel Structures.* Canadian Standards Association, Rexdale (Toronto), 1994.

[2.31] KUNZ, P.: *Probabilistisches Verfahren zur Beurteilung der Ermüdungssicherheit bestehender Brücken aus Stahl.* Ph.D. Thesis No. 1023, Swiss Federal Institute of Technology, Lausanne, 1992.

[2.32] WILSON, W. M.; THOMAS, F. P.: *Fatigue Tests of Riveted Joints.* Bulletin 302, Engineering Experiment Station, University of Illinois, 1938.

[2.33] KLOEPPEL, K.; SEEGER, T.: *Dauerversuche mit einschnittigen HV-Verbindungen aus ST 37.* Der Stahlbau, Vol. 33, No. 8, 1964, pp. 225-245 and No. 11, 1964, pp. 335-346.

[2.34] MIKI, C.; FAN, H.; KAWAI, Y.: *Fatigue Performance of Single Spliced Bolted Joints in Prefabricated Steel Bridge Decks.* Structural Eng./Earthquake Eng., Japanese Society of Civil Engineers, Vol. 8, No. 2, 1991, pp. 59-62.

[2.35] ALBRECHT, P.; SAHLI, A. H.; WATTAR, F.: *Fatigue Strength of Bolted Joints.* Journal of Structural Engineering, ASCE, Vol. 113, No. 8, 1987, pp. 1834-1849.

[2.36] FRANK, K. H.; YURA, J. A.: *An Experimental Study of Bolted Shear Connections.* Report No. FHWA/RD-81/148, Department of Civil Engineering, University of Texas, Austin, 1981.

[2.37] BARON, F.; LARSON, E. W., Jr.: *The Effect of Grip on the Fatigue Strength of Riveted and Bolted Joints.* Proceedings of the American Railway Engineering Association, Vol. 54, 1953, pp. 175-190.

[2.38] STEINHARDT, O.; MOEHLER, K.: *Versuche zur Anwendung vorgespannter Schrauben im Stahlbau, Teil II.* Bericht des Deutschen Ausschusses für Stahlbau, Stahlbau Verlag GmbH, Cologne, 1959.

[2.39] CHESSON, E., Jr.; MUNSE, W. H.: *Studies of the Behavior of High-Strength Bolts and Bolted Joints.* Engineering Experiment Station Bulletin 469, University of Illinois, Urbana, 1965.

[2.40] BIRKEMOE, P. C.; MEINHEIT, A. M.; MUNSE, W. H.: *Fatigue of A514 Steel in Bolted Connections.* Journal of the Structural Division, ASCE, Vol. 95, ST 10, 1969, pp. 2011-2031.

[2.41] LIEURADE, H.-P.: *Etude de la tenue à la fatigue des assemblages boulonnés en aciers à haute limite d'élasticité.* Report RE 339, Institut de Recherches de la Sidérurgie Française, Saint-Germain-en-Laye, 1976.

[2.42] SAHLI, A.; ALBRECHT, P.; VANNOY, D. W.: *Fatigue Strength of Retrofitted Cover Plates.* Journal of Structural Engineering, ASCE, Vol. 110, No. 6, 1984, pp. 1374-1388.

[2.43] GRAF, O: *Versuche an geschraubten Verbindungen.* Bericht 16, Deutscher Ausschuss für Stahlbau, Stahlbau Verlag GmbH, Cologne, 1951.

[2.44] LENZEN, K. H.: *The Effect of Various Fasteners on the Fatigue Strength of a Structural Joints.* Proceedings of the American Railway Engineering Association, Vol. 51, 1950, pp. 1-28.

[2.45] CULLIMORE, M. S. G.: *Fatigue of HSFG Bolted Joints – Effects of Design Parameters.* Proceedings of the IABSE Colloquium "Fatigue of Steel and Concrete Structures" held in Lausanne, International Association for Bridge and Structural Engineering, Vol. 37, Zurich, 1982, pp. 715-723.

[2.46] MUNSE, W. H.; WRIGHT, D. T.; NEWMARK, N. M.: *Laboratory Tests of Bolted Joints.* Proceedings of the American Society of Civil Engineers, Structural Division, Vol. 80, May, 1954, Separate No. 441.

[2.47] YIN, W.-S.; FANG, Q.-H.; WANG, S.-X.; WANG, X.-H.: *Fatigue Strength of High Strength Bolted Joints.* Proceedings of the IABSE Colloquium "Fatigue of Steel and Concrete Structures" held in Lausanne, International Association for Bridge and Structural Engineering, Vol. 37, Zurich, 1982, pp. 707-714.

[2.48] HANSEN, N. G.: *Fatigue Tests of Joints of High Strength Steels.* Journal of the Structural Division, ASCE, Vol. 85, ST 3, 1959, pp. 51-69.

[2.49] BIRKEMOE, P. C.; SRINIVASAN, R.: *Fatigue of Bolted High Strength Structural Steels.* Journal of the Structural Division, ASCE, Vol. 97, ST 3, 1971, pp. 935-950.

[2.50] MAS, E; JANSS, J.: *Assemblages par boulons à haute résistance Fatigue des assemblages à double couvre-joint.* Report MT 10, Centre de Recherches Scientifiques et Techniques de l'Industrie des Fabrications Métalliques, Section Construction Métallique, Brussels, 1964.

[2.51] ENV 1993-1-1:1992: *Design of Steel Structures - Part 1-1: General Rules and Rules for Buildings.* Comité Européen de Normalisation, Brussels, 1992.

[2.52] REEMSNYDER, H. S.: *Fatigue Life Extension of Riveted Connections.* Journal of the Structural Division, ASCE, Vol. 101, ST 12, 1975, pp. 2591-2608.

[2.53] DIBATTISTA, J. D.; KULAK, G. L.: *Fatigue of Riveted Tension Members.* Structural Engineering Report No. 211, Department of Civil Engineering, University of Alberta, Edmonton, 1995.

[2.54] DIBATTISTA, J. D.; ADAMSON, D. E. J.; KULAK, G. L.: *Fatigue Strength of Riveted Connections.* Journal of Structural Engineering, ASCE, Vol. 124, No. 7, 1998, pp. 792-797.

[2.55] JOSI, G.; KUNZ, P.; LIECHTI, P.: *Aarebrücke Felsenau: Ermüdungsversuche an vier Diagonalen.* ICOM Report 667-3, Swiss Federal Institute of Technology, Lausanne, 1996.

[2.56] ABE, H.; ICHIJO, M.; TAKAGI, Y.: *Fatigue Strength of Joints with Bolts in Staggered Patterns.* Proceedings of the IABSE Colloquium "Fatigue of Steel and Concrete Structures" held in Lausanne, International Association for Bridge and Structural Engineering, Vol. 37, Zurich, 1982, pp. 699-706.

[2.57] KELLER, A.; BEZ, R.; BRÜHWILER, E.; HIRT, M. A.: *Aarebrücke Felsenau: Beurteilung der Ermüdungssicherheit und der Restnutzungsdauer*. ICOM Report 667-2, Swiss Federal Institute of Technology, Lausanne, 1995.

[3.1] HIBBIT, KARLSSON & SORENSEN, INC.: *ABAQUS/Standard User's Manual, Version 5.7.* Hibbit, Karlsson & Sorensen, Inc., Pawtucket, Rhode Island, 1997.

[3.2] BATHE, K.-J.: *Finite Element Procedures.* Prentice Hall, New Jersey, 1996.

[3.3] ELBER, W.: *Fatigue Crack Closure under Cyclic Tension.* Engineering Fracture Mechanics, Vol. 2, 1970, pp. 37-45.

[3.4] FROCHT, M. M.: *Photoelastic Studies in Stress Concentration.* Mechanical Engineering, August 1936, pp. 485-489.

[4.1] KULAK, G. L.; ADAMS, P. F.; GILMOR, M. I.: *Limit States Design in Structural Steel.* Fifth Edition, Canadian Institute for Steel Construction. Printed by Universal Offset Limited, Markham, Ontario, 1998.

[4.2] CAN/CSA G40.21-M92: *Structural Quality Steels.* Canadian Standards Association, Rexdale (Toronto), 1992.

[4.3] ASTM A 370-94: *Standard Test Methods and Definitions for Mechanical Testing of Steel Products.* American Society for Testing and Materials, West Conshohocken, Pennsylvania, 1994.

[5.1] KENNEDY, J. B.; NEVILLE, A. M.: *Basic Statistical Methods for Engineers and Scientists.* Second Edition, Published by Harper & Row, New York, 1976.

[5.2] REEMSNYDER, H. S.: *Procurement and Analysis of Structural Fatigue Data.* Journal of the Structural Division, ASCE, Vol. 95, No. 7, 1969, pp. 1533-1551.

[5.3] BENJAMIN, J. R.; CORNELL, C. A.: *Probability, Statistics, and Decision for Civil Engineers.* McGraw-Hill Book Company, New York, 1970.

[5.4] FISHER, J. W.; YEN, B. T.; WANG, D.: *Fatigue of Bridge Structures–A Commentary and Guide for Design, Evaluation and Investigation of Cracking.* ATLSS Report No. 89-02, Lehigh University, Bethlehem, PA, 1989.

[5.5] KLIPPSTEIN, K. H.: *Variable Amplitude Load Fatigue, Task A - Literature Review, Volume III – Supplementary Information on Constant Amplitude Fatigue Behavior.* U.S. Department of Transportation Report No. DTFH61-86-C-00036-III, Washington, D.C., 1987.

[5.6] BROZETTI, J.; HIRT, M. A.; RYAN, I.; SEDLACEK, G.; SMITH, I. F. C.: *Eurocode 3: Background Informations on Fatigue Design Rules, Statistical Evaluation.* First Draft of Background Document No. 9.01, University of Technology in Aachen, Germany, 1989.

[5.7] AREA: *Manuel for Railway Engineering.* American Railway Engineering Association, , 1994.

[5.8] HERTZBERG, R. W.: *Deformation and Fracture Mechanics of Engineering Materials.* Fourth Edition, John Wiley & Sons, New York, 1996.

[B.1] NATRELLA, M. G.: *Experimental Statistics.* National Bureau of Standards Handbook 91, United States Department of Commerce, Washington, D.C., 1963.

[B.2] ASTM E 739-80: *Standard Practice for Statistical Analysis of Linear or Linearized Stress-Life (S-N) and Strain-Life (e-N) Fatigue Data.* American Society for Testing and Materials, West Conshohocken, Pennsylvania, 1980.

[B.3] MILLER, I.; FREUND, J. E.; JOHNSON, R. A.: *Probability and Statistics for Engineers.* Fourth Edition, Prentice Hall, Englewood Cliffs, N. J., 1990.

APPENDIX A

Results of Tension Coupon Tests

Results of Tension Coupon Tests

Three tension coupons (TC1, TC2, and TC3) from the splice plate material were tested prior to the fatigue study. The tension coupons were prepared in accordance with the requirements of ASTM A 370-94 [4.1], with a gage length of 50 mm and a reduced section width of 12.5 mm. The material tests were conducted at a strain rate of about 15 $\mu\varepsilon$/sec in the elastic range and at about 50 $\mu\varepsilon$/sec in the plastic range. Strains in the first tested coupon were measured using two electrical resistance strain gages and a clip-on extensometer. After verifying that the average strains measured with the strain gages corresponded to the strains measured with the extensometer, only the extensometer was used for the subsequent tests. All three specimens showed elastic behavior followed by a yield plateau and strain hardening. Four static stress values—two in the yield stress plateau, one near the ultimate stress, and one near the failure stress—were obtained for each test when the strain rate was reduced to zero for an interval of two minutes. Table A.1 shows specific results from each of the tension coupon tests. The static yield stress was obtained by calculating the mean of the two static values measured in the yield plateau and the dynamic yield stress was obtained by averaging several values in the yield plateau. All other values were read directly from the stress-strain curves.

Table A.1 – Tension coupon test results (engineering stresses and strains).

	TC1	**TC2**	**TC3**
Static Yield Stress [MPa]	420	420	420
Dynamic Yield Stress [MPa]	455	460	460
Modulus of Elasticity [MPa]	212 000	212 000	212 000
Strain at Onset of Strain Hardening	0.031	0.029	0.032
Static Ultimate Stress [MPa]	480	475	475
Dynamic Ultimate Stress [MPa]	500	495	500
Strain at Ultimate Stress	0.140	0.142	0.142
Rupture Strain	0.27	0.31	0.30

APPENDIX B

Statistical Analysis of Test Data

B.1 Comparison of Variances Using the F Test

In order to be able to compare mean values from different sets of tests, it first has to be shown with some degree of certainty that their variances do not differ significantly. If there are only two variances ($s_{y,1}$ and $s_{y,2}$) the F test can be applied, where the value of F is calculated as [5.1]:

$$F = \left(\frac{s_{y,1}}{s_{y,2}} \right)^2 \qquad \text{with } s_{y,1} > s_{y,2} \tag{B.1}$$

Subscript 1 corresponds to the first set of data and subscript 2 refers to the second set of data. If F is smaller than a tabulated value for a certain level of significance, then the difference between the two variances can be assumed to be insignificant. The tabulated value of F depends on the number of degrees of freedom, DOF, for each set of tests ($DOF = n-1$ where n is the sample size) and the desired level of significance. All the sets discussed in Chapter 5 consisted of three test data points; therefore $DOF = 2$ for each set. If a level of confidence of 95 percent is defined, then F should not be greater than 19.0 in order to conclude there is no significant difference between the two variances [B.1].

B.2 Comparison of Mean Values Using Student's t Test

A statistical comparison of the mean values of two sets of test results ($y_{av,1}$ and $y_{av,2}$) can be carried out using Student's t test, where t is defined as [5.1]:

$$t = \frac{\left| \bar{y}_1 - \bar{y}_2 \right|}{\sqrt{\dfrac{\sum (y_1 - \bar{y}_1)^2 + \sum (y_2 - \bar{y}_2)^2}{(n_1 - 1) + (n_2 - 1)} \times \left(\dfrac{n_1 + n_2}{n_1 n_2} \right)}} \tag{B.2}$$

For simplification, the subscript i in the summations was omitted. If t is smaller than a tabulated value for a certain level of confidence, then the difference between the two mean values can be assumed to be insignificant. The tabulated value of t depends on the number of degrees of freedom for the total of the tests of the two sets, which is for all the comparisons carried out in Chapter 5 equal to $DOF = n_1 + n_2 - 2 = 4$, and the desired level of confidence. If a 95 percent level of confidence is defined, then t should not be greater than 2.776 in order to conclude there is no significant difference between the two variances [B.1].

B.3 Regression Analysis

Regression analysis of the test data was used to derive the sloped portion of the $\Delta s - N$ curve, which can be described by the following equation:

$$\log(N) = \log(C) - m\log(\Delta s) \tag{B.3}$$

For simplicity, the subscript sc for the adjusted gross section stresses is omitted. The notation can be further simplified by replacing $log(\Delta\sigma)$ by x (independent variable), $log(N)$ by y (dependent variable), $log(C)$ by a (intercept), and $-m$ by b (slope):

$$y = a + bx \tag{B.4}$$

Using the method of least squares, the slope b and the intercept a of the best fit line with n test results are obtained from [B.2]:

$$b = \frac{S_{xy}}{S_{yy}} \tag{B.5}$$

with: $$S_{xy} = \sum_{i=1}^{n}\left(x_i - \overline{x}\right)\left(y_i - \overline{y}\right)$$

$$S_{yy} = \sum_{i=1}^{n}\left(y_i - \overline{y}\right)^2$$

$$a = \overline{y} - b\overline{x} \tag{B.6}$$

The goodness of fit of the regression model is measured using the correlation coefficient, r, given by [5.1]:

$$r = \sqrt{\frac{S_{xy}{}^2}{S_{xx}S_{yy}}} \tag{B.7}$$

with: $$S_{xx} = \sum_{i=1}^{n}\left(x_i - \overline{x}\right)^2$$

An r value of zero indicates that y is not linearly predicted in any useful way by x, and an r value of 1.0 indicates that y is linearly predicted perfectly by x.

Existing $\Delta s - N$ curves have, with a few exceptions, a slope of $m = 3$. It is therefore interesting to determine whether there is a significant difference between $m = -b$ and $m = 3$. This is done using the t test [5.1]:

$$t = \frac{|3-(-b)|}{s_b} \tag{B.8}$$

with $$s_b = \sqrt{\frac{\sum \left(y_i - (a + bx_i)\right)^2}{(n-2)S_{xx}}}$$

If the calculated value of t is greater than the tabulated value of t for a required level of significance and a number of degrees of freedom, $DOF = n-2$, then there is a significant difference between $m = -b$ and $m = 3$.

The values of $\log(N)$ obtained using the regression curve are estimated values, and it is therefore useful to calculate their standard error of estimate, s_e, given by [B.3]:

$$s_e = \sqrt{\frac{S_{yy} - bS_{xy}}{n-2}} \tag{B.9}$$

B.4 Determination of the Design Fatigue Curve

A simplified confidence interval of about 95% for the regression curve can be obtained by subtracting two standard errors of the estimate from the mean regression curve [5.5]. This results in a new intercept, $a' = \overline{y} - 2s_e - b\overline{x}$, which is equal to $6.063 - 2 \cdot 0.255 + 7 \cdot 2.008 = 19.6$ for the investigated shear splices. Consequently, the $\Delta s - N$ relationship can be written as:

$$\log(N) = 19.6 - 7\log(\Delta s\ ) \tag{B.10}$$